UNIVERSITY OF LEEDS

Real-Time State of Charge Estimation Algorithm for Electrical Batteries

Onur Kadem

Submitted in accordance with the requirements for the degree of PhD. Mechanical Engineering

The University of Leeds

Faculty of Engineering

School of Mechanical Engineering

September 2022

Intellectual Property

The candidate confirms that the work submitted is his own and that appropriate credit has been given where reference has been made to the work of others.

This copy has been supplied on the understanding that it is copyright material and that no quotation from the thesis may be published without proper acknowledgment.

Acknowledgements

I would like to express my gratitude to my supervisor, Dr. Jongrae Kim, for his guidance during my Ph.D. study. Thanks to him, I had a great opportunity to learn a lot about optimal estimation techniques.

None of these would be possible without the support, encouragement, and love of my mom Miyesser, my father Celil, and my sister Şennur. I also want to thank my niece Naz, and my nephew Ömür for giving me lots of smiles.

Special thanks to the Republic of Türkiye Ministry of National Education for their financial support for my Ph.D. and MSc studies.

I also want to thank my friends from different disciplines who shared their experiences regarding their Ph.D. studies and spent time with me at social events.

Abstract

While 21st-century society is shifting towards eco-friendly infrastructures, the main interest of the automotive industry has been transferring to electric vehicles. This transformation is dependent on the development of reliable battery management systems (BMSs). A BMS in electric cars provides vital information about the battery states including the state of charge (SoC). Optimal and robust SoC estimation algorithms to deploy with minimal effort are vital for the future electric car industry.

The equivalent circuit model (ECM) based SoC estimation algorithms are widely used in practice. These algorithms suffer from two dominant error sources, i.e., inaccurate SoC-OCV relationship and input current measurement noise. In the ECM-based SoC estimation, these error sources have not been fully mitigated. Firstly, we present a novel technique to construct the SoC-OCV relation, which is eventually converted to a single parameter estimation problem. The Kalman filter is implemented to estimate the SoC and the related battery states using the proposed parameter estimation and the SoC-OCV construction technique. Secondly, we develop a novel technique to mitigate the error in the current input measurement. The error is calculated based on difference between the calculated output and the measured output. Correcting the current input measurement significantly reduces the SoC estimation error.

We validate the proposed algorithms through computer simulations and battery experiments. The numerical simulations and the battery experiment demonstrate that the SoC-OCV relationship is accurately constructed in real-time. The SoC estimation error remains below 2% in numerical simulations whereas the SoC estimation error remains within 2.5% in the battery experiment. The current noise mitigation algorithm reduces the SoC error from 11.3% to 0.56% in the numerical simulations. In the battery experiment, the SoC error is reduced from 1.74% to 1.12%.

Contents

1 Introduction **1**

1.1 Introduction 1

1.2 Research questions 6

1.3 Aim and objectives 7

1.4 Contributions and organisation of this thesis 7

2 Literature review **9**

2.1 Battery modelling 9

2.1.1 Modelling strategies 9

2.1.2 Electrochemical modelling of a battery 10

2.1.3 Equivalent Circuit-based models 12

2.2 Battery estimation 17

2.2.1 Parameter identification 17

2.2.2 State of charge estimation 27

2.3 Current sensor noise & its estimation 44

2.4 Discussion 48

3 Battery modelling and parameter identification **51**

3.1 Battery modelling 51

3.2 Model parameter identification 53

3.2.1 Linear parametric model derivation 54

3.2.2 Online parameter estimator design 56

3.2.3 Stability analysis using Lyapunov method 58

3.3 Simulations 60

3.4 Results 61

3.5 Battery experiment 64
3.6 Discussion 66

4 The SoC and OCV Relationship 68
4.1 The SoC-OCV relationship modelling 69
4.1.1 OCV Estimation Using Kalman Filter 70
4.1.2 Model construction in real-time 71
4.2 Simulations 74
4.3 Battery experiment 76
4.3.1 Battery capacity calculation 76
4.3.2 The SoC-OCV relationship calculation 77
4.4 Results 78
4.5 Discussion 86

5 Current measurement noise mitigation 88
5.1 Current sensor model 89
5.1.1 Gaussian white noise with zero mean 90
5.1.2 Current bias noise 90
5.2 Battery modelling for bias estimation 91
5.3 Modification of standard Kalman filter for batteries 94
5.4 Simulation 98
5.5 Results 100
5.6 Discussion 109

6 Conclusion and future work 111
6.1 Conclusion 111
6.2 Future work 113

References 115

A Appendix Chapter 138
A.1 Battery model algorithm 138
A.2 Parameter estimation algorithm 139
A.3 SoC-OCV curve construction algorithm 141
A.4 Bias estimation algorithm 144

List of Figures

1.1 Overview of the real-time SoC estimation algorithm 2

2.1 Electrochemical model by (Doyle et al. 1993) 11
2.2 Single particle model by (Park et al. 2017) 12
2.3 Typical relationship between the SoC and the OCV 13
2.4 Rint battery model 14
2.5 RC battery model (Hongwen et al. 2011) 14
2.6 Thevenin battery model 16
2.7 PNGV battery model 16
2.8 Ohmic resistance variations for different SoC levels, temperatures and battery ageing (Barcellona et al. 2022) 18
2.9 HPPC discharge test 20
2.10 Magnified plot of Figure 2.9 iii) 21
2.11 Wiener configuration by Naseri et al. 2022 23
2.12 Flowchart of the model-based state of charge estimation method 29
2.13 The percentage of commonly used SoC estimation algorithms by (Shrivastava et al. 2019) 30
2.14 Variations in the SoC-OCV relationship depending on the battery ageing, current rate, temperature and using different batteries by (C. Chen et al. 2022) 38
2.15 The effect of current rate on the SoC-OCV characteristic by (Yuan et al. 2022) 38
2.16 Variations in the SoC-OCV characteristic with respect to the ambient temperature by (R. Zhang et al. 2018) 39

2.17 The SoC-OCV variations at different ambient temperatures by (Z. Wang et al. 2022) . . . 39
2.18 The SoC-OCV characteristic depending on the ambient temperature by (Choi et al. 2020) . . . 40
2.19 The SoC-OCV variations for different batteries by (Han et al. 2014) . . 42

3.1 1st order Thevenin battery model . . . 52
3.2 ECM model parameter estimation results under 1C constant current discharge . . . 61
3.3 Physical parameter estimation results under sine discharge . . . 62
3.4 Physical parameter estimation results under HPPC current profile . . . 63
3.5 Physical parameter estimation results under dynamic stress test . . . 64
3.6 Battery test rig . . . 65
3.7 Battery model parameter estimation results by a battery experiment . . 66

4.1 V_{oc} and I_a estimation under constant current discharge . . . 76
4.2 SoC and SoC-OCV curve coefficients estimation under constant current discharge . . . 77
4.3 V_{oc} and I_a estimation under sinusoidal current discharge . . . 78
4.4 SoC and SoC-OCV curve coefficients estimation under sinusoidal current discharge . . . 79
4.5 Dynamic stress test Voc estimation . . . 81
4.6 Dynamic stress test I_a estimation . . . 81
4.7 SoC and SoC-OCV curve coefficients estimation under DST cycle discharge . . . 82
4.8 HPPC Voc estimation . . . 83
4.9 HPPC I_a estimation . . . 83
4.10 SoC and SoC-OCV curve coefficients estimation under HPPC cycle discharge . . . 84
4.11 Estimated & True SoC-OCV curves at different temperatures . . . 85
4.12 Real battery's V_{oc} estimation in comparison with the experimental V_{oc} . 85
4.13 Real battery's SoC estimation in comparison with the experimental SoC & Real battery's SoC-OCV curve coefficients . . . 86
4.14 Errors in OCV and SoC . . . 87

5.1 Beta estimatior 93
5.2 Current bias estimation under constant current discharge 98
5.3 SoC estimation under constant current discharge 99
5.4 Bias estimation under sinusoidal current discharge 101
5.5 SoC estimation under sinusoidal current discharge 101
5.6 Bias estimation under HPPC current discharge 102
5.7 SoC estimation under HPPC current discharge 103
5.8 Bias estimation under DST current discharge 103
5.9 SoC estimation under DST current discharge 104
5.10 The SoC and β estimation when $\sigma_{V_t} = 0.01$ and $\sigma_i = 0.01$ 105
5.11 The SoC and β estimation when $\sigma_V = 0.005$ and $\sigma_i = 0.005$ 106
5.12 The SoC and β estimation when $\sigma_V = 0.002$ and $\sigma_i = 0.002$ 106
5.13 The SoC and β estimation when $\sigma_V = 0.001$ and $\sigma_i = 0.001$ 107
5.14 The SoC and β estimation when $\sigma_{V_t} = 0.0005$ and $\sigma_i = 0.0005$ 107
5.15 The experimental β estimation result 109

Nomenclature

α	The exponential time constant
β	The bias noise in the current measurement
$\bigtriangledown(\cdot)$	The gradient of $(\cdot)$
Δt	The time interval between two sampling points
ΔV_{hl}	The difference between the higher and lower cut-off voltages
δ	The small positive constant in the SoC-OCV model
ϵ	The estimation error in the output
η	The random number from the normal distribution
Γ	The adaptive gain matrix
ϕ	The measured input vector
ρ	A positive scalar
σ	The standard deviation
σ^2	The variance
τ	The polarisation time constant
$\mathrm{I_{n\times n}}$	The n-by-n identity matrix
θ	The unknown parameter vector
ϱ	The third element of the unknown parameter vector
A	The state propagation matrix
a	The coefficient of the logarithmic term in the SoC-OCV model

B	The input matrix
b	The coefficient of the exponential term in the SoC-OCV model
C	The state measurement vector
c	The constant in the SoC-OCV model
C_p	The battery polarisation capacitance
D	The input measurement vector
e	The measurement difference error
e_s	The zero-mean white noise error
f	The nonlinear function
H	The Hessian matrix
I	The battery load current
I_a	The current flowing over R_p
I_b	The current flowing over C_p
J	The quadratic cost function
K	The Kalman gain
N_s	The number of samples
P	The error covariance matrix
Q	The process error covariance matrix
Q_{max}	The maximum capacity of a battery
Q_r	The remaining capacity of a battery
R	The measurement error covariance matrix
r	The measurement variance
R_0	The battery internal resistance
R_p	The battery polarisation resistance
T	The trace operator

u	The input
V	The Lyapunov function
v	The measurement white noise
v_i	The white noise in the current measurement
V_p	The battery polarisation voltage
V_t	The battery terminal voltage
V_{high}	The higher cut-off voltage
V_{low}	The lower cut-off voltage
V_{oc}	Open circuit voltage
w	The process white noise
x	The state vector
y	The output
z	State of charge

Chapter 1

Introduction

1.1 Introduction

In the last few years, there has been a significant technology conversion in the automotive industry towards electric vehicles (EVs) (Macioszek 2020). The number of EV owners has increased rapidly during the last decade and the global EV stock has surpassed 10 million in 2020 (Shi et al. 2022). There were 3.125 million EVs sold in 2020, which is equal to 4% of the total annual vehicle sales (Shijian Zhang et al. 2022). Although there is a 14% monotonous decreasing trend in the annual number of vehicles sold, the EV sales went up 41% against this trend in 2020 (Shijian Zhang et al. 2022). This trend is expected to keep increasing in the upcoming decades depending on the development of EVs' performance.

The EV's performance is very much dependent on the development of battery technologies and battery management systems (BMSs). In the last few decades, new battery technologies have been introduced, which has contributed to the expansion of the EV sector. Using batteries in EVs brings a challenge in making the driver comfortable about the EV in terms of range anxiety, safety, maintenance cost, and reliability. This challenge can be significantly overcome by developing efficient BMSs.

Considering batteries are a vital component of an EV powertrain, it requires accurate control and monitoring in real-time. In EVs, this requirement is fulfilled via a BMS. This is an electronic system designed to manage a rechargeable battery. This could be a single battery cell or a battery pack consisting of multiple battery cells depending

upon the application (Pastor-Fernández et al. 2016). One of its functions is to monitor the battery states using the observed data to ensure the battery or the battery pack operates safely and efficiently. A BMS provides the estimation of important parameters including the state of charge (SoC).

Existing EVs have a significantly lower driving range when compared to traditional internal combustion engine-based vehicles. Another concern regarding EVs is to miscalculate the remaining power, leaving passengers stranded. These are due to the lack of an efficient BMS that can accurately estimate the remaining power of a battery. Recent developments in the automotive industry have increased the need for more efficient BMSs (Hu et al. 2021). Providing the driver with a piece of reliable information regarding the available driving range is one of the several challenges in EVs. The SoC is a key parameter to ensure the driving range and remaining power are reliable. Thus, accurate information on the SoC is vital for EVs. The SoC cannot be directly measured by sensors, however, it could be estimated based on the observed data with a suitable method. Thus, the development of an accurate battery SoC estimation is one of the hot topics. The development of the real-time SoC estimation algorithm requires several steps to be addressed. Figure 1.1 shows these steps.

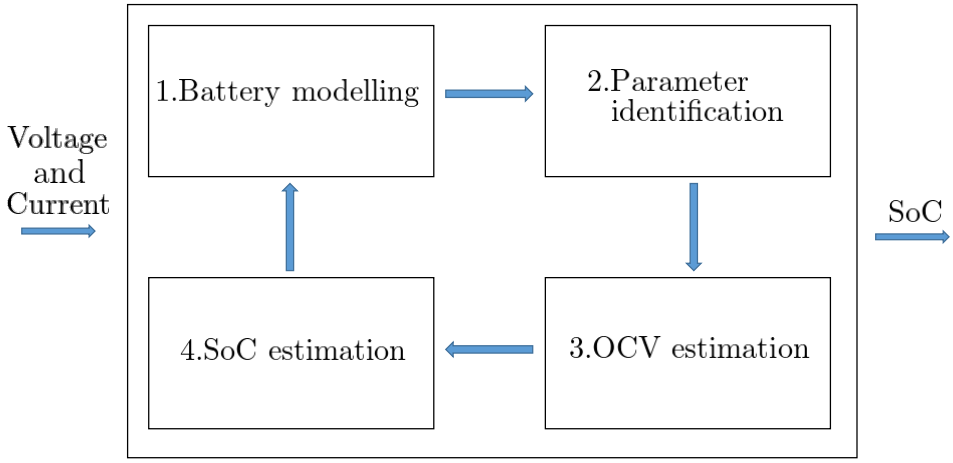

Figure 1.1: Overview of the real-time SoC estimation algorithm

The SoC is defined as the ratio of the remaining capacity to the maximum capacity given by the battery manufacturer (Cui et al. 2022).

$$z = \frac{Q_r}{Q_{max}} \tag{1.1}$$

where z represents the SoC, Q_r is the remaining capacity and Q_{max} is the maximum capacity. There are various methods to calculate the SoC. Each one of these methods has its advantages and disadvantages subject to the application, required precision, type of battery, and computational availability. In general, these methods can be classified according to whether the battery model is used or not. If the SoC is estimated based on a battery model, it is called the model-based estimation method. Otherwise, it is called the model-free estimation method.

One of the most common model-free estimation methods is the Coulomb counting (CC) method. It is a very simple method that relies on the measurement of the load current and the initial estimation of the SoC (Ko et al. 2022).

$$z(t) = z(t_0) - \int_{t_0}^{t} \frac{\tilde{I} dt}{Q_{max}} \tag{1.2}$$

where $z(t_0)$ is the initial SoC, $\tilde{I}$ is the measured load current, Q_{max} is the maximum battery capacity. In the CC method, even when $z(t_0)$ is known accurately and the current measurement sensor has very high precision, the CC method continues integrating the noises. Eventually, this method provides an inaccurate SoC estimation, which generates a lack of reliability in the CC method.

Another model-free estimation method is the open circuit voltage (OCV) measurement method. This method correlates the OCV of the battery with the SoC through a look-up table that is predefined by a battery drop-test experiment. It is not applicable in practice because the OCV can only be measured when the battery reaches the equilibrium state which may take up to a few hours depending on the battery type (M. Hannan et al. 2017).

On the other hand, model-based methods adopt a battery model. The two most common battery models are electrochemical models and empirical models which are usually in the form of equivalent circuit models (ECMs). These methods firstly predict the SoC based on the battery model and $\tilde{I}$. Then, the predicted SoC is corrected based on the measured terminal voltage $\tilde{V}_t$ that is the measured voltage difference between the battery poles. This feedback loop makes model-based methods more reliable by considering the modelling inaccuracies, the system noise, and the measurement noise.

Electrochemical battery modelling utilises electrochemical kinetics and transport phe-

nomena. Therefore, these models include several coupled differential equations to describe the chemical reactions taking place in the battery (Doyle et al. 1993). The pseudo-two-dimensional (P2D) and the single-particle model (SPM) are the most common electrochemical battery models (Hashemzadeh et al. 2022). The P2D model is a physics-based model that represents the electrochemical reactions, mass transport, and thermodynamics inside a lithium-ion battery (Newman et al. 2004). The SPM has been introduced to reduce the modelling complexity of the P2D model (Baba et al. 2014). Although the SPM is the simplified version of the P2D model, the challenges of the solution of the differential equations and parametric uncertainties remain. These models are not preferred in practice due to their modelling complexity but they are commonly used for the optimisation of battery designs in laboratories.

ECMs are usually adopted to reflect the battery behaviour in the context of a larger system. ECMs describe the response of the battery to different usage scenarios. These models are extensively used in EV applications due to their easy implementation in real-time applications (X. Liu et al. 2020). There are various kinds of ECM and they all have at least a voltage source, an internal resistor (ohmic resistor), and a load or a source. They are named according to other circuit elements utilised in the ECM. For example, the ECM that has a serially connected internal resistor and parallel resistor-capacitor (RC) branch is called the first-order Thevenin model. If there are two RC branches are connected serially to the ohmic resistor, these models are called the second-order Thevenin model. To estimate the SoC, ECMs are used with optimal state estimation algorithms (H. He et al. 2011), (R. Xiong et al. 2013), and (X. Wu et al. 2018).

Using a battery model requires the identification of the battery model parameters to prepare the state estimation algorithm to be executed. Compared to the electrochemical models, ECMs have a smaller number of parameters to be tuned. The battery parameters vary according to the operational conditions and battery aging in real-time applications. Therefore, the calculation of the model parameters is challenging. There are two main methods to calculate the model parameters: an offline method and an online method. The offline method is a battery experiment. Therefore, the model parameters acquired through the battery experiment are constant during the battery operation. Moreover, these identified parameters are only accurate under the condi-

tions of the battery experiment (Tang et al. 2011). Thus, using the offline method to identify the model parameters leads to an erroneous SoC estimation in EV applications. On the other hand, the online parameter identification method tunes the battery parameters according to the operational conditions and battery aging. Therefore, it is more appropriate to use in practice (Partovibakhsh et al. 2015), (X. Liu et al. 2020), and (Q. Ouyang et al. 2020).

ECM-based SoC estimation algorithms firstly estimate the OCV of the battery according to the previously identified model parameters (C. Zhang et al. 2015). They then convert the estimated OCV into the SoC by using a nonlinear OCV-SoC relationship. Therefore, the nonlinear relationship between the OCV and the SoC must be previously identified. Similar to the parameter estimation, the SoC-OCV relation could be obtained through a battery experiment. However, this relation is unique for a specific battery used during the battery test and cannot apply to different batteries and conditions. Moreover, Jokić et al. 2018, Aung et al. 2015, and Shehab El Din et al. 2018 showed that the relationship is vulnerable to a change in operational conditions and battery ageing. The inaccurate SoC-OCV relationship reduces the accuracy of SoC estimation. Therefore, an online method is required to calculate the SoC-OCV characteristic during the battery operation. This leads to more reliable SoC estimations as well as an increase in the trust in EVs.

The SoC is estimated using two measurable signals in batteries: the terminal voltage and the load current. The measurement noises in these signals are inevitable. The input signal in the SoC estimation problem is the measured current input. Zheng et al. 2018 showed that the current measurement is corrupted by the current bias (also known as current drift noise) and the white noise. The corrupted current measurement reduces the accuracy of the SoC estimation, which causes overcharging/discharging of the battery in real-time applications. The majority of available SoC estimation algorithms do not consider the noisy current input measurement. The development of a more realistic SoC estimation algorithm taking into account the impact of the noisy input current remains challenging.

The standard Kalman filter (KF) has been widely used in SoC estimation due to its simplicity and powerful estimation ability. The KF can only provide a good estimation when the input signal is noiseless (Ma et al. 2019). However, the input measurement

is also corrupted by a sensor noise in batteries. Therefore, the standard KF-based SoC estimation algorithms provide unreliable estimation results. Different dynamic loading profiles are used to assess the performance of the SoC estimation algorithms used in EVs. The dynamic stress test (DST) profile and hybrid pulse power characterisation (HPPC) profile are commonly used for this purpose Rui Xiong, J. Huang, et al. 2022a. These profiles along with constant discharge and sinusoidal discharge profiles are used to assess the performance of the algorithms proposed in this research.

In conclusion, the popularity of EVs is on an increasing trend. This increase brings some challenges to be addressed in the development of more reliable EVs. The SoC estimation is one of the most important tasks to be fulfilled by a BMS in EVs. Therefore, developing an SoC estimation algorithm is a popular research topic in the development of EVs. The SoC estimation methods have several steps including battery modelling, model parameter identification, and the SoC-OCV relationship calculation. Furthermore, there are error sources that reduce the accuracy of the SoC estimation. These error sources need to be mitigated to develop more realistic SoC estimation algorithms. In this research, we clarified the gaps in the available SoC estimation methods found in the literature and provided our novel methods to contribute to the literature.

1.2 Research questions

Rechargeable batteries are being more common as a primary power source in practical applications. This presents technical challenges to be addressed. One of the challenges is the robust real-time estimation of the SoC. Thus, this research answers the following points:

1. Real-time calculation of the battery model parameters and their impact on the SoC estimation accuracy, as well as the implementation steps of an online parameter identification technique.

2. Real-time construction of the SoC-OCV nonlinear relationship for ECM-based SoC estimation algorithms based on the battery boundary conditions (cut-off voltages) and current sensor measurement.

3. Mitigation of the SoC estimation error due to the corrupted current measurement by developing a more realistic current sensor measurement model and modifica-

tion of the standard KF based on the proposed current sensor model.

1.3 Aim and objectives

The objective of this research is to develop a real-time KF-based SoC estimation algorithm for rechargeable batteries based on an adaptive SoC-OCV model to environmental changes. Further, a new current measurement sensor model is to be derived and an engineering framework is proposed to mitigate the error source due to the corrupted current measurement in the SoC estimation problem. Finally, the results are compared to state-of-the-art SOC estimators in the literature.

1.4 Contributions and organisation of this thesis

This work is based on the optimal adaptive estimation theory and the objectives including the development of the methodologies for the real-time SoC estimation algorithm. Firstly, the adaptive law-based parameter estimation method is used to calculate the model parameters. Secondly, a novel method to construct the nonlinear SoC-OCV relationship in real-time is proposed and the SoC is estimated using the EKF. Finally, the effect of current measurement bias on the accuracy of the SoC estimation is investigated. A mitigation method is proposed to eliminate the error in the SoC estimation due to the current input measurement bias. Research gaps in the SoC estimation problem are addressed to provide a more realistic SoC estimation algorithm for real-time applications. The contributions are as follows:

1. Adaptive law based battery model parameter identification to guarantee the convergence of the parameter estimation
2. A novel real-time OCV-SoC nonlinear curve construction based on the boundary conditions and measurements
3. A novel method to correct the current input measurement by calculating the current input bias noise in real-time
4. Modification of the standard KF considering the white noise and the current measurement bias to increase the accuracy in the SoC estimation

The organisation of the thesis is as follows:

Chapter 2 covers the work has been done in the literature.

Chapter 3 introduces the battery model and the online parameter identification method based on the adaptive law.

Chapter 4 develops a new methodology for the SoC-OCV curve construction in real-time.

Chapter 5 introduces a mitigation method for the noisy current input measurement for batteries.

Chapter 6 shows the conclusion and the future work.

Chapter 2

Literature review

This chapter firstly introduces the review of the battery modelling techniques and the battery model parameter identification techniques found in the literature. Secondly, the state of the art of SoC estimation algorithms and the construction techniques for the nonlinear SoC-OCV relationship and its behaviour depending on the operational conditions and battery ageing are reviewed. Finally, the literature review on the impact of the noisy current input on the SoC estimation error is undertaken.

2.1 Battery modelling

Battery modelling is significant in predicting battery behaviour to ensure the safe and efficient operation of the battery. The model is used to estimate the battery states including the SoC, which is vital to avoid abnormal operations. Modelling the battery is the starting point to develop an efficient BMS. Numerous battery modelling techniques have been introduced in the literature with different complexities. These techniques can be useful in different application areas. According to the physical interpretation, Seaman et al. 2014 fundamentally separated the battery models into two groups: electrochemical models and ECMs.

2.1.1 Modelling strategies

A wide variety of battery models are adopted to interpret the battery dynamical behaviour in the BMS design of EVs. Complicated battery models are unsuitable to implement in real-time applications; besides very simple battery models cannot pre-

cisely replicate the battery's dynamic behaviour under different operational conditions. Hence, modelling the battery is of great importance without compromising model accuracy and ease of implementation. There are three sub-steps in battery modelling: battery model selection, model parameter identification, and model performance validation. The primary stage of battery modelling is the selection of the battery model. In this chapter, two fundamental battery models are introduced and discussed with their advantages and disadvantages.

2.1.2 Electrochemical modelling of a battery

Yonghuang Ye et al. 2012 summarised the discharge process of Lithium-ion (Li-ion) batteries as follows: electrons (e^-) move from the negative electrode (cathode) to the positive electrode (anode) via the external circuit. This consequently causes an electrical potential difference between the anode and the cathode. On the other hand, the Li-ions move from the anode to the cathode through the electrolyte. This is to make the sum of the negative electric charges on Li-ions equal to the sum of the positive electric charges on Li-ions. This process is reversed by applying an external source to the battery, which is called the charging process. The battery models built based on the theoretical aspect of this electrochemical process are called electrochemical battery models. There are two common types of electrochemical battery models: the P2D model and the SPM.

Pseudo two-dimensional model

Doyle et al. 1993 developed the original P2D electrochemical model. The evolution of Li-ions concentration in the two electrodes is shown in Figure 2.1 where Li_xC_6 is the lithiated carbon, $Li_{1-x}MO_2$ is the lithium metal oxide, Li^+ represents the Li-ions, c_{ss}^- and c_{ss}^+ are the concentration at particle surface in cathode and anode, respectively. c_s^- and c_s^+ are Li concentration in the cathode solid and the anode solid, respectively. c_e is the Li concentration in the electrolyte. L^- and L^+ are the thickness of the cathode and anode electrodes, respectively.

Electrochemical modelling describes the battery chemistry that relies on electrochemical reactions occurring in the electrodes and the electrolyte. These chemical reactions are depicted by using a set of coupled partial differential equations (PDEs). Doyle

et al. 1993 modelled the galvanostatic charge and discharge behaviour of a lithium anode/solid polymer separator/insertion cathode cell based on a concentrated solution theory. It is concluded that the model is generic enough to consider a large range of polymeric separator materials, composite insertion materials, and lithium salts. The solution of this model requires powerful computational tools and theoretical knowledge of computational fluid dynamics (Tamilselvi et al. 2021).

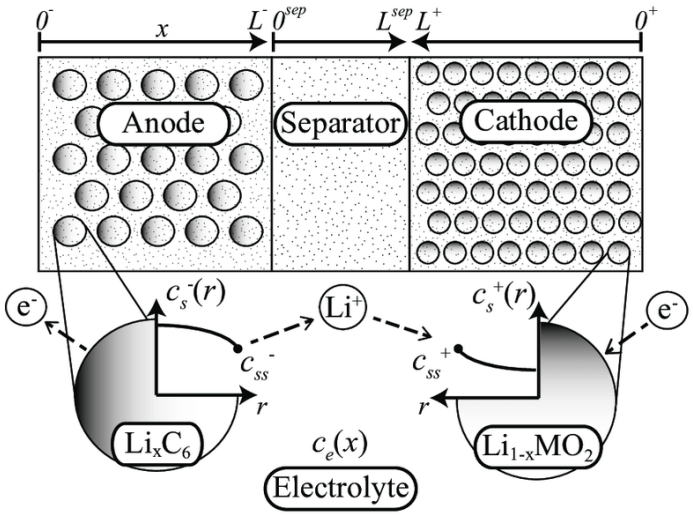

Figure 2.1: Electrochemical model by (Doyle et al. 1993)

Single particle model

Atlung et al. 1979 introduced the SPM as shown in Figure 2.2 where $V(t)$ is the voltage and $I(t)$ is the current. R_s^- and R_s^+ represent the particle radius in the cathode and anode, respectively. The SPM assumes that electrodes are formed by identical size spherical particles. Guo et al. 2011 highlighted the main simplification compared to the P2D model as follows: the SPM does not consider the electrolyte dynamics and thus assumes a constant reaction rate for each electrode. The SPM is relatively simple compared to the P2D battery model but it is also not common due to its availability for only low current densities (Guo et al. 2011).

To sum up, electrochemical models are very complicated battery models including several coupled PDEs. Therefore, their onsite applications are restricted. These two models are generally used for the optimisation of the battery design in laboratories (Corno et al. 2015).

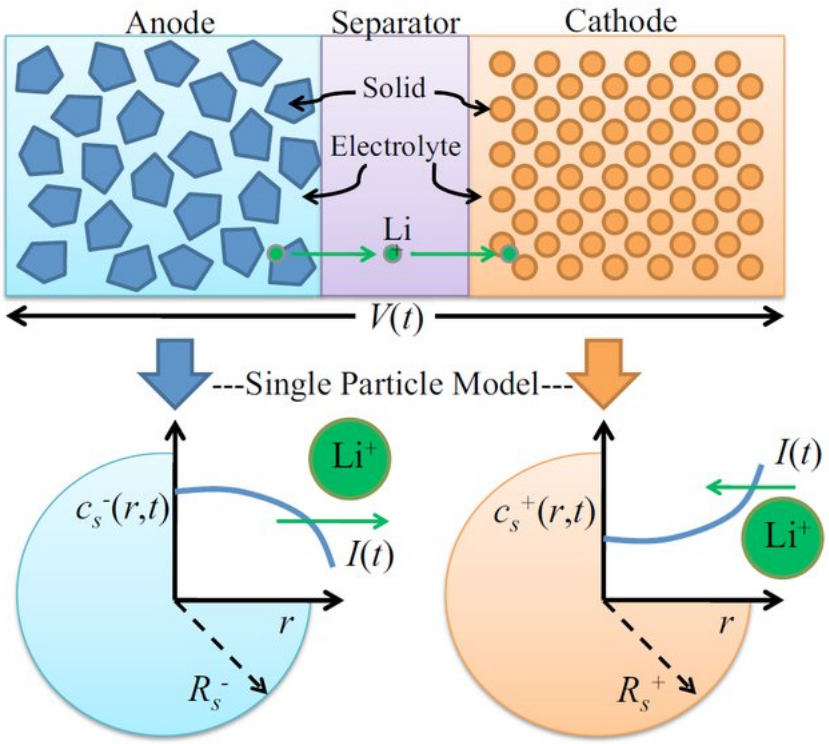

Figure 2.2: Single particle model by (Park et al. 2017)

2.1.3 Equivalent Circuit-based models

In contrast with electrochemical battery modelling, ECMs are widely employed in practice (Rui Xiong, J. Huang, et al. 2022b). These models use electrical circuit elements to reflect the charging and discharging behaviour of batteries. They remove the difficulty of understanding the details of the electrochemical reactions taking place inside a battery. In addition to that, it only requires fewer model parameters to be identified for the state estimation. Therefore, complicated mathematical and numerical calculations are avoided, which leads to a fast calculation of results.

ECM describes the battery's voltage-current characteristic that appears very simple. They also relate the battery's OCV to the SoC with a nonlinear relationship shown in Figure 2.3. Designing an accurate ECM provides a practical way to estimate the SoC with relatively less effort compared to the electrochemical model-based techniques. A generic ECM includes three major parts (Yann Liaw et al. 2004): a static part that represents the battery's thermodynamic properties such as the battery capacity and the OCV, a dynamic part that represents the battery's internal impedance behaviour, and a source or a load is the third part to complete the circuit for charging/discharging regimes. There is various kind of ECMs to be discussed with their advantages and

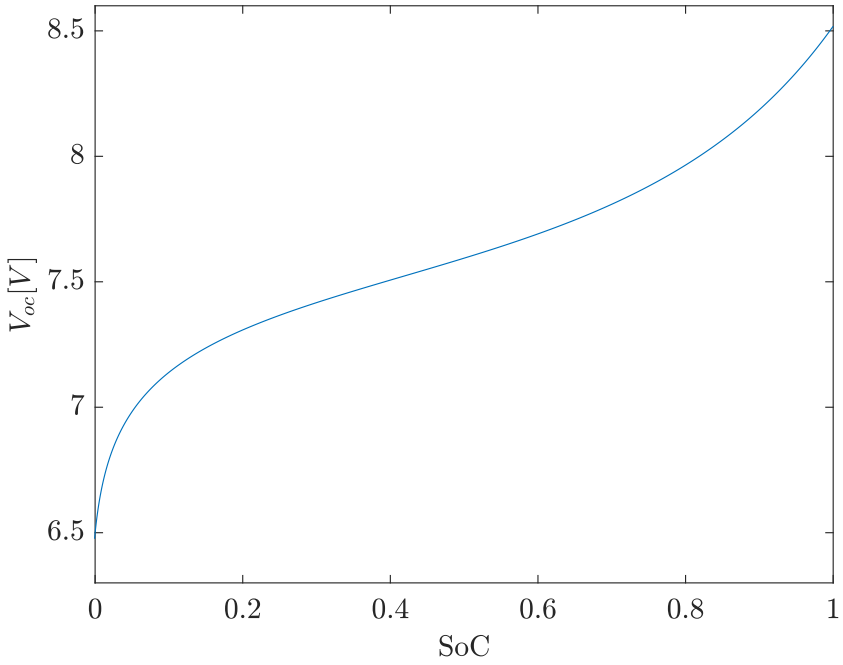

Figure 2.3: Typical relationship between the SoC and the OCV

disadvantages.

The battery model which is defined by the OCV is the simplest battery modelling found in the literature and it is given as follows (Tamilselvi et al. 2021):

$$V_t(t) = V_{oc} \tag{2.1}$$

where V_t is the terminal voltage and V_{oc} is the OCV, which is a function of the SoC. The SoC is 100% when the battery is fully charged and the SoC is 0% when the battery is fully discharged.

Rint battery model

Johnson 2002 described the Rint model as the internal resistance model shown in Figure 2.4. It has an ideal voltage source to describe the battery's OCV (V_{oc}). Additionally, it has an internal resistor (R_0) which is serially connected to V_{oc}. V_{oc} is assumed to be equal to the terminal voltage (V_t) in the equilibrium state when the battery is not loaded. I is the charge/discharge current.

The measurement equation of the Rint model is expressed as follows:

$$V_t(t) = V_{oc}(z) - I(t)R_0 \tag{2.2}$$

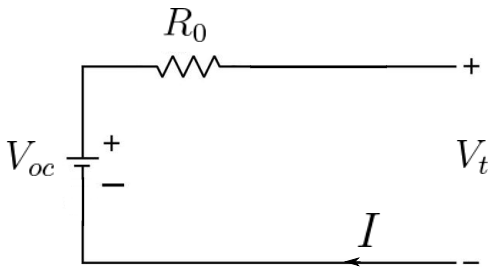

Figure 2.4: Rint battery model

where z represents the SoC.

$$z(t) = z(t_0) - \int_{t_0}^{t} \frac{I(t)dt}{Q_{max}} \tag{2.3}$$

where Q_{max} is the battery capacity. The Rint battery model is not an accurate battery model because the load transfer polarisation and diffusion polarisation are ignored. Therefore, it is not a preferred battery model for the SoC estimation problem.

Resistor-capacitor battery model

X. Zhang et al. 2016 described the RC battery model consisting of two capacitors (C_s, C_e) and three resistors (R_t, R_e, R_s) as shown in Figure 2.5. The capacitor C_s has a small capacitance compared to C_e. C_s represents the surface capacity of the battery, therefore it is also called a surface capacitor. The capacitor C_e is the bulk capacitor, which represents the electric-charge-storage capability of the battery. R_s, R_t, and R_e are the surface resistance, the terminal resistance, and the end resistance, respectively. The state-space representation of the RC battery model is as follows:

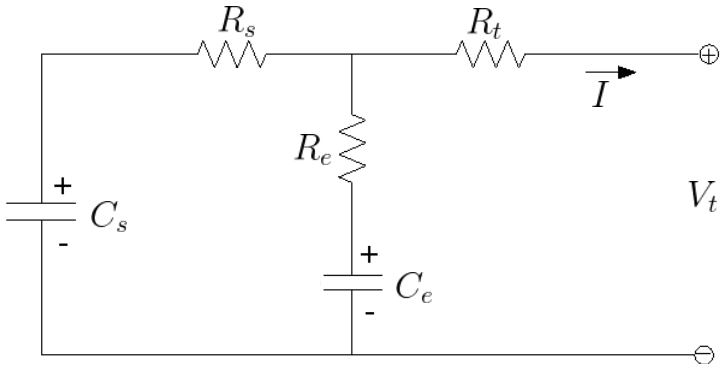

Figure 2.5: RC battery model (Hongwen et al. 2011)

$$\begin{bmatrix} \dot{V}_{c_e} \\ \dot{V}_{c_s} \end{bmatrix} = \begin{bmatrix} -\frac{1}{(R_s+R_e)C_e} & \frac{1}{(R_s+R_e)C_e} \\ \frac{1}{(R_s+R_e)C_s} & -\frac{1}{(R_s+R_e)C_s} \end{bmatrix} \begin{bmatrix} V_{c_e} \\ V_{c_s} \end{bmatrix} + \begin{bmatrix} \frac{R_s}{(R_s+R_e)C_e} \\ \frac{R_e}{(R_s+R_e)C_s} \end{bmatrix} I \tag{2.4}$$

and V_t is given by

$$V_t = \begin{bmatrix} \frac{R_s}{R_e+R_s} & \frac{R_e}{R_e+R_s} \end{bmatrix} \begin{bmatrix} V_{c_e} \\ V_{c_s} \end{bmatrix} + \left(\frac{R_e R_s}{R_e+R_s} + R_t \right) I \tag{2.5}$$

where V_{c_e} and V_{c_s} are the voltages across the capacitor C_e and C_s, respectively. I is the terminal current flowing between the battery terminals and V_t is the terminal voltage. In this model, V_{c_e} and V_{c_s} are the system states, I is the measured input and V_t is the measured output. This battery model is used to describe the dynamics of the lead acid battery by Loukil et al. 2017. Having five model parameters to be identified restricts its use in practice. Moreover, it does not have an ideal voltage source that remains its voltage output without depending on the current drawn from the battery. This makes building the relationship between the SoC and the OCV impossible. Therefore, it is not commonly used in practice.

Thevenin battery model

Ding et al. 2019 describe the Thevenin model. It connects the RC pair to the Rint model in series as shown in Figure 2.6. Compared to the Rint model, it takes into account the load transfer polarisation and diffusion polarisation. It consists of three parts; the OCV as a static part, the internal resistance and the RC pair as a dynamic part, and the load. R_0 is the internal resistance similar to the Rint model. R_p is commonly called the polarisation resistance which is the resistance between the plate and electrolyte. C_p is the equivalent capacitance of the electrode plate, which describes the transient response of the battery for charging and discharging processes. V_t is the terminal voltage. The Thevenin model dynamic characteristic is defined by the following equations:

$$V_t = V_{oc} - IR_0 - V_p \tag{2.6a}$$

$$\dot{V}_p = -\frac{V_p}{R_p C_p} + \frac{I}{C_p} \tag{2.6b}$$

Thevenin ECMs could have more than one RC branch. If the number of the RC pair is

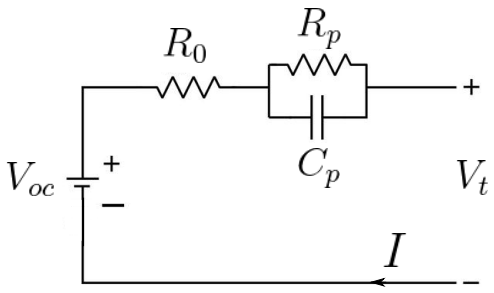

Figure 2.6: Thevenin battery model

n, the model is called nth order Thevenin model. Hong et al. 2022 performed a battery modelling validation test for the first order Thevenin ECM. The results indicated that the ECM achieved a 95% accuracy in representing the actual battery. In consequence of its comparable simplicity and capability to fulfil the basic requirements of batteries, it has been extensively adopted in BMSs in practice (Gholizadeh et al. 2014).

PNGV battery model

Xiangyong Liu et al. 2018 explained the PNGV battery model shown in Figure 2.7. It is achieved by adding a capacitor C_0 to the Thevenin model in series. The capacitor describes the change in the OCV generated in time due to the accumulation of the load current.

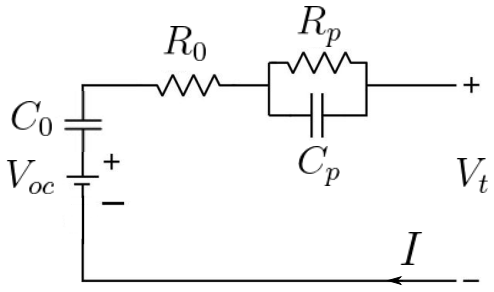

Figure 2.7: PNGV battery model

The integral change of the V_{oc} is described by using a large capacitance, which describes the relationship between the V_{oc} and the battery capacity.

$$\begin{bmatrix} \dot{V}_{c_0} \\ \dot{V}_{c_p} \end{bmatrix} = \begin{bmatrix} 0 & 0 \\ 0 & -\frac{1}{R_p C_p} \end{bmatrix} \begin{bmatrix} V_{c_0} \\ V_{c_p} \end{bmatrix} + \begin{bmatrix} \frac{1}{C_0} \\ \frac{1}{C_p} \end{bmatrix} I \tag{2.7a}$$

$$V_t = \begin{bmatrix} 1 & 1 \end{bmatrix} \begin{bmatrix} V_{c_0} \\ V_{c_p} \end{bmatrix} + R_0 I + V_{oc} \tag{2.7b}$$

The battery capacity degradation happens in a long term. Therefore, its simultaneous calculation with the battery states increases the computational cost. Thus, this battery model is not commonly used in the SoC estimation.

Compared to electrochemical battery models having several partially differential equations to mimic the battery dynamics, ECMs use relatively simple equations based on the circuit theory. Moreover, ECMs have fewer parameters to be calculated. Therefore, ECMs significantly reduce the computational cost in practical applications. Considering all the advantages and disadvantages of the aforementioned battery models, the first-order Thevenin model is a good candidate for battery modelling (J. Kim et al. 2012).

2.2 Battery estimation

The first step in the battery SoC estimation is to calculate the model parameters. The SoC is then estimated based on the calculated model parameters. Thus, this section first undertakes the literature review regarding the battery model parameter calculation. After that, different SoC estimation techniques are introduced with SoC-OCV curve construction techniques.

2.2.1 Parameter identification

Adopting a battery model requires the identification of the battery model parameters. These parameters must be identified before the execution of the SoC estimation algorithm. There are two main methods found in the literature for parameter identification. The first one is the offline method (Barsali et al. 2002). This method includes a battery experiment under a pulse input. The essential disadvantage of this method is that the calculated model parameters remain constant during the battery operation. However, these parameters vary with the operational conditions and battery ageing. Furthermore, identical batteries may have different model parameter values. For example, Barcellona et al. 2022 showed the different internal resistances for different temperatures, SoC levels and battery ageing in Figure 2.8, where R_s represents the internal resistance. The internal resistance decreases exponentially as the temperature increases. The battery's internal resistance is greater in higher SoC regions. It is also observed that the internal resistance increases as the battery ages. This is due to the

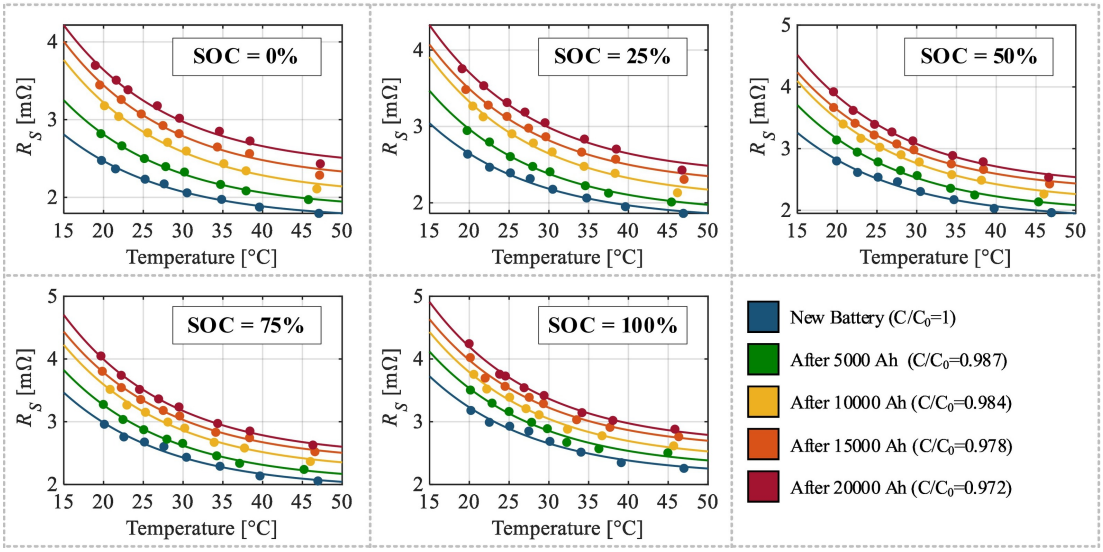

Figure 2.8: Ohmic resistance variations for different SoC levels, temperatures and battery ageing (Barcellona et al. 2022)

increase in the residual products of the electrochemical reactions taking place inside the battery. Thus, the battery model parameters need to be updated during the battery operation to capture these variations. The second method is the online method (Tran et al. 2017). In online parameter identification, the parameters are updated at each calculation step. Hence, variations in the model parameters are considered as the operational conditions change and the battery ages.

Reliable parameter identification methods play an important role in the accuracy of the SoC estimation. Different model identification algorithms are proposed in the literature. Xia et al. 2017 estimated the battery model parameters based on a forgetting factor recursive least squares (FFRLS), Yu et al. 2017 utilised H-infinity filter, Li et al. 2020 used the RLS algorithm, and Fang et al. 2021 proposed an adaptive genetic algorithm (AGA). Zhao et al. 2020 and Gao et al. 2017 estimated the first order Thevenin ECM parameters using the FFRLS algorithm. The voltage difference between V_t and V_{oc} is firstly written in the linear parametric model (LPM) form. Then the FFRLS algorithm is used to solve the voltage difference equation. Partovibakhsh et al. 2015 used the FFRLS method to estimate the parameters of the RC battery model. Adaikkappan et al. 2022 showed that the FFRLS method is used to estimate the model parameters of various types of battery models. Hicham Chaoui et al. 2015 adopted the adaptive strategy for the model parameter estimation.

In real-time applications, the FFRLS and the RLS algorithms are commonly used

in the parameter identification of the battery models. FFRLS method reduces the effect of the old data on the current estimate so that the bias due to the old data is significantly removed from the current estimates. In comparison with the RLS, the FFRLS improves the convergence speed. AGA is a popular method for the optimisation of the model parameters, yet it is not applicable in real-time due to its iterative process. The adaptive law guarantees the stability of the parameter convergence based on a Lyapunov direct method (Hicham Chaoui et al. 2015). Furthermore, measurement errors in the current input and voltage output cause identification biases. Zhu et al. 2020 showed that the RLS suffers from current and voltage measurement errors, which leads to a bias in calculated parameters. To reduce the identification bias, the recursive restricted total least squares method is introduced. In the model-based SoC estimation methods, model parameter identification methods draw great attention because the accuracy of the model parameters is the basis of the accurate SoC estimation.

Offline parameter identification

The offline method is based on laborious experimental work. These tests are usually performed under HPPC cycles (H. Zhang et al. 2014). Figure 2.9 shows the dynamic response of the first order Thevenin battery model to the HPPC discharge cycle. (D. Deng et al. 2021) presents the following procedure:

- To identify the battery's model parameters, the HPPC input cycle is applied to a battery. Once the pulse input is injected/removed to/from the system, the voltage jump/drop takes place due to R_0. In Figure 2.10, the battery's terminal voltage changes suddenly from V_1 to V_2 and V_3 to V_4. The internal resistance R_0 mainly causes these sudden voltage changes. Therefore, it can be calculated based on the average of the two voltage differences divided by the load current. The expression to calculate R_0 is given as follows:

$$R_0 = \frac{1}{2} \cdot \frac{(V_1 - V_2) + (V_4 - V_3)}{I} \tag{2.8}$$

- The relaxation periods of the battery can be seen in Figure 2.10, which take place between V_2-V_3 and V_4-V_5. These periods are a zero input stage of the voltage. In Figure 2.10, the terminal voltage drops slowly from V_2 to V_3. This is due to the

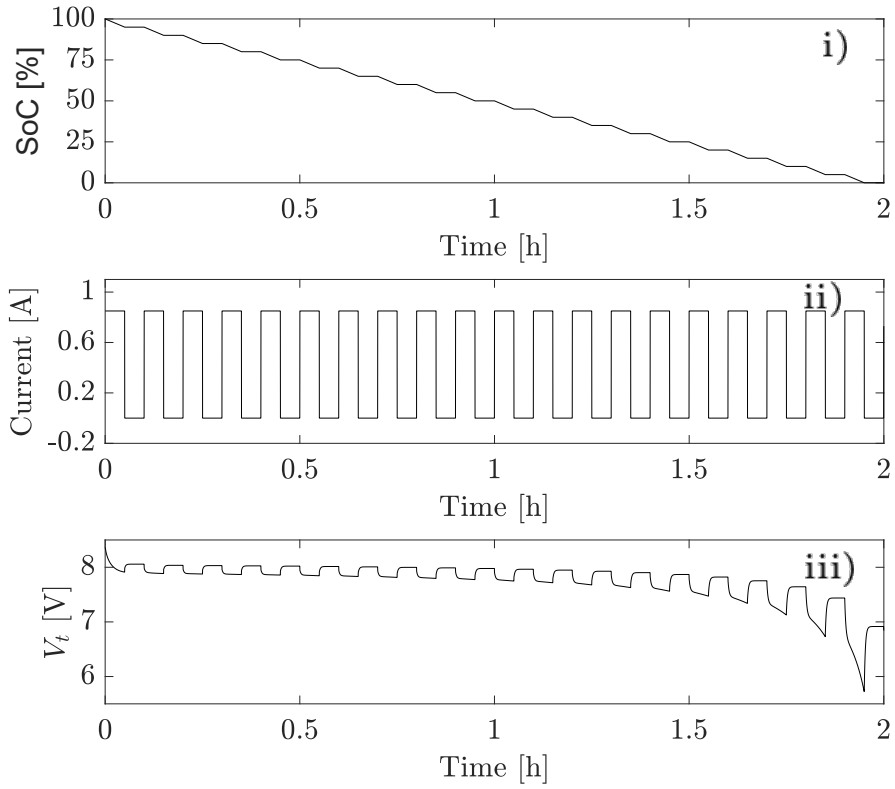

Figure 2.9: HPPC discharge test

polarisation dynamic of the RC branch. The expression to calculate R_p is given as follows:

$$V_t(t) = V_2 - IR_p\left(1 - e^{-\frac{t}{\tau}}\right) \tag{2.9}$$

where V_2 is the initial voltage when the relaxation period starts. The collected data is curve-fitted to the expression given in (2.9). Once R_p and the battery's time constant τ are calculated, C_p can be calculated by diving τ by R_p.

- Let the battery rest for some time until it reaches the equilibrium state. The measured battery voltage does not vary after the battery reaches the equilibrium state. In this state, the potential difference between the positive and negative poles of the battery can be considered to be the OCV. Therefore, V_1 in Figure 2.10 is assumed to be approximately equal to the battery OCV under the corresponding SOC value. The pair OCV and SoC data can be similarly collected for different SoC regions. The nonlinear relationship is then constructed by curve-fitting the appropriate model to the data.

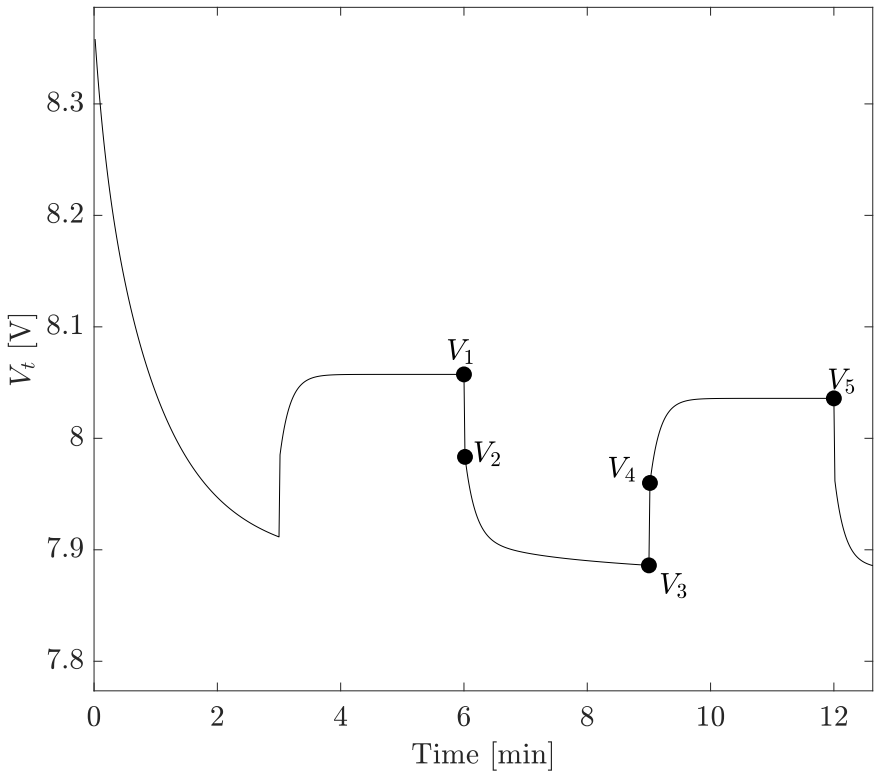

Figure 2.10: Magnified plot of Figure 2.9 iii)

Online parameter identification

Model parameter identification is a challenging task in the development of the real-time SoC estimation algorithm. The model parameters varying under different conditions have a significant effect on the SoC estimation. Thus, parameter estimation methods are widely investigated in the literature. One of the most common parameter identification methods is the RLS-based method. The performance of the RLS-based method is increased by employing the forgetting factor (Ciochina et al. 2009). Hence, the effect of the old data on the parameter estimation is reduced. An alternative to the RLS-based methods is the adaptive law-based parameter identification method. The adaptive law-based parameter estimator firstly expresses the unknown parameters in a parametric model. Secondly, the estimation model is built using the same parametric model. The estimation error is then calculated using the estimated output and the measured output. This error is used to derive the adaptive parameter estimator. Compared to the RLS methods, the adaptive law-based parameter estimation algorithm guarantees the convergence of the model parameters (Ioannou et al. 2006). Therefore, it is commonly used to in the model parameter estimation of the adaptive systems (Aburakhis et al. 2022), (Tao et al. 1995).

The first-order Thevenin model is commonly used in real-time SoC estimation algorithms. One of the reasons for its common use is that the online estimation of its model parameters requires a small amount of a priori information (W. Zhang et al. 2022). Xia et al. 2018, J. Wei et al. 2020, and Prashant et al. 2021 applied RLS to estimate the model parameters of Thevenin based battery model. To apply the RLS, the battery measurement equation must be converted into the LPM form given as follows:

$$y_k = \theta_k^T \phi_k \tag{2.10}$$

where y_k is the terminal voltage of the battery, θ_k is the parameter vector to be calculated and ϕ_k is the observation matrix. W.-Y. Kim et al. 2019 and Shu et al. 2020 converted the measurement equation into the LPM form and then employed the RLS method to estimate the 1^{st} order Thevenin ECM parameters. They used the one-step voltage difference equation to derive the LPM form. However, the performance of the RLS method decreases with an increase in the number of similar or repetitive data. Moreover, the effect of the old data needs to be reduced by using the forgetting factor.

The online parameter identification can be used as an indicator regarding battery ageing. For example, Topan et al. 2016 estimated the first order Thevenin ECM parameters using the RLS method. It is explained that the change in the battery's internal resistance can be used as an indicator of the battery's state of health. After many charging/discharging cycles, an increase in the internal resistance is a sign of battery ageing.

The performance of the parameter identification methods is not always satisfying. Therefore, there are different approaches to improve the performance of the parameter identification algorithms. For example, T. Ouyang et al. 2021 used the RLS method to calculate the model parameters of the first order Thevenin battery model. They highlighted the data saturation phenomenon in the RLS method. This phenomenon is briefly explained as follows: the capability of the RLS method to reduce the error in the parameter estimation decreases with an increase in the number of similar or irregular samples. This problem was mitigated by introducing a variable forgetting factor (VFF). This improved the performance of the RLS method by eliminating the

effect of the old data. Ping et al. 2018 also used the forgetting factor RLS method to improve the accuracy of the model parameter identification. The battery tests showed that increasing the accuracy in the calculated model parameters decreases the error in the SoC estimation. However, choosing the optimal forgetting factor is ambiguous.

The performance of the model parameter identification algorithms is attempted to increase by separating the linearity of the battery model and the nonlinear characteristic of the batteries. The model parameter estimation process is facilitated by combining the linear ECM and the static nonlinear output block by Naseri et al. 2022. They intro-

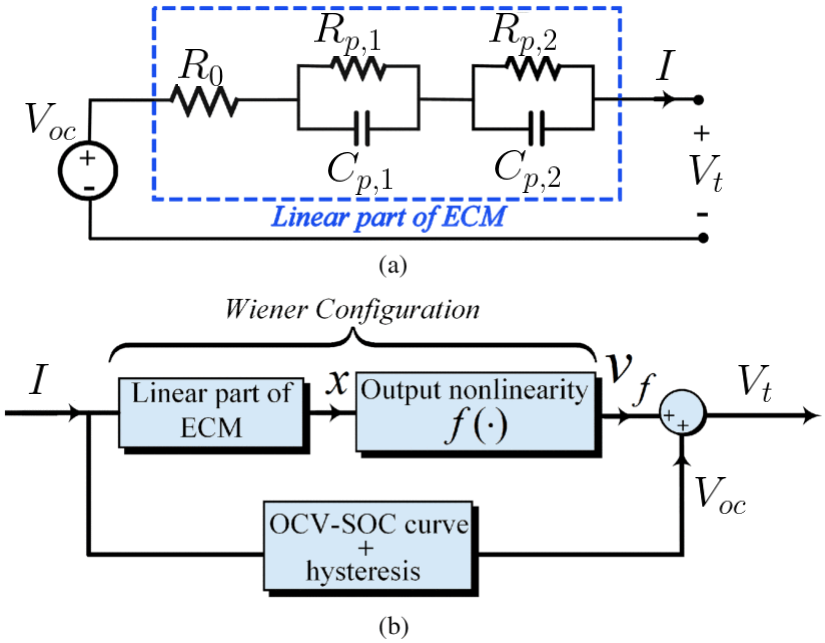

Figure 2.11: Wiener configuration by Naseri et al. 2022

duced a new battery modelling to better capture the nonlinearities of Li-ion batteries. The Wiener configuration shown in Figure 2.11 is utilised to enhance the nonlinear mapping capacity of the linear ECM. This contributes to the decomposition of the nonlinear input-output relationship into linear and nonlinear segments. The output signal V_t is expressed as follows:

$$V_t = f[x(k)] + V_{oc} \tag{2.11}$$

where $x(k)$ is the intermediate signal and $f[\cdot]$ is the nonlinear function in the Wiener configuration. The second order polynomial model is chosen for $f[\cdot]$, i.e., $v_f(k) = \gamma_1 x(k) + \gamma_2 x^2(k)$. After that, the regression model including both linear and nonlinear segments is derived and the extended kernel iterative recursive least-squares (EKIRLS)

algorithm is implemented to calculate the model parameters. The EKIRLS algorithm removes the estimation difficulty due to the unavailability of the intermediate signal $x(k)$. However, the ECM-based battery models are not highly nonlinear systems and the nonlinearity originates from the nonlinear mapping relationship between the SoC and OCV. In the literature, it is shown that the EKF-based SoC estimation algorithms can successfully tackle the nonlinearity without making any difference in the battery model.

The majority of the online parameter estimation algorithms calculate the model parameters based on the terminal voltage. Therefore, the more accurate prediction of the terminal voltage would increase the accuracy of the model parameter estimation. It is found that the fractional order battery models simulate the variations in the terminal voltage more precisely. The fractional-second-order Thevenin ECM for Li-ion batteries is established by Ling et al. 2021. The battery parameters are modelled as a constant that is disrupted by the state noise only because the model parameters vary slowly compared to the battery states. Fractional order EKF is used to calculate the model parameters. Hu et al. 2018 also used the fractional-second-order Thevenin ECM for Li-ion batteries. In various driving cycle tests, the voltage response of the model is predicted with a root-mean-squared error of less than 10 mV. The model parameters are identified by an AGA-based parameter estimation method. The accuracy of the estimated terminal voltage also suffers from the corrupted current measurement. Thus, considering the realistic current sensor model would significantly increase the accuracy of the estimated terminal voltage. This would lead to more accurate parameter estimation.

There are different battery modelling approaches to improve the model parameter accuracy. Pang et al. 2020 presented a new enhanced temperature-dependent equivalent circuit model (eTECM). An integrated RC branch is structured by combining a series RC branch and a parallel RC branch. The static hysteresis and temperature compensation voltages are introduced to establish eTECM. The forgetting factor least square (FFLS) method is used to calculate the model parameters to overcome a large accumulated error due to a big amount of test data. Modelling the RC branch considering the impact of ambient temperature on the dynamics of the LIBs increased the model parameter estimation accuracy in the battery experiments conducted under different

temperatures. Online parameter estimation algorithms adopt the model parameters to operational conditions automatically and adding temperature modelling is not necessary. Hence, adding the temperature modelling needs to be decided according to the trade-off between the computational cost and the improvement in the parameter estimation accuracy.

Meng et al. 2019 proposed a dynamic linear battery model which enables the use of standard KF for SoC estimation and removes the need of using online parameter estimation methods. The relationship between the voltage and current is assumed piecewise linear for a sufficiently short time period so that the battery model can be linearised. This makes the model parameters automatically updated and reduces the order of the state-space function to one. The linear piecewise battery model is established based on a partial least squares (PLS) and the moving window method whose window width is denoted as M. The PLS battery model is given as follows:

$$V_t = B^{PLS} X^{PLS} = b_1 + b_2 \cdot z + b_3 \cdot I \tag{2.12}$$

where $B^{PLS} = [b_1\ b_2\ b_3]$ is the coefficient matrix and $X^{PLS} = [1\ z\ I]^T$. The first PLS model is calculated based on M samples collected in advance. The next PLS model is calculated based on samples collected according to the estimation results during the previous moving window. Once the collection of M samples is completed, the PLS model is updated. Therefore, the moving window method allows the battery model to be updated with a small number of samples.

Another approach to estimating the model parameters is to augment the state vector by adding model parameters. Therefore, the model parameters and the battery's actual states are estimated simultaneously. W. Zhang et al. 2022 added the ECM parameters into the state vector along with the battery's actual states. However, the adaptive battery state estimation (ABSE) method does not consider the effect of the load current in the parameter's control equations. Consequently, the ABSE may provide erroneous parameter estimates when the load current is high. W. Zhang et al. 2022 proposed an improved version of ABSE to estimate the model parameters simultaneously with the battery states. They defined R_{sum} as a sum of resistors in the

ECM. The relation between R_{sum} and the measured signals are given as follows:

$$R_{sum} = \frac{V_t - V_{oc}}{I} \tag{2.13}$$

R_{sum} is used as a feedback element to reduce the error in the parameter estimations regarding the ECM modelling error. It is concluded that the improved ABSE identifies the ECM parameters more precisely thanks to the control equation of the improved ABSE. Increasing the number of elements in the state vector increases the computational cost. Thus, the model parameters and the battery states must be calculated separately.

Finally, different parameter estimation algorithms are used to compare the parameter estimation accuracy. For example, Jarrraya et al. 2022 compared the hybrid Nelder-Mead particle swarm optimization (PSO-NM) and open circuit voltage-recursive least square (OCV-RLS) for the battery parameters estimation. The PSO-NM technique requires a long period, i.e., around 2 hours, to calculate the model parameter accurately under dynamic working conditions. On the other hand, the OCV-RLS technique can momentarily provide fast and robust parameter estimation. Both methods show excellent performance in battery experiments by predicting the battery model parameters with less 2% error. In conclusion, these two techniques can be used to identify the model parameters on different current ranges and at different temperatures. C. Huang et al. 2018 investigated the robustness analysis of the EKF and UKF for SoC estimation under unknown initial SoC, current noise, and various temperature conditions. A new model parameter estimation algorithm called multi-swarm particle swarm optimization (MPSO) is proposed to estimate the model parameters of the first-order Thevenin ECM. ΔV_t is defined as the difference between two consecutive V_t, which is eventually expressed as the LPM. The model parameters R_0, R_p, and C_p are formulated as an optimisation problem by minimizing the mean squared error between the measured ΔV_t and calculated $\Delta \hat{V}_t$. $\Delta \hat{V}_t$ is calculated based on $\hat{R}_0$, $\hat{R}_p$, and $\hat{C}_p$ previously calculated using the RLS method. The results show that the MPSO-based method can accurately estimate the battery model parameters.

2.2.2 State of charge estimation

The load current and the terminal voltage are the measurable signals in BMSs. However, the SoC is not a measurable signal. A reliable BMS must accurately estimate the SoC using these measurements. The definition of the SoC is the ratio of the remaining capacity to the maximum capacity (Plett 2004a). The SoC estimation is a challenging task since different error sources may contribute to the error in the SoC estimation. For example, the current input sensor measurement has a great influence on the SoC estimation accuracy and imprecise current sensor measurements cause false SoC estimation. Another error source might be inaccurate model parameters and the SoC-OCV characteristic if the SoC estimation algorithm is model based. The operational conditions including ambient temperature have an impact on the model parameters and the SoC-OCV characteristic. Therefore, SoC estimation algorithms must be adaptive to the changes in the operational conditions.

In EV applications, a reliable SoC estimation prevents unwanted incidents including running out of available energy due to the wrong estimation, and the explosion of the batteries due to overcharging. An accurate SoC estimation provides the driver with the optimal use of the battery pack in EVs. Thus, there is a wide variety of SoC estimation algorithms grouped into two main groups: model-free methods and model-based methods. Model-free methods include the OCV method (Piller et al. 2001) and the Coulomb counting (CC) method (Ng et al. 2009), (Z. Deng et al. 2016). Model-based methods include the KF, the extended Kalman filter (EKF), the uncented Kalman filter (UKF), the fading Kalman filter (FKF), the cubature Kalman filter (CKF), the particle filter (PF), the H-infinity observer algorithms (L. He et al. 2022), (Ren et al. 2022), (Ali et al. 2022), (Adaikkappan et al. 2022), (Bian et al. 2020), (Zou et al. 2014), and artificial neural network (ANN) methods (M. A. Hannan et al. 2020).

Model-free methods:

Coulomb counting method

The CC method measures the battery's charging/discharging current and integrates it over time to estimate the SoC (Ng et al. 2009). The main advantage of the CC method is that it can be easily applied to any type of battery (J. Zhang et al. 2010). However, it is not only sensitive to the unknown initial SoC value but also accumu-

lates errors from the current measurement sensor over time because of the integration process (Wadi et al. 2019). The CC technique can be used to calculate an acceptable SoC estimation when additional information is added, such as current sensor fault, charge/discharge efficiency, and capacity degradation due to battery ageing. Nevertheless, regular calibration must be performed by conducting completely charged and discharged scenarios, which limits its use in practice. Ng et al. 2009 proposed an enhanced CC method. Their method eliminates the effect of charge losses and takes charging/discharging efficiency into account. In the proposed method, maximum available capacity is also calculated by a state of health estimation technique. In order to remove the initial guess error, the initial SoC is calculated based on V_t calculated through a constant current constant voltage curve.

Open circuit voltage measurement method

In this method, the SoC is estimated based on the battery OCV since there is a one-to-one nonlinear relationship between SOC and OCV. The V_t is measured after the battery reaches the equilibrium state where the battery's OCV is assumed to equal to V_t. The OCV measurement method provides accurate SoC estimations but it requires a look-up table for the SoC-OCV relationship (Farmann et al. 2015). Once the OCV is measured, the corresponding SoC can be easily found from the look-up table. However, accurate measurement of the OCV requires a long relaxation time in the range of hours and this is not suitable for online applications (J.-N. Shen et al. 2019). Furthermore, the SoC-OCV relationship is assumed not to vary depending on the various temperatures and different C-rates (the unit to measure the charging/discharging speed of the battery), which is not realistic in practical applications.

Model-based methods:

The generic flowchart of the model-based SoC estimation methods is shown in Figure 2.12. The standard KF has been developed for linear systems. When the dynamic system is nonlinear, an additional linearisation of the system is required to implement KF. This KF version is called the EKF and Zhi et al. 2017 developed an SoC estimation algorithm based on the EKF. However, if the system's nonlinearity increases, the linearisation approximation fails, which causes the failure of the EKF. In case of high non-linearity, the UKF may be an alternative to the EKF by eliminating the lin-

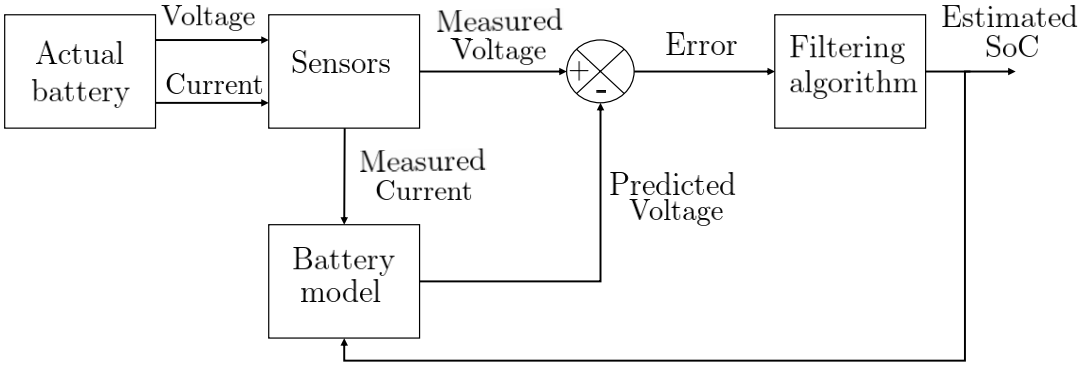

Figure 2.12: Flowchart of the model-based state of charge estimation method

earisation problem (Wan et al. 2001). However, the selection of the sigma points may deteriorate the performance of the UKF (S. Liu et al. 2020). KF family algorithms assume the measurement and system noises to be Gaussian noise. In case these noises are non-Gaussian, the PF can be implemented for the SoC estimation (Tulsyan et al. 2016). If the goal is the reduce the modelling error, adopting an H-infinity filter could be another solution (Z. Chen et al. 2021). The ANN methods are also used in SoC estimation. Piao et al. 2010 developed a real-time SoC estimation method based on ANN, which is validated by simulations and battery experiments. ANNs are mathematical models that can learn and recognise patterns similar to human brains. In brief, these models manage to map the input to output based on interconnected neurons with different weights. In SoC estimation based on the ANN method, the input data include the load current, the terminal voltage, and the temperature. The output signal is the SoC. ANN based SoC estimation algorithms are applicable to any battery chemistry but it necessitates specific data set to train the battery model.

Considering all these advantages and disadvantages, Figure 2.13 shows that the KF family algorithms are the most favored SoC estimation method based on the literature results according to the Institute of Electrical and Electronics Engineers (IEEE) Data given by Shrivastava et al. 2019.

The performance of the KF in SoC estimation is extensively investigated and different approaches are proposed to upgrade it. To improve the performance of the SoC estimation accuracy, the combination of two different SoC estimation methods is used. D. Liu et al. 2019 combined the deep belief network with the KF algorithm. T. Wu et al. 2011 combined the CC method with the EKF algorithm. However, combining

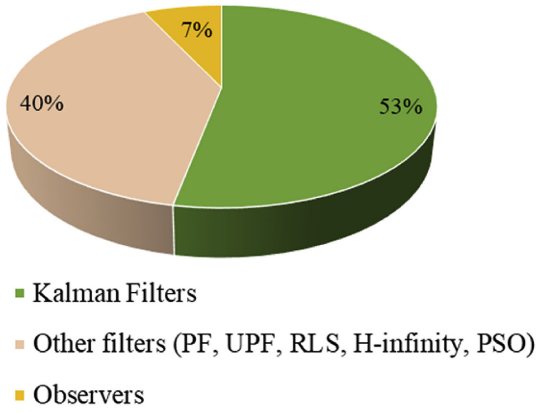

Figure 2.13: The percentage of commonly used SoC estimation algorithms by (Shrivastava et al. 2019)

two algorithms would increase the computational time and cost. Çelikten et al. 2022 introduced a hybrid SoC estimation method combining the CC method and sigma point Kalman Filter (SPKF) method. However, both methods do not run simultaneously. Therefore, the hybrid method reduces the execution time and complexity. The SoC and the output voltage (V_t) estimations start using the SPKF. The estimated V_t is compared to the measured V_t. Root mean squared error (RMSE) in V_t is calculated with a sliding window. In detail, the RMSE is calculated for each data for 60 s which is called the window length. If the RMSE is less than 5 mV, the CC method is used to calculate the SoC. For the next 60 s, the RMSE is calculated based on the estimate from the CC method. If it is greater than 20 mV, the SoC estimation becomes inaccurate and the SoC method is switched to the SPKF method. The inaccuracy in the SoC estimation using the CC method is expected due to its open-loop structure. The SPKF is more reliable and used to readjust the accuracy in the SoC estimation because of its closed-loop structure.

Yuanmao Ye et al. 2022 proposed a new online model-based SoC estimation technique for Lithium-ion batteries. The second order ECM based battery modelling is used due to the high compatibility and low complexity. The SoC-OCV relationship is obtained offline by a battery test. The collected data is then curve-fitted to the 6^{th} order polynomial function. The extended stochastic gradient (ESG) method is adopted for the parameter estimation based on a gradient search (Xiao et al. 2010). ESG method propagates the parameter vector by the following equation:

$$\hat{\theta}_k = \hat{\theta}_{k-1} + \frac{e_k}{r_k}\phi_k \tag{2.14}$$

where θ_k is the unknown parameter vector, ϕ_k is the measured input vector, e_k is the innovation and r_k is the gradient coefficient expressed as follows: $r_k = r_{k-1} + ||\phi_k||^2$ where the initial $r_0 = 1$ and $||\phi_k||$ is the norm of ϕ_k. The measurement equation is written as follows: $V_{t,k} = V_{oc,k} - \phi_k^T \theta_k$. This measurement equation is then used in the SoC estimation algorithm. The model parameters are firstly calculated using the ESG method based on the initial values. Once the model parameters are calculated, the parameter matrices are constructed to prepare the state estimation. The adaptive EKF is then utilised to estimate battery states based on the online estimated model parameters. The parameter estimation and state estimation algorithms are combined into one closed-loop algorithm. The root mean squared error (RMSE) in the SoC estimation under the dynamic stress test cycle is 1.96%. This work did not fully consider the model parameters including the SoC-OCV nonlinear model parameters. Therefore, it is not a fully online SoC estimation algorithm and it cannot be used in practical cases.

Another approach to improving the performance of the KF algorithms is filter modification. The KF algorithms are modified to eliminate their disadvantages and improve their performance in the SoC estimation. For example, L. He et al. 2022 introduced a central difference Kalman Filter (CDKF) for the SoC estimation. The first and second derivatives in Taylor expansion are replaced by the central difference transformation (CDT). The CDT is defined as follows:

$$f(x) = f(\bar{x}) + \bar{D}_{\Delta x} f + \frac{1}{2!} \bar{D}_{\Delta x}^2 f \tag{2.15}$$

where

$$\bar{D}_{\Delta x} f = \Delta x \frac{f(\bar{x} + h) - f(\bar{x} - h)}{2h} \tag{2.16}$$

and

$$\bar{D}_{\Delta x}^2 f = \Delta x^2 \frac{f(\bar{x} + h) + f(\bar{x} - h) - 2f(\bar{x})}{h^2} \tag{2.17}$$

where x is the state, $\bar{x}$ is the mean of the state, f is the nonlinear function, $\Delta x = x - \bar{x}$ and h is the half of the length from the central difference that implies the sigma points' distribution around the mean. The maximum SoC estimation error is around 2%. The existing EKF-based SoC estimation error has similar estimation performance so the proposed transformation technique does not increase the accuracy

of the SoC estimation. However, the complicated derivations are avoided, which is one of the disadvantages of the EKF. This modification allows the use of more complicated nonlinear models for the SoC estimation based on the EKF.

Finally, the system uncertainties due to the battery model and sensor measurements vary according to the operational conditions. Therefore, predetermined fixed noise parameters deteriorate the KF performance in SoC estimation. Z. He et al. 2020 proposed a new adaptive EKF for the SoC estimation that can track the system noise, making it adapted to priori error covariance. The new method is based on the feature of slowly changing Lithium-ion battery system parameters during the battery operation. Therefore, it is proved that the priori state error covariance $P_{k|k-1}$ is convergent. Note that $P_{k|k-1}$ is defined as follows:

$$P_{k|k-1} = \mathrm{E}[(x_k - \hat{x}_{k|k-1})(x_k - \hat{x}_{k|k-1})^T] \tag{2.18}$$

where E is the expectation operator, $x(k)$ is the true state, $\hat{x}_{k|k-1}$ is the priori estimated state. Assuming $P_{k|k-1}$ as a constant is unrealistic in practice, which may deteriorate the filtering effect and lead to filtering divergence. However, the assumption is asymptotically efficient and used to estimate $P_{k|k-1}$ based on a maximum likelihood method and the innovation data set gathered from the initial time step to $k-1$.

In BMS, the estimated OCV can be transformed into the SoC through lookup tables. An alternative approach is to shift between linear models, each linearly fitted to the corresponding region of the SoC-OCV relationship. Haus et al. 2020 proposed a model-adaptive EKF, which uses a single fit with state-dependent coefficients but a higher-order polynomial equation for the SoC-OCV relationship. This relaxes the Taylor-based linearisation tool in EKF. The higher-order polynomial fit has 3 coefficients to be estimated. The coefficients of the polynomial equation are considered as states and estimated by the KF. It is concluded that the SoC estimation is stable and proved by the experimental results. Analysing the work of Haus et al. 2020 from a critical perspective, the SoC-OCV relationship is modelled with a 11^{th} degree polynomial equation. This would increase the sensitivity of the model to small changes in the states and would deteriorate the robustness of the algorithm.

In the majority of the SoC estimation problems, the model parameters are commonly

assumed to slowly vary over time, i.e., $\theta_{k+1} \approx \theta_k$, where θ is the model parameters vector. The model parameter vector can be implemented into the state vector, and it is jointly estimated with the battery states, i.e., $x = [z\ V_p\ \theta]^T$. Beelen et al. 2021 collectively estimated the battery model parameters and SoC using EKF based on a single-parameter tuning approach. It is found that the dynamic system becomes unobservable or poorly observable when both the system input and the polarisation voltage (V_p) become 0. Therefore, the robust-observer approaches cannot be used for the joint estimation of the SoC and model parameters. This may prevent the SoC estimate from converging. The joint EKF can be used as an alternative way on the condition that EKF must consider cross-correlated noise and have a forgetting factor to ensure that the state and model parameter is estimated based on recent data. The forgetting factor is added to the KF steps. The tuning procedure of the forgetting factor is as follows (Beelen et al. 2021): the algorithm execution starts with the forgetting factor of 1, which implies "no forgetting". Then, the forgetting factor is gradually decreased until the algorithm reaches satisfactory performance in terms of the state estimation error. The proposed method is validated using the battery experimental drive cycles. When the system input and the polarisation voltage are zero, the battery is in the steady-state resting. Therefore, the estimation of the battery SoC can be directly calculated from the terminal voltage measurement.

Different filtering algorithms are utilised in SoC estimation. W. Xu et al. 2019 proposed a multi-timescale SoC and state of energy estimator based on an H-infinity filter that is a developed form of KF. It is very effective to restrict the unknown input disturbances on the system output. The main goal of H-infinity filtering is to find the linear combinations of the states. The following standard linear discrete system is used:

$$\begin{aligned} x_{k+1} &= A_k x_k + w_k \\ y_k &= C_k x_k + v_k \\ \psi_k &= L_k x_k \end{aligned} \tag{2.19}$$

where x_k, y_k, A_k and C_k are the state vector, output vector, and nonlinear system functions, respectively. w_k and v_k are the noises. ψ_k is a linear combination of states and L_k is the matrix chosen by the user. The battery states are calculated at micro-timescale whereas the slowly-varying model parameters are calculated at macro-timescale. This

reduces the computational cost in BMS applications. The accuracy and stability are dependent on the coefficient matrices which are dependent on the timescale (L_{ts}) of the parameter identification. It is found that a small L_{ts} reduces the parameter estimation error by increasing the frequency of the parameter update. Although this is reported in a positive context, the increases in computational cost are overlooked. More specifically, the optimal value of L_{ts} must be calculated according to the trade-off between the computational cost and the estimation accuracy. Moreover, using the H-infinity filtering, the predicted terminal voltage is found very close to the measured terminal voltage by the battery experiment. Therefore, the model parameters and the states are calculated with high accuracy. The SoC estimation error is within 1.5% under dynamic loading profiles.

J.-N. Shen et al. 2019 introduced a joint moving horizon estimation (MHE) approach to simultaneously estimate the model parameters and the battery states. The battery is modelled as the first order Thevenin ECM. The model parameters are modelled as a polynomial function of SoC. According to the sensitivity analysis of the polynomial coefficients, it is concluded that slight changes in the high-order polynomial coefficients cause drastic variations in the model parameters, which may lead to an unstable V_t estimation. Additionally, the model parameters are of the same order of magnitude as the constant terms in the polynomial functions. Thus, if these constant terms are updated in real-time, it would be accurate enough to update the model parameters in real-time. The state vector is augmented by adding the constant coefficients of the model parameters. However, the battery model parameters are slowly changing with time. They can be modelled as a constant parameter to reduce computational complexity. Moreover, treating the parameters as a state increases the computational cost. It is less costly to calculate model parameters before the execution of the SoC estimation algorithm. This approach provides an update for the circuit parameters that may vary due to the operational conditions and battery ageing. The optimal state estimation is transformed into the maximisation of the conditional probability density function through the Bayesian rule, which is an optimisation problem. The MHE is used to solve the optimisation problem to prevent the increase in the computational cost with the sampling time. The horizon length (L_h) is introduced and the time interval is separated into two parts, i.e., $[0, \ldots, t_{T-L_h}]$ and $[t_{T-L_h+1}, \ldots, t_T]$ where t_T

is the sampling time. The optimisation problem is solved according to this separation of the sampling interval.

In practice, the system states may not be normally distributed due to the hysteresis phenomenon. The complicated OCV characteristic may cause a nonlinear and non-Gaussian error distribution of the states. This may restrict the use of the methods derived based on the Gaussian distribution assumption of the states. Dong et al. 2019 proposed a novel method to estimate the SoC and the model parameters based on a sequential Monte Carlo filter (SMCF) and an auto-regressive exogenous model (ARXM). The SMCF calculates the system states based on a set of random samples with associated weights. In ARXM, the past input and output data are used to build a linear model to be used in the current time (Jiang et al. 2020). However, each battery has unique model parameters and the SoC-OCV relationship. Calculating these parameters and the relationship according to the previously collected data for a specific battery restricts the use of this method for different batteries. The battery model adopts a nonlinear voltage source to mimic the OCV characteristic. The ARXM is utilised to mimic the battery's transient response. It is concluded that the proposed algorithm can estimate the states under non-Gaussian noises. Ren et al. 2022 proposed a forgetting factor dual particle filter (FFDPF) algorithm for the SoC estimation. The performance of the PF-based SoC estimation algorithm depends on the accuracy of the parameter identification. In order to prevent the data saturation leading to large errors in model parameters, a forgetting factor recursive least square method is introduced. The performance of the FFDPF is compared to the EKF, UKF, and PF algorithms. In all simulations, the FFDPF algorithm showed superiority in terms of SoC estimation accuracy.

Rahimifard et al. 2021 modelled the Li-ion battery by utilising the third-order Thevenin ECM. It is highlighted that the internal resistance R_0 indicates the ageing and power capability. Thus, R_0 is the only model parameter taken into account as one of the state elements to be estimated. The CC method is combined with a model-based technique to eliminate the error sources in the CC method. The calculated SoC using the CC method is treated as a measurement reflecting the current sensor measurement. The

SoC bias is assumed to be a slowly-varying state and it is expressed as follows:

$$e^b_{k+1} = e^b_k + w_{e^b_k} \tag{2.20}$$

where $w_{e^b_k}$ is a white noise. Therefore, the SoC measurement includes this bias as follows:

$$SoC_{m,k} = SoC_k + e^b_k \tag{2.21}$$

The generic state space form is then defined with the following state vector and measurement signals: $x_k = [V_{1,k}\ V_{2,k}\ V_{3,k}\ SoC_k\ R_{0,k}\ e^b_k]^T$ and $y_k = [V_{t,k}\ SoC_{m,k}]^T$. However, the other parameters including R_p and C_p are equally important because the measurement equation is the summation of terms calculated based on these parameters. Therefore, only estimating R_0 reduces the accuracy of the SoC estimation.

Eddahech et al. 2012 estimated the SoC of the Lithium-polymer cell using an ANN based method. In their work, an ANN was used to consider the previous input signals along with the current ones to calculate the SoC estimate, which is called a recurrent ANN. The SoC-OCV characteristic is dependent on the battery chemistry, operational conditions, and battery ageing. Considering these factors in the model training, an SoC estimation method based on an ANN is proposed by Grewal et al. 2001. A three layered ANNs is utilised to map the input data to the output signal. The ANNs are trained using the back propagation algorithm by optimising the number of neurons to estimate the SoC accurately. However, the back propagation algorithm may have a local minima problem. To prevent this, Bo et al. 2008 trained the ANN based on an evolutionary algorithm. Five different input data including the load current, the battery terminal voltage, the battery terminal voltage first derivative, the battery terminal voltage second derivative, and the temperature are used.

There are several standard drive cycles to assess the performance of the SoC estimation algorithms in EV applications. DST and HPPC cycles are widely used in the performance assessment of the SoC algorithms (Hongwen et al. 2012). Hongwen et al. 2011 estimated the SoC using an ECM-based EKF. Additional RC brach is adopted to increase modelling accuracy representing the concentration polarisation and the electrochemical polarisation. The model parameters are calculated using a genetic algorithm. DST and the federal urban driving schedules (FUDS) are used to evaluate the

performance of the proposed technique. Xiaosong et al. 2012 presented a comparison study of twelve ECMs for Li-ion batteries. The performance of each ECM is evaluated using an HPPC test.

The SoC-OCV relationship

The majority of the model-based SoC estimation algorithms firstly calculate the OCV. When the OCV estimate is available, the estimated OCV is converted to the SoC estimate. The nonlinear relationship between the SoC and the OCV is required for this conversion. The nonlinear SoC-OCV relationship can be calculated by either battery experiments or real-time estimation methods. However, using an experimentally calculated SoC-OCV relationship reduces the accuracy of the SoC estimation due to its fixed property. This relationship varies depending on the ambient temperature, battery ageing, and the current rate. To capture these variations in the relationship, the SoC-OCV relationship must be either updated or constructed in real-time.

C. Chen et al. 2022 investigated the SoC-OCV characteristic of different batteries considering different battery ageing, current rates, and temperatures. The results are shown in Figure 2.14. It is observed that the shape of the curve does not significantly change due to the battery ageing. The relationship is very similar between the SoC of 98% and the SoC of 8%. The maximum OCV difference at the same SoC value is less than 2.3mV. The maximum OCV difference in the same SoC range is 2.9 mV for the different current rates whereas it increases to 7.6 mV due to the ambient temperature. The greatest difference in the OCV is observed among different batteries. When a different battery is used, the maximum OCV difference in the same SoC range increases to 10 mV. It is concluded that the SoC-OCV characteristic can be used as an indicator of battery health. It is recommended that the effect of the current rate, the ambient temperature, and the inconsistency among different batteries should be considered in the SoC estimation.

Yuan et al. 2022 investigated the effect of the current rate on the SoC-OCV relationship conducting a battery experiment. In Figure 2.15, OCV1 indicates the OCV when the battery is charged with 0.5A and 1A whereas OCV2 is the OCV under 2A of constant charging current. Finally, OCV3 shows the OCV under 2A of constant discharging current. It is observed that the battery OCV changes fast in low SoC regions whereas

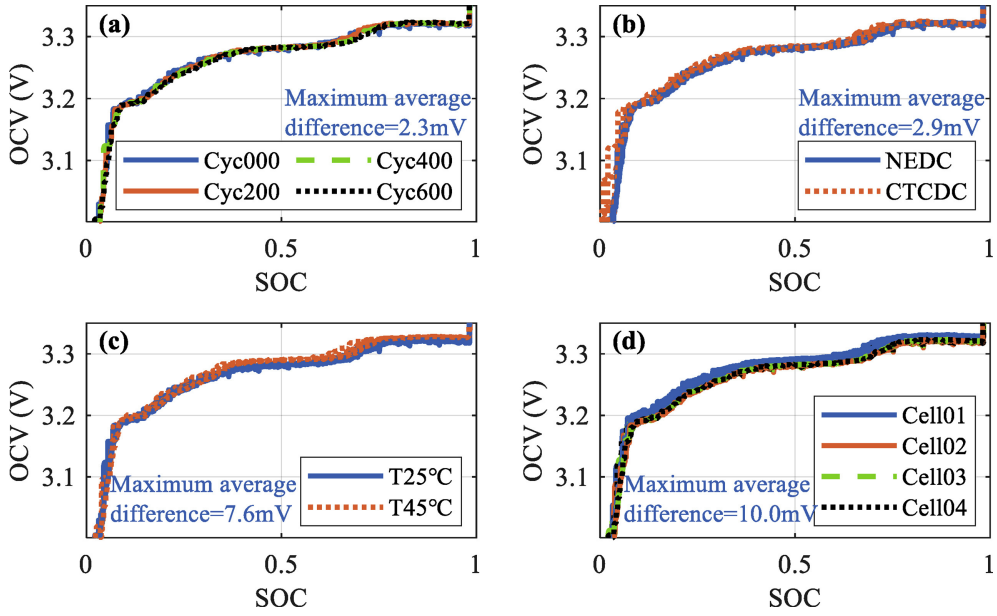

Figure 2.14: Variations in the SoC-OCV relationship depending on the battery ageing, current rate, temperature and using different batteries by (C. Chen et al. 2022)

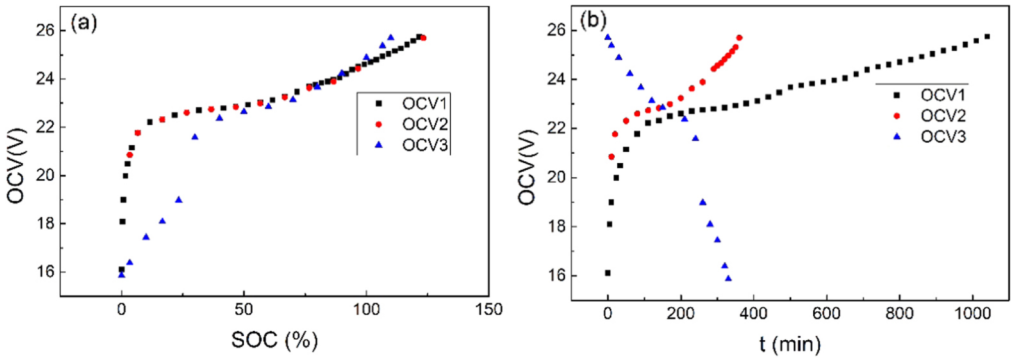

Figure 2.15: The effect of current rate on the SoC-OCV characteristic by (Yuan et al. 2022)

it changes slowly in high SoC regions as the SoC changes. The OCV at the same SoC is different at the charging and discharging cycles.

R. Zhang et al. 2018 investigated the effect of the ambient temperature on the SoC-OCV characteristic. The battery drop test is conducted at different temperatures and the results are shown in Figure 2.16. When the ambient temperature is lower, the OCV becomes higher or vice versa. However, this behaviour is not significant at high SoC regions, i.e. SoC $>$ 90%. However, Z. Wang et al. 2022 expressed the opposite impact of the ambient temperature on the SoC-OCV curve. As the ambient temperature increases, the OCV at the same SoC increases as shown in Figure 2.17. The difference in the battery experiment results show that the real-time estimation of the SoC-OCV relationship is required. The SoC-OCV data is curve-fitted to the 5^{th} order SoC and

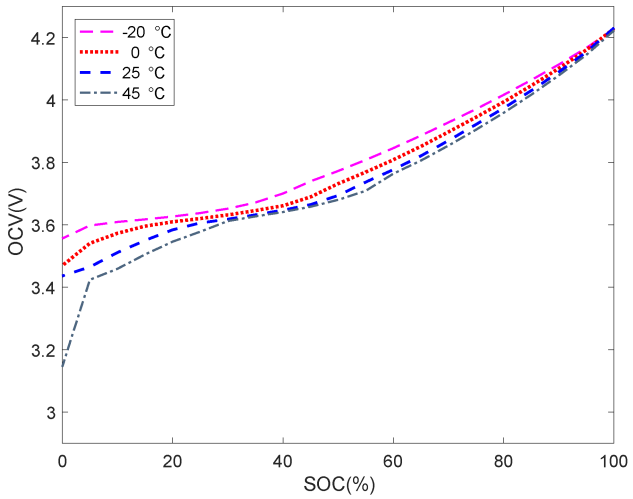

Figure 2.16: Variations in the SoC-OCV characteristic with respect to the ambient temperature by (R. Zhang et al. 2018)

1st order temperature polynomial function. J. Shen et al. 2021 modelled the battery

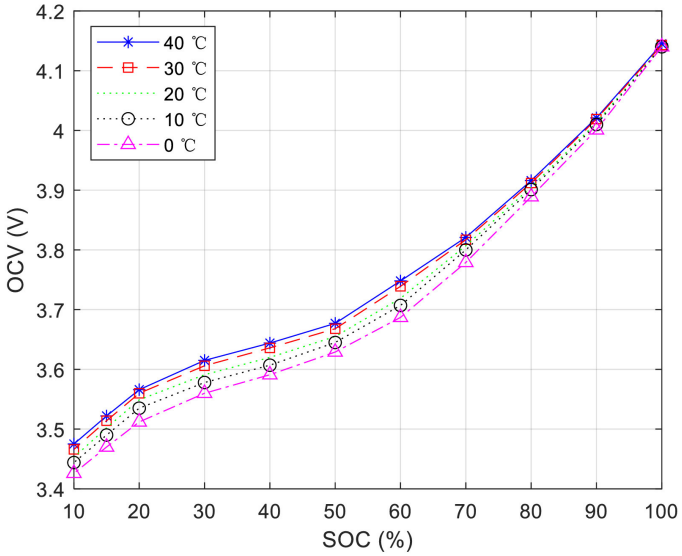

Figure 2.17: The SoC-OCV variations at different ambient temperatures by (Z. Wang et al. 2022)

OCV as a function of the SoC and the ambient temperature. They conducted a battery experiment in a wide range of temperatures, i.e., from -20^oC to 60 ^oC. It is found that the OCV decreases with an increase in the ambient temperature in low SoC regions. However, this trend is the opposite in the SoC regions which is greater than 60%. The maximum absolute error (MAAE) in SoC estimation is 1.75% under laboratory conditions. However, this error would be greater in practice depending on the variations in the SoC-OCV relationship due to real-world conditions. As a result, the battery can be overcharged or over-discharged. Choi et al. 2020 also investigated

the temperature impact on the SoC-OCV characteristic. The experimental SoC-OCV characteristics are determined in the laboratory using the HPPC cycle including 20 discharge pulses at the rate of C/10. The same procedure is repeated to completely charge the battery as well. After completing these two cycles, the average of the charge and discharge curves are calculated to consider the hysteresis characteristics. The results indicate that the OCV increases as the ambient temperature decreases as shown in Figure 2.18. The SoC-OCV relationship is dependent on many aforementioned factors. Therefore, its online calculation is required to increase the SoC estimation accuracy in practice.

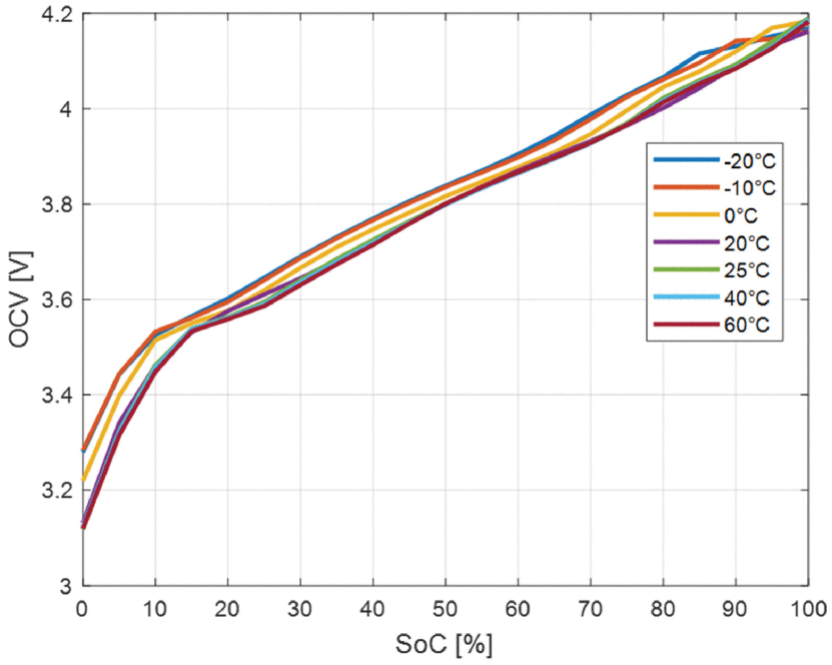

Figure 2.18: The SoC-OCV characteristic depending on the ambient temperature by (Choi et al. 2020)

Shuzhi Zhang et al. 2022 partially constructed the SoC-OCV relationship without conducting a battery drop test. It is expressed that the difficulty in the relationship's construction is the calculation of the SoC. The SoC is calculated using the CC method by neglecting the current drift. The battery's OCV is calculated along with the first-order Thevenin ECM parameter using the RLS method. When the SoC and OCV data are available, the SoC-OCV relationship is partially constructed around the sampling point. The RMSE in the SoC estimation is calculated to be 0.63% when the fresh battery is used. The RMSE increased to 1.02% when the aged battery is used in the battery experiment. In practice, the error is likely to increase due to the CC method.

Furthermore, this method is vulnerable to the current measurement noise and it always requires the correct initial guess of the SoC estimate.

Long 2022 highlighted the difficulties in the OCV drop test to acquire the SoC-OCV relationship. It is expressed that the relaxation period of the battery to reach a steady state is uncertain. Therefore, building the SoC-OCV relation experimentally may be erroneous. To prevent this, the OCV is estimated in real-time. The corresponding SoC values are calculated using the CC method. The coupled SoC-OCV data are curve-fitted to the nonlinear model. The average SoC estimation error is 2.617%. However, this error would be greater in practice due to the lack of initial SoC guess and noisy current sensor measurement.

Siva Suriya Narayanan et al. 2022 utilised the machine learning (ML) technique to construct the SoC-OCV relationship. The static SoC-OCV relationship is built based on experimental data at different temperatures using the proposed ML technique. 201 experimental data points are collected in total. 141 data points are used to train the ML algorithm whereas 30 data points are used to test the algorithm. The other 30 data points are used to validate the algorithm. This work aims to eliminate the error in the curve-fitting techniques. The proposed method showed superiority over existing techniques adopting different nonlinear functions. The SoC-OCV relationship is unique for every battery. Therefore, constructing this relationship according to a specific battery does not propose a general technique that can be used for every battery. Its application to practical cases is limited.

Jibhkate et al. 2022 used a rational polynomial function to model the SoC-OCV relationship. The function is expressed as follows:

$$V_{oc}(z) = \frac{N_1 + N_2 z + N_3 z^2 + N_4 z^3}{1 + D_1 z + D_2 z^2 + D_3 z^3} \tag{2.22}$$

where z is the SoC, N_i for $i = 1, \ldots, 4$ and and D_j for $j = 1, 2, 3$ are coefficients. Firstly, the experimental data are curve-fitted to the model to calculate the coefficients. In order to assess the deviations in the coefficients, the battery's remaining useful life (RUL) is used. As the RUL decreases, the OCV at the same SoC decreases at the low SoC regions. The inverse function of (2.22) is calculated. It is plotted over the range of RUL from 0%RUL to 100% RUL and changes in the coefficients are compared. The

coefficients N_4, D_1, D_2, and D_3 remained almost constant whereas N_3 varied linearly over the lifetime of the battery. N_1, and N_2 showed a reverse trend during the entire range of the RUL. These coefficients are modelled by using a 2^{nd}order polynomial functions. The coefficient of these functions are calculated as a function of RUL. The model is given in (2.22) now considers the changes in the SoC-OCV relationship with respect to the battery's RUL. The SoC-OCV curve estimation error is 3.4481% at 50% of SoC, which is the maximum error observed in this work. It is concluded that the error range is under the usable range.

B.-C. Chen et al. 2017 approximated the SoC-OCV relation with a local linearisation. The nonlinear SoC-OCV relation around the operating point is constructed by a straight line with 2 unknown modelling parameters. The linear relation is expressed as follows:

$$V_{oc} = V_{oc}(z^*) + \left.\frac{\partial V_{oc}}{\partial z}\right|_{z^*} (z - z^*) \tag{2.23}$$

where z^* is the operating SoC point. The estimated OCV is converted into the SoC value using this relationship. X. Chen et al. 2019 investigated the reconstruction of the SoC-OCV relationship. The SoC is calculated using the CC method. The OCV is chosen as one of the battery model parameters and estimated using an online parameter identification algorithm. Once the OCV estimate is calculated, the SoC and OCV couple data is curve-fitted by the SoC-OCV nonlinear model that is chosen as n^{th} order polynomial function.

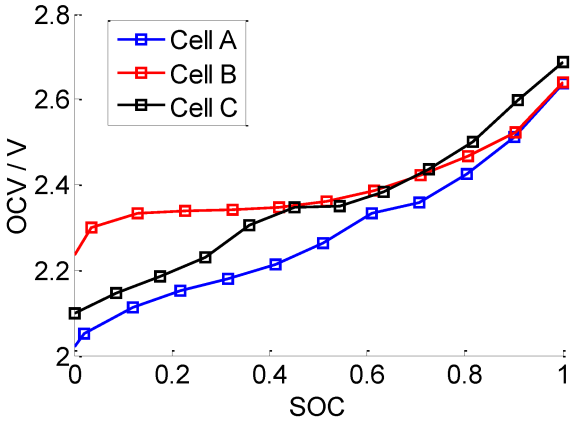

Figure 2.19: The SoC-OCV variations for different batteries by (Han et al. 2014)

In Figure 2.19, Han et al. 2014 showed the difference in the SoC-OCV curve for three batteries manufactured from the same production line. Lee et al. 2008 explained that each battery with the same capacity has a different SoC-OCV characteristic even

though these characteristics are measured under the same conditions. In order to prevent the variations in the SoC-OCV relationship, a new capacity concept is introduced with respect to the OCV. The SoC is then recalculated based on the new capacity. They choose the lower cut-off OCV value arbitrarily, i.e., 3.6 V. This voltage value is used to calculate the new SoC-OCV relationship for each battery. Each battery's SoC-OCV characteristic shows similarities after the procedure is completed.

C.-S. Huang et al. 2021 investigated the observability problem when the slope of the SoC-OCV curve is close to zero. The battery is modelled as the first order Thevenin model. The nonlinear SoC-OCV relation is approximated by a piece-wise linear functions:

$$V_{oc}(z) = \begin{cases} a_{1,o}z + b_{1,o} \text{ for } z_0 \leq z \leq z_1 \\ a_{2,o}z + b_{2,o} \text{ for } z_1 \leq z \leq z_2 \\ \vdots \\ a_{i,o}z + b_{i,o} \text{ for } z_{i-1} \leq z \leq z_i \end{cases} \tag{2.24}$$

where $a_{i,o}$ and $b_{i,o}$ are the coefficients of the linear equation, i is the particular section of the relation, o represents the charging or discharging regime of the battery. The different piece-wise linear functions for the same particular sections are used with respect to the charging or discharging regime due to the hysteresis effect. The coefficients $a_{i,o}$ and $b_{i,o}$ are continuously calculated. In the derivations, the subscript o is skipped for the simplicity purpose. Firstly, the state space model of the first order Thevenin model is formulated as follows:

$$\begin{aligned} \dot{x} &= Ax + Bu \\ y &= Cx + Du \end{aligned} \tag{2.25}$$

where

$$\begin{aligned} x &= \begin{bmatrix} z & V_p \end{bmatrix}^T, \ y = V_t, \ u = I \\ A &= \begin{bmatrix} 0 & 0 \\ 0 & \frac{-1}{R_p C_p} \end{bmatrix}, \ B = \begin{bmatrix} \frac{1}{Q_{max}} \\ \frac{1}{C_p} \end{bmatrix}, C = \begin{bmatrix} a_i & 1 \end{bmatrix}, \ D = R_0, \end{aligned} \tag{2.26}$$

The estimation error is defined as follows:

$$e = \begin{bmatrix} e_z \\ e_{V_p} \end{bmatrix} = \hat{x} - x \tag{2.27}$$

It is proved that the SoC estimation error is vulnerable to the slope of the SoC-OCV curve. This dependence is prevented by replacing z by V_{oc} in the state vector. The estimated V_{oc} is then used to calculate the coefficients. The results demonstrated that the SoC estimation accuracy increased with the proposed method.

2.3 Current sensor noise & its estimation

In batteries, the input signal is the current measurement. Since it is a measured signal, it is corrupted by the sensor noises. The error in the current input is challenging because the amount of noise may cause the divergence of the state estimations. Therefore, the effect of the current input noise must be investigated thoroughly and it must be considered in the SoC estimations.

The error analysis of the SoC observer was carried out by P. Shen et al. 2018. The second order Thevenin model is utilised to model a Lithium-ion battery. It is found that the current measurement error is one of the error sources deteriorating the SoC estimation. This error can be defined as the summation of the bias error and noise in the current measurement process. Thus, the true current I can be expressed by subtracting the bias noise and the white noise from the measured current $\tilde{I}$, i.e., $I = \tilde{I} - \beta - v_i$ where β is the bias noise, v_i is the white noise. Using an appropriate feedback gain is proposed to mitigate the SoC estimation error by claiming the voltage correction in the update part can cancel out the error caused by the current measurement. However, the voltage measurement equation is as follows:

$$V_t = V_{oc} + \tilde{I}R_0 + I_{a,1}R_{p,1} + I_{a,2}R_{p,2}. \tag{2.28}$$

where $I_{a,i}$ is the current flowing over $R_{p,i}$ for $i = 1, 2$. According to the current measurement equation, the error in the current measurement is directly added to the voltage estimation therefore the difference between the measured voltage and the estimated voltage will be biased due to the error in the current measurement. This leads to erroneous SoC estimation.

Y. Xu et al. 2020 proposed a dual Kalman Filter (DKF) algorithm to filter the SoC twice to reduce the current measurement error and battery modelling error. The DKF based SoC estimation algorithm combines the Ampere-hour (Ah) counting method

with the EKF. Another KF is used to suppress the estimation error by the EKF. The SoC is initially estimated using the EKF depending on the difference between the measured output voltage and the model output voltage. This is to surpass the battery modelling error. Secondly, the SoC is estimated and updated using the KF algorithm depending on the difference between the SoC estimated using the Ah counting method and the SoC previously estimated by the EKF. The second estimation of the SoC is to surpass the current measurement error accumulated in the Ah counting method. It is found that the dual KF suppresses the current measurement error. However, the standard KF is derived for the system with noiseless input. Since the current input is a measured signal in the battery-powered systems, the standard Kalman filter estimation algorithm must be rearranged considering the noisy input current. Moreover, the error in the current measurement is not explicitly defined. Therefore, it cannot be claimed that dual KF can reduce the error without defining the type of the error since KF derivation depends on the Gaussian noise assumptions.

The effect of the current measurement accuracy on the state prediction error is highlighted by Tingting et al. 2011. They explained that the impact of the current measurement error is reflected in the state propagation step. However, the current input measurement is also used in the update equation. Therefore, it is expected to see the impact in the update step as well. It is also found that the Gaussian white noise with zero means does not affect the results of the entire SoC estimation algorithm. However, it is emphasised that the input current measurement has a current bias in practice. In order to see the effect of the current bias on the SoC estimation, computer simulations are performed by adding the current bias to the current input measurement. The simulation results show that the accuracy of the SoC estimation decreases with the increase in the current bias. Similarly, Z. Wei et al. 2021 scrutinises the effect of sensor noise on the estimation of physical model parameters and SoC. The first-order Thevenin equivalent circuit is used to model the battery. The sensor noises are assumed to be zero-mean, ergodic, and random. It is concluded that the solution of the LPM based on the least squares technique is asymptotically biased due to the corrupted system input and output measurements. The current bias is modelled as a constant in this work, which is not a realistic bias modelling. There is no information about the bias noise. Thus, modelling the bias noise as a random walk is a more suitable approach

to tackle the current measurement problem.

Z. Liu et al. 2015 tested the effect of the current measurement bias on the SoC estimation. The current sensor bias of ∓ 10 A was injected into the SoC estimation algorithm in the middle of the simulation. Once the bias was added to the current measurement, a significant deterioration in the SoC estimation was observed. Under the faulty current sensor measurement, the SoC estimation error is out of the tolerable range by 5%. It is concluded that this error may cause overcharging/over-discharging of the battery in real-time applications. The EKF-based fault diagnosis algorithm was proposed to prevent an error due to the current sensor measurement bias. The bias noise is a random walk. Therefore, its magnitude cannot be limited to a certain value. In practice, the error in SoC estimation can be greater than 5%.

J. Xu et al. 2016 estimated the current sensor fault by using the proportional integral observer (PIO) based method. The current sensor fault is designed as the integral of the difference between the measured output and the estimated output, i.e., it is expressed as follows:

$$\dot{\hat{f}}_c = K_i(\tilde{y} - \hat{y}) \tag{2.29}$$

where f_c is the estimated current sensor fault, $\tilde{y}$ is the output measurement, $\hat{y}$ is the estimated output, and K_i is the integral gain. Once the current sensor fault is calculated, it is subtracted from the current measurement to estimate the current input. The estimated current input is then used to estimate the battery states. Firstly, the proposed algorithm is tested for the scenario that the current sensor measurement does not have the current sensor bias. The experimental result indicates that the SoC estimation error is within 0.01%. Secondly, the current bias of -20 A is intentionally added to the current measurement at 2500 s. However, the current fault estimator is not used. The estimated SoC accurately traces the reference SoC before the current bias is injected into the current measurement. After this point, the SoC estimation diverges from the reference SoC and the error in the SoC estimation keeps increasing. The latter scenario is then repeated by utilising the current bias estimator. The SoC estimation error is less than 2%. However, bias modelling is not explicitly shown in this work. Furthermore, the proposed algorithm is executed under a constant bias. The performance of the algorithm is not tested with variable bias noise.

Chun et al. 2016 developed a method to estimate the SoC without sensing the current measurement. The method only uses the filtered $\tilde{V}_t$ measurements of each cells in the battery pack. The current applied to the battery is estimated by using the filtered $\tilde{V}_t$. The simple RC battery model is adopted to model the battery. Its V_{oc} is calculated based on the specifications given by the manufacturer as follows:

$$V_{oc} = C_n \frac{dSoC}{dV_{oc}} \tag{2.30}$$

where C_n is the nominal capacity given by the manufacturer and the SoC-OCV relation is also given by the manufacturer. Therefore, the estimated current and estimated SoC are expressed by the followings:

$$\hat{I}(k) = (1 - f_s) \left\{ \hat{I}(k-1) - \frac{[V_t(k) - V_t(k-1)]}{R} \right\} \tag{2.31a}$$

$$\hat{z}(k) = \hat{z}(k-1) - \frac{\hat{I}(k)}{C_n} \Delta t \tag{2.31b}$$

where $f_s = \Delta t/(\Delta t + RC)$ is the smoothing factor, R is the resistor, C is the equivalent capacitor and Δt is the sampling time. The proposed algorithm is validated by a battery experiment. In the battery experiment, the current estimation error is around +5 mA and the error in the SoC estimation is within 3%. However, the current estimation model is built based on the simple RC battery model. This battery model is not good enough to capture the transient response of the battery under dynamic loading. Therefore, it cannot be applicable to practical applications including EVs.

Lin 2018 analysed the SoC estimation error due to the sensor noises. The sensor is modelled by taking into account the bias and the variance as follows:

$$\tilde{I}_k = I_k - \Delta I - \delta I_k \tag{2.32}$$

where ΔI is the current bias and δI is the random noise identically distributed with zero mean and constant variance. ΔI is assumed to slowly vary over time. The least-square estimation method is defined to minimise the residual between the measured $\tilde{V}_t$ and estimated $\hat{V}_t$. The partial derivative of the residual with respect to the SoC is equalised to zero and solved for SoC. This yields the estimated SoC. However, a more realistic approach is to model the bias noise as a random walk. In this case, the bias

noise is expected to change fast.

Hong et al. 2022 highlighted that the accuracy of the BMS is dependent on the precision of the sensors and the state estimation algorithms. It is also added that the biased sensor data is possible due to the malfunction of the sensors and communication errors. The current sensor bias reaches up to 2% according to the actual EV experiments. Mohammadi 2022 expressed the current input measurement as the summation of the actual current input and the current input uncertainty. It is noted that the actual current flows from one battery's terminal to the other one and the current uncertainty is a fault in the measurement process.

Yan et al. 2013 designed an improved fuzzy adaptive KF to estimate the SoC of EVs working under poor sensor measurements. The filter monitors the variations in the residual, utilises its mean and variances as an input of the fuzzy controller and finally adjusts the weight of noises using fuzzy logic. This reduces the estimation error in SoC in real-time. However, the system noise and the measurement noise are assumed to be zero mean white noise, and the proposed method only updates their statistical properties. In practice, current measurement is corrupted by two stochastic noises, i.e., white noise and bias noise. Therefore, considering the bias noise in the current measurement would be a more realistic approach for SoC estimation for EVs. Y. Wang et al. 2021 investigated the effect of the current sensor accuracy on the SoC estimation. The results show that the error of the current sensor must be controlled within 4% to maintain the SoC error within 5%.

2.4 Discussion

This chapter undertakes the literature review regarding the battery modelling, the model parameter identification methods, the SoC estimation methods, the SoC-OCV curve construction and its variations, and the current sensor measurement noises. The most common battery models are discussed and the most suitable one is chosen comparing their reliability and applicability in practice. A reliable battery model should have low complexity yet be able to describe the battery dynamics. Various battery technologies including lithium-ion battery technologies use and adopt Thevenin ECMs for real-time utilisation. To prevent large matrix operations, the first-order

Thevenin ECM is a good candidate to accurately represent the battery dynamics.

The ECM consists of basic circuit elements including resistors, capacitors, and voltage sources. The majority of SoC estimation algorithms are based on a battery model whose parameters are initially unknown. This implies that a parameter identification procedure is necessary to prepare the model for SoC estimation. The battery model parameters can be identified through either offline or online methods. The offline parameter identification method is a heavily laborious experimental task. Although a set of batteries can originate from the same production line, deviations in parameter values between these batteries are natural. Thus, the experiment has to be conducted for each battery. Moreover, the experimental conditions and battery ageing also affect the parameter values. These aforementioned reasons make the model parameters need to be updated in real-time. Therefore, the online parameter estimation is the only appropriate way to estimate model parameters. There are different approaches to estimating the model parameters online. The RLS methods are commonly used in the literature. However, the convergence and the stability of the proposed RLS techniques have not been guaranteed. An alternative to the RLS-based parameter estimation is the adaptive law-based method. This method guarantees the convergence and stability of the parameter estimation based on the Lyapunov stability theory. Consequently, the adaptive law-based parameter estimation method is found more appropriate in the model parameter estimation.

The nonlinear SoC-OCV relation is used to map the OCV to its corresponding SoC value. The SoC-OCV relation could be obtained through an offline method or an online method. Similar to the parameter estimation, the SoC-OCV relationship is unique for a specific battery used during the test and cannot apply to different batteries. Furthermore, it is vulnerable to a change in the operational conditions and battery ageing. For example, an increase in the ambient temperature either increase or decrease the OCV at the same SoC for different batteries. Therefore, empirical modelling of the SoC-OCV curve would provide an erroneous SoC-OCV relationship in practice. This error is directly reflected as an error in SoC estimation. Therefore, real-time construction of the SoC-OCV relationship is required. This increases the accuracy in the SoC estimation considering the variations in the SoC-OCV characteristic and different battery types.

The current measurement is corrupted by the current bias and the white noise. The impact of these noises is considerably different. The white noise does not have a significant effect on the SoC estimation error. The EKF can accurately estimate the SoC based on the current sensor measurement with random white noise. However, it is found that the current bias significantly increases the error in the SoC estimation. In the literature, the majority of available SoC estimation algorithms do not realistically consider the bias noise in the current input measurement. For example, most of them consider a constant current bias noise, which does not reflect the actual bias noise characteristic. Moreover, it is commonly concluded that the KF can estimate the SoC under noisy current input measurement. However, the bias noise has a random walk characteristic and it may reach large values. In the case of larger bias noise, the KF is expected to fail. Therefore, the development of a more realistic SoC estimation algorithm is required taking into account these two current measurement noises with a correct current sensor modelling.

The standard KF has been widely used in many engineering applications due to its simplicity and powerful estimation ability, especially for linear systems. The EKF and UKF are developed for nonlinear systems based on the idea of the standard KF. The KF provides an accurate estimation when the input signal is noiseless. In literature, the majority of the SoC estimation algorithms are based on the standard KF without considering the current input measurement noises. In battery systems, the current input measurement is corrupted by two sensor noises. Therefore, the standard KF is expected to provide unreliable SoC estimation. To increase the SoC estimation accuracy, the standard KF needs to be modified based on the current sensor model.

There are still gaps in the real-time SoC estimation algorithms. Firstly, more realistic SoC estimation algorithms have to be adaptive to the changes in the operational conditions and battery ageing. Therefore, the model parameters and the SoC-OCV relationship have to be calculated together in real-time using robust estimation algorithms. Secondly, the current sensor bias has a significant effect on the SoC estimation error. Thus, the current input measurement needs to be corrected by estimating the bias noise modelled as a random walk. Considering the noisy current input requires the modification of the standard KF. Therefore, the standard KF algorithm must be modified based on the current sensor model.

Chapter 3

Battery modelling and parameter identification

Battery models are used to reflect the battery's dynamic behaviour. An appropriate battery model should be chosen according to the trade-off between the computational cost and model accuracy. Adopting a battery model requires the identification of the model parameters that change slowly with time. Therefore, these parameters need to be calculated online.

This chapter introduces the first-order Thevenin ECM. It summarises the battery model parameters identification method based on the adaptive law and its stability analysis. Additionally, the battery test rig is introduced, which is designed to validate the battery model and the preferred parameter identification method. Finally, simulation and experimental results are presented along with a discussion regarding the battery model and the proposed parameter estimation method.

3.1 Battery modelling

The essential strategy used for selecting a suitable battery model is as follows: the potential candidate should accurately simulate the charge/discharge process and dynamic response of the battery with a minimum computational cost. The first order Thevenin model given in Figure 3.1 robustly mimics the dynamic behaviour of the battery. It also associates the OCV with the SoC using a nonlinear SoC-OCV charac-

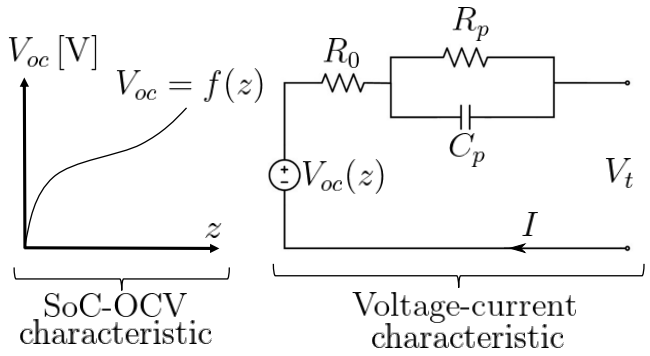

Figure 3.1: 1st order Thevenin battery model

teristic. Besides, it reduces the calculation effort compared to the high order Thevenin models. Consequently, the first order Thevenin model is used to model the battery in this work.

Firstly, the relationship between the load current I and the terminal voltage V_t is required. It can be calculated by distributing I to the RC branch components. Based on the Kirchhoff's current law:

$$I = I_a + I_b \tag{3.1}$$

where I_a is the current flows over R_p, and I_b is the current flows over C_p. The polarisation voltage V_p across the RC branch is obtained by the Ohm's law as follows:

$$V_p = I_a R_p \tag{3.2}$$

The differential equation of the voltage across C_p is given by

$$\frac{dV_c}{dt} = \frac{I_b}{C_p} \tag{3.3}$$

As C_p and R_p are connected in parallel, the voltage across R_p (V_p) and the voltage across C_p (V_c) are equal to each other, i.e., $V_c = V_p$. Rearranging (3.2) and (3.3) substituting into (3.1) yield the continuous-time dynamic equation of V_p

$$\dot{V}_p = -\frac{V_p}{\tau} + \frac{I}{C_p} \tag{3.4}$$

where $\dot{(\cdot)} = d(\cdot)/dt$ and $\tau = R_p C_p$. Divide both sides of (3.4) by R_p

$$\dot{I}_a = -\frac{I_a}{\tau} + \frac{I}{\tau} \tag{3.5}$$

Equation (3.5) is the governing differential equation for I_a and it reflects the battery's polarisation behaviour depending on variations in I. The terminal voltage V_t is given by

$$V_t = V_{oc} - IR_0 - V_p \tag{3.6}$$

where $V_{oc} = f(z)$ and $f(z)$ is the SoC-OCV function, which is known to be a nonlinear function. Equations (3.5) and (3.6) define the voltage-current characteristic of the battery.

The OCV is assumed to vary slowly therefore the dynamic equation for the OCV is approximated by

$$\dot{V}_{oc} \approx 0 \tag{3.7}$$

Discrete-time expressions of (3.5), (3.6), and (3.7) are of the form:

$$I_{a,k+1} = \alpha I_{a,k} + (1-\alpha) I_k \tag{3.8a}$$

$$V_{oc,k+1} = V_{oc,k} \tag{3.8b}$$

$$V_{t,k} = V_{oc,k} - I_k R_0 - V_{p,k} \tag{3.8c}$$

where $(\cdot)_k$ is the k^{th} sample of $(\cdot)$, $\alpha = e^{-\Delta t/\tau}$, and Δt is the sampling time for the discrete-time equations.

For the SoC estimation, the nonlinear SoC-OCV relationship, $V_{oc} = f(z)$, needs to be identified to convert the estimated OCV to the SoC after the OCV estimate is available. To prepare the battery model for the SoC estimation, the nonlinear relationship and the model parameters R_0, R_p, and C_p must be calculated first. The following section introduces the identification method of the model parameters.

3.2 Model parameter identification

As it is highlighted in Chapter 2, the battery model parameters can be identified by two fundamental methods; offline method and online method. These parameters vary depending on the operational conditions including temperature and battery aging. Hence, parameters calculated using the offline method are constant values and they do not adapt to changes in the operational conditions. This disadvantage leads to erroneous identification of model parameters for different operational conditions. The

error in the estimated parameter may cause large errors in the SoC estimation. Online methods are more suitable to identify and update these parameters in real-time. Therefore, an online parameter identification method is adopted in this work. The online parameter estimation of the battery model parameters includes the following three steps:

1. Derivation of the linear parametric model
2. Setting up the estimation model
3. Presenting the convergence condition

3.2.1 Linear parametric model derivation

The above three steps are followed in order to derive the online parameter estimation algorithm. First of all, the LPM form of the battery model needs to be derived. The one sampling step difference of (3.8c) can be used to derive the LPM.

Discretise (3.4)

$$V_{p,k+1} = \alpha V_{p,k} + (1-\alpha) R_p I_k \tag{3.9}$$

Rewrite (3.8c) for step $k+1$

$$V_{t,k+1} = V_{oc,k+1} - V_{p,k+1} - R_0 I_{k+1} \tag{3.10}$$

Substituting (3.9) into (3.10)

$$V_{t,k+1} = V_{oc,k+1} - \alpha V_{p,k} - (1-\alpha) R_p I_k - R_0 I_{k+1} \tag{3.11}$$

Rearrange (3.8c) for $V_{p,k}$ and substitute into (3.11)

$$\begin{aligned} V_{t,k+1} =& \alpha V_{t,k} - R_0 I_{k+1} + \left[\alpha R_0 + (\alpha - 1) R_p\right] I_k \\ &+ V_{oc,k+1} - \alpha V_{oc,k} \end{aligned} \tag{3.12}$$

Define

$$\Delta V_{t,k+1} = V_{t,k+1} - V_{t,k} \tag{3.13}$$

Substitute (3.12) into (3.13) for k and $k+1$ sampling time

$$\begin{aligned}\Delta V_{t,k+1} = \alpha \Delta V_{t,k} - R_0 \alpha I_{k+1} + \varrho \Delta I_k \\ + \Delta V_{oc,k+1} - \alpha \Delta V_{oc,k}\end{aligned} \tag{3.14}$$

where $\Delta(\cdot)_{k+1} = (\cdot)_{k+1} - (\cdot)_k$ and $\varrho = \alpha R_0 + (\alpha - 1)R_p$. V_{oc} is known to vary slowly compared to V_t, and the change in V_{oc} is assumed to be negligible during the sampling interval (H. Chaoui et al. 2017). Equation (3.14) is approximated as

$$\Delta V_{t,k+1} \cong \alpha \Delta V_{t,k} - R_0 \Delta I_{k+1} + \varrho \Delta I_k \tag{3.15}$$

and it is written in a linear parametric model as follows:

$$y_{k+1} = \boldsymbol{\theta}_{k+1}^T \boldsymbol{\phi}_{k+1} \tag{3.16}$$

where

$$\boldsymbol{\theta}_{k+1} = \begin{bmatrix} \alpha & -R_0 & \varrho \end{bmatrix}^T \tag{3.17}$$

which is the unknown to be estimated, and the state vector is given by

$$\boldsymbol{\phi}_{k+1} = \begin{bmatrix} \Delta V_{t,k} & \Delta I_{k+1} & \Delta I_k \end{bmatrix}^T \tag{3.18}$$

Once the estimation, $\hat{\boldsymbol{\theta}}_{k+1}$, is available, the parameters in the model are obtained by

$$\hat{R}_0 = -\hat{\boldsymbol{\theta}}_{k+1}^{(2)} \tag{3.19a}$$

$$\hat{R}_p = \frac{\hat{\boldsymbol{\theta}}_{k+1}^{(3)} + \hat{\boldsymbol{\theta}}_{k+1}^{(1)} \hat{R}_0}{1 - \hat{\boldsymbol{\theta}}_{k+1}^{(1)}} \tag{3.19b}$$

$$\hat{C}_p = \frac{-\Delta t_s}{\hat{R}_p \log \hat{\boldsymbol{\theta}}_{k+1}^{(1)}} \tag{3.19c}$$

where $(\cdot)^{(i)}$ for $i = 1, 2, 3$ is the i^{th} element of $(\cdot)$. As the terminal voltage is measured, the terminal voltage difference is obtained from two measurement samples. The measurement equation for the parameter estimation is defined by

$$\tilde{y}_{k+1} = \Delta V_{t,k+1} + e_{k+1} \tag{3.20}$$

where e_{k+1} is the measurement noise.

3.2.2 Online parameter estimator design

In this section, we summarize one of the standard parameter estimation algorithms (Ioannou et al. 2006). The majority of the dynamic systems are continuous-time systems, which are represented with continuous-time expressions. However, the measured signals are in discrete time. Therefore, the implementation of the online parameter identification algorithm needs to be in discrete time. Consequently, the online parameter estimation algorithm can be derived based on the continuous-time system equations first, and then it can be transformed into the discrete-time version.

Consider a system defined by the following algebraic equation

$$y(t) = \boldsymbol{\theta}^T(t)\boldsymbol{\phi}(t) \tag{3.21}$$

where $\boldsymbol{\phi}(t)$, $y(t)$, and $\boldsymbol{\theta}(t)$ are the input vector, the output scalar, and an unknown parameter vector, respectively. Note that $\boldsymbol{\phi}(t)$ and $y(t)$ are measured signals and $\boldsymbol{\theta}(t)$ is to be calculated at each time step.

This section attempts to derive a recursive online method to calculate $\boldsymbol{\theta}$. It is therefore necessary to estimate the output using an equation based on the input signals and the estimated parameters. The estimate of the output is given by

$$\hat{y}(t) = \hat{\boldsymbol{\theta}}^T(t)\boldsymbol{\phi}(t) \tag{3.22}$$

where $\hat{\boldsymbol{\theta}}(t)$ is the estimate of $\boldsymbol{\theta}(t)$. Now the estimation error in the output can be calculated as follows:

$$\epsilon = y - \hat{y} = y - \hat{\boldsymbol{\theta}}^T\boldsymbol{\phi} \tag{3.23}$$

Substitute (3.21) into (3.23)

$$\epsilon = \boldsymbol{\theta}^T\boldsymbol{\phi} - \hat{\boldsymbol{\theta}}^T\boldsymbol{\phi} = -\tilde{\boldsymbol{\theta}}^T\boldsymbol{\phi} \tag{3.24}$$

where $\tilde{\boldsymbol{\theta}} = \hat{\boldsymbol{\theta}} - \boldsymbol{\theta}$. Minimizing the cost criteria of ϵ with respect to $\hat{\boldsymbol{\theta}}$ yields the differential equation to generate $\hat{\boldsymbol{\theta}}$. The following quadratic cost function is a common

choice:

$$J(\hat{\boldsymbol{\theta}}) = \frac{\epsilon^2}{2} = \frac{\left(y - \hat{\boldsymbol{\theta}}^T \boldsymbol{\phi}\right)^2}{2} \tag{3.25}$$

Assume that $\hat{\boldsymbol{\theta}}_k$ is the estimate of $\boldsymbol{\theta}$ at instant k. Then the gradient of $J(\hat{\boldsymbol{\theta}})$, $\bigtriangledown J(\hat{\boldsymbol{\theta}})$ at $\hat{\boldsymbol{\theta}}_{k+1}$ is approximated by the Taylor's series expansion.

$$\bigtriangledown J(\hat{\boldsymbol{\theta}}_{k+1}) \simeq \bigtriangledown J(\hat{\boldsymbol{\theta}}_k) + \frac{\partial}{\partial \boldsymbol{\theta}} \bigtriangledown J(\hat{\boldsymbol{\theta}})|_{\hat{\boldsymbol{\theta}}=\hat{\boldsymbol{\theta}}_k} \left(\hat{\boldsymbol{\theta}}_{k+1} - \hat{\boldsymbol{\theta}}_k\right) \tag{3.26}$$

Solving (3.26) for $\hat{\boldsymbol{\theta}} = \hat{\boldsymbol{\theta}}_{k+1}$ by setting the right hand side of (3.26) equal to zero provides $\hat{\boldsymbol{\theta}}_{k+1}$ of $\boldsymbol{\theta}$ at $k+1$, i.e.,

$$\hat{\boldsymbol{\theta}}_{k+1} = \hat{\boldsymbol{\theta}}_k - H^{-1}(\hat{\boldsymbol{\theta}}_k) \bigtriangledown J(\hat{\boldsymbol{\theta}}_k) \tag{3.27}$$

where $H(\hat{\boldsymbol{\theta}}_k) = \frac{\partial}{\partial \boldsymbol{\theta}} \bigtriangledown J(\hat{\boldsymbol{\theta}}_k) = \bigtriangledown^2 J(\hat{\boldsymbol{\theta}}_k)$ refers to the invertible Hessian matrix. Note that J is continuously differentiable function, i.e., all first and second order partial derivatives of J exist for each $\boldsymbol{\theta}$ and all are continuous function of $\boldsymbol{\theta}$. The Hessian of $J(\boldsymbol{\theta})$ is defined to be 3-by-3 symmetric matrix as follows:

$$\bigtriangledown^2 J(\hat{\boldsymbol{\theta}}) \triangleq \left[\frac{\partial^2 J(\boldsymbol{\theta})}{\partial \boldsymbol{\theta}^{(i)} \partial \boldsymbol{\theta}^{(j)}}\right]_{3\times 3} \tag{3.28}$$

where $\partial^2 J(\boldsymbol{\theta})/(\partial \boldsymbol{\theta}^{(i)} \partial \boldsymbol{\theta}^{(j)})$ is the i^{th} row and j^{th} column element of the Hessian. A domain S is a convex set if for all $\boldsymbol{\theta}^{(i)}$, $\boldsymbol{\theta}^{(j)} \in S$ and $\vartheta \in [0,1]$, $\vartheta \boldsymbol{\theta}^{(i)} + (1-\vartheta)\boldsymbol{\theta}^{(j)} \in S$. Furthermore, J is convex over the domain S if the following is satisfied:

$$J\left(\vartheta \boldsymbol{\theta}^{(i)} + (1-\vartheta)\boldsymbol{\theta}^{(j)}\right) \leq \vartheta J\left(\boldsymbol{\theta}^{(i)}\right) + (1-\vartheta) f\left(\boldsymbol{\theta}^{(j)}\right) \tag{3.29}$$

If the above condition is satisfied, the Hessian of J is said to be invertible. Assuming $\boldsymbol{\theta}(t)$ as a differentiable function in continuous time, the continuous version of (3.27) can be developed by taking the time derivative of $\bigtriangledown J(\hat{\boldsymbol{\theta}}(t))$ as follows:

$$\frac{d}{dt} \bigtriangledown J(\hat{\boldsymbol{\theta}}(t)) = \frac{\partial}{\partial \hat{\boldsymbol{\theta}}} \bigtriangledown J(\hat{\boldsymbol{\theta}}) \dot{\hat{\boldsymbol{\theta}}} = H(\hat{\boldsymbol{\theta}}) \dot{\hat{\boldsymbol{\theta}}} \tag{3.30}$$

If $\dot{\hat{\boldsymbol{\theta}}}$ is chosen as $\dot{\hat{\boldsymbol{\theta}}} = -\rho H^{-1}(\hat{\boldsymbol{\theta}}) \bigtriangledown J(\hat{\boldsymbol{\theta}})$ where ρ is a positive-definite matrix, the time

derivative of $\bigtriangledown J(\hat{\boldsymbol{\theta}}(t))$ can be written as follows:

$$\frac{d}{dt} \bigtriangledown J(\hat{\boldsymbol{\theta}}(t)) = -\rho \bigtriangledown J(\hat{\boldsymbol{\theta}}) \tag{3.31}$$

or

$$\bigtriangledown J(\hat{\boldsymbol{\theta}}(t)) = e^{-\rho(t-t_0)} \bigtriangledown J(\hat{\boldsymbol{\theta}}_0) \tag{3.32}$$

For $\rho > 0$, it is clear that $e^{-\rho(t-t_0)}$ part of (3.32) implies that this solution will converge to the root of $\bigtriangledown J = 0$ as $t \to \infty$, if the solution exists for $\forall t \geq t_0 \geq 0$. Note that $\bigtriangledown J$ is equal to zero at any global minimum $\boldsymbol{\theta^*}$, i.e.,

$$\bigtriangledown J(\boldsymbol{\theta}^*) = 0 \tag{3.33}$$

The recursive scheme for $\hat{\boldsymbol{\theta}}$ is now obtained, which can be written in a general form as follows:

$$\dot{\hat{\boldsymbol{\theta}}} = -\Gamma \bigtriangledown J(\hat{\boldsymbol{\theta}}) = \Gamma(y - \hat{\boldsymbol{\theta}}\boldsymbol{\phi})\boldsymbol{\phi} = \Gamma\epsilon\boldsymbol{\phi} \tag{3.34}$$

where Γ is a positive-definite adaptive gain matrix. The discrete-time version of (3.34) is in the form of :

$$\hat{\boldsymbol{\theta}}_{k+1} = \hat{\boldsymbol{\theta}}_k + \Gamma\Delta t\epsilon_{k+1}\boldsymbol{\phi}_{k+1} \tag{3.35}$$

where

$$\epsilon_{k+1} = \tilde{y}_{k+1} - \hat{\boldsymbol{\theta}}_k^T \boldsymbol{\phi}_{k+1} \tag{3.36}$$

Equations (3.35) and (3.36) describe one of the standard online parameter estimation algorithms (Ioannou et al. 2006).

3.2.3 Stability analysis using Lyapunov method

The stability analysis of the adaptive law based parameter estimation is summarised in this section (Ioannou et al. 2006). The stability properties of (3.34) can be analysed by defining the continuous-time parameter error, i.e.,

$$\dot{\tilde{\boldsymbol{\theta}}} = \dot{\hat{\boldsymbol{\theta}}} - \dot{\boldsymbol{\theta}} = \Gamma\epsilon\boldsymbol{\phi} - \dot{\boldsymbol{\theta}} \tag{3.37}$$

where the true parameter $\boldsymbol{\theta}$ is assumed to be constant, therefore, $\dot{\boldsymbol{\theta}} = 0$. Rewrite (3.37) as follows:

$$\dot{\tilde{\boldsymbol{\theta}}} = \Gamma \boldsymbol{\phi} \epsilon \tag{3.38}$$

The error ϵ is defined as follows:

$$\epsilon = \boldsymbol{\theta}^T \boldsymbol{\phi} - \hat{\boldsymbol{\theta}}^T \boldsymbol{\phi} = -\tilde{\boldsymbol{\theta}}^T \boldsymbol{\phi} = -\boldsymbol{\phi}^T \tilde{\boldsymbol{\theta}} \tag{3.39}$$

The following function is selected as the Lyapunov function:

$$V(\tilde{\boldsymbol{\theta}}) = \frac{\tilde{\boldsymbol{\theta}}^T \Gamma^{-1} \tilde{\boldsymbol{\theta}}}{2} \tag{3.40}$$

Take the time derivative of $V(\tilde{\boldsymbol{\theta}})$

$$\dot{V}(\tilde{\boldsymbol{\theta}}) = \tilde{\boldsymbol{\theta}}^T \boldsymbol{\phi} \epsilon = -\epsilon^2 < 0 \tag{3.41}$$

In conclusion, $V(t)$ has a limit because $V > 0$ and $\dot{V} < 0$, i.e.,

$$\lim_{t \to \infty} V[\tilde{\boldsymbol{\theta}}(t)] = V_\infty < \infty \tag{3.42}$$

Stability means that the initial $\boldsymbol{\theta}_0$ approaches the equilibrium point and always remain close to the equilibrium point. However, this does not imply that $\hat{\boldsymbol{\theta}}$ converges to $\boldsymbol{\theta}$. The sufficient and necessary condition for this convergence is that the input signal must be persistently exciting (PE).

The input signal is PE if it satisfies the following (Ioannou et al. 2006):

$$\int_{t_0}^{t_0+T_0} \boldsymbol{\phi}(t) \boldsymbol{\phi}^T(t) dt \geq \alpha_0 T_0 I \tag{3.43}$$

for $\forall t_0 \geq 0$ and for some $\alpha_0 \quad \& \quad T_0 > 0$. Under the PE input signal, the model parameters converges to their actual values.

This parameter estimation method is commonly called the adaptive law in literature (Ioannou et al. 2006). It is important to highlight that the design of the adaptive law ensures the stability of the adaptive estimator. The combination of an online parameter estimation algorithm based on the adaptive law and the state estimation

algorithm may be considered as an adaptive state estimator.

3.3 Simulations

This section describes the parameter estimation simulation based on the adaptive law. Different types of dynamic loading conditions are simulated to assess the performance of the proposed algorithm. For this purpose, four different current input profiles including standard cycles DST and HPPC, constant-current discharge profile, and sinusoidal-current discharge profile are used. The capacity of the simulated battery is 0.85 Ah. The adaptive gain matrix Γ is set to different values for each current input profile. It is adjusted according to the frequency of the input current and its values for each simulation are given in Table 3.1 in where $I_{3\times3}$ is the 3-by-3 identity matrix. For example, the current input profile with the higher frequency requires using a smaller Γ. This is because the input signal excites the system better with high frequency. As a result, the estimated parameters converge to the actual parameters faster. However, the adaptation speed (the rate of change in $\dot{\hat{\boldsymbol{\theta}}}$) decreases with time and eventually approaches zero. The time interval between two sampling points is 0.01s. The measurement noise variance is 0.1 for both the load current and the terminal voltage. The battery's initial SoC is 100% in every simulation and it is completely discharged at the end of each simulation. Note that the standard DST cycle initially charges the battery for 7 seconds. Only in the DST cycle simulation, the initial SoC is 99.95% not to overcharge the battery. The time duration to complete each simulation is different due to the different charge/discharge rates and profiles. For simulation purposes, the battery has the following true model parameters:

$$\boldsymbol{\theta} = \begin{bmatrix} \alpha & -R_0 & \varrho \end{bmatrix}^T = \begin{bmatrix} 0.99 & -0.1\Omega & 0.2960 \end{bmatrix}^T \tag{3.44}$$

The initial values for the parameters are chosen as follows:

$$\hat{\boldsymbol{\theta}}_0 = \begin{bmatrix} \alpha_0 & -R_{0,0} & \varrho_0 \end{bmatrix}^T = \begin{bmatrix} 0.5 & -0.01\Omega & 0.01 \end{bmatrix}^T \tag{3.45}$$

where initial parameters are intentionally chosen with large errors to assess if the parameter estimation algorithm is dependent on the initial value.

Table 3.1: The adaptive gain, Γ, for each simulation scenario

Current input profile in the simulation	Γ
CC discharge	500 $I_{3\times3}$
Sinusoidal discharge	100 $I_{3\times3}$
HPPC	0.15 $I_{3\times3}$
DST	0.1 $I_{3\times3}$

3.4 Results

The following results show that the adaptive law-based parameter estimation algorithm can accurately determine the battery's parameters for various charge/discharge rates and profiles. One of the main findings from the simulation results is that increasing Γ increases the rate of parameter convergence and reduces the impact of the current input frequency on the parameter convergence speed.

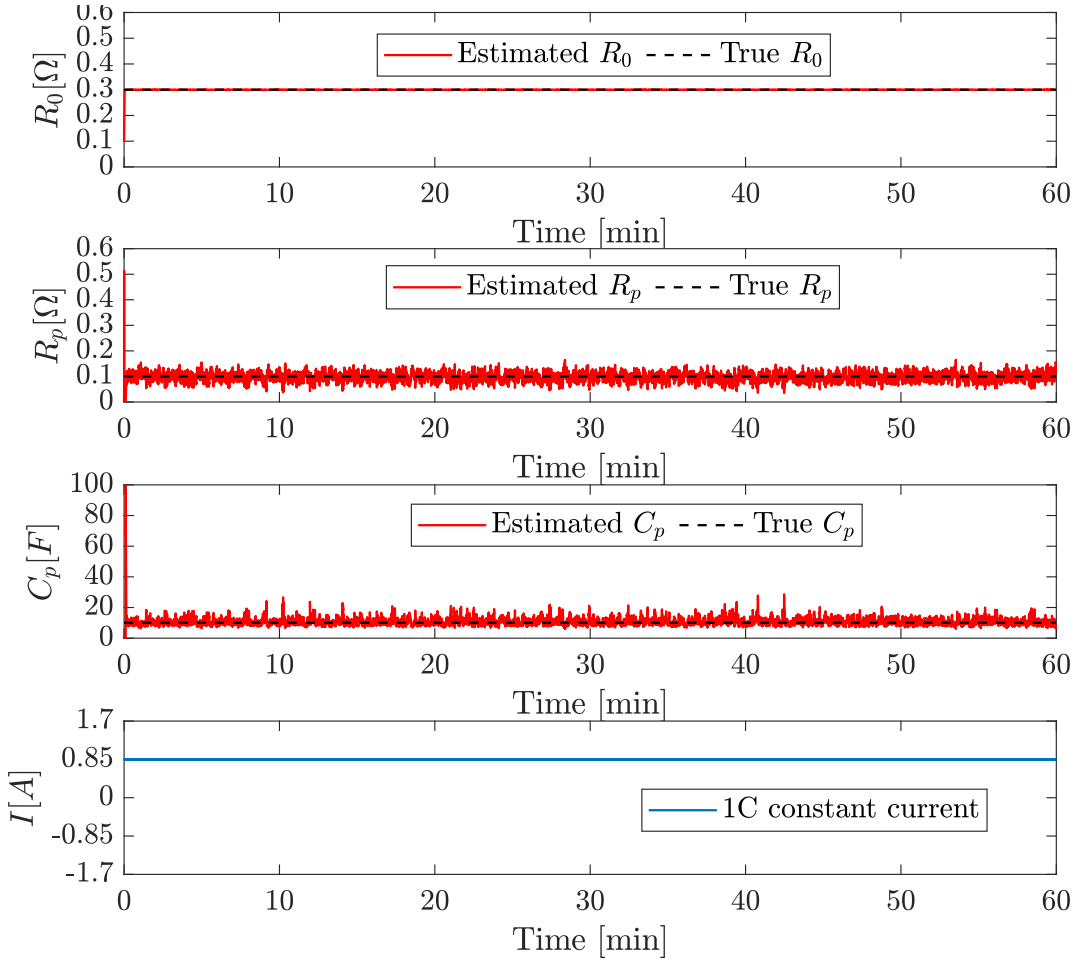

Figure 3.2: ECM model parameter estimation results under 1C constant current discharge

Figures 3.2, 3.3, 3.4, and 3.5 illustrate the convergence of the battery model parameters

under different charge/discharge current profiles. The convergence time is slightly different for each current input profile due to using different Γ and different input signal frequencies. For example, parameters converge almost instantly within 10 seconds under a constant current discharge profile as shown in Figure 3.2. This is because Γ is set to a large value. The estimation of R_0 exhibits a persistent trend of around the actual R_0. On the other hand, R_p fluctuates due to the noisy input current.

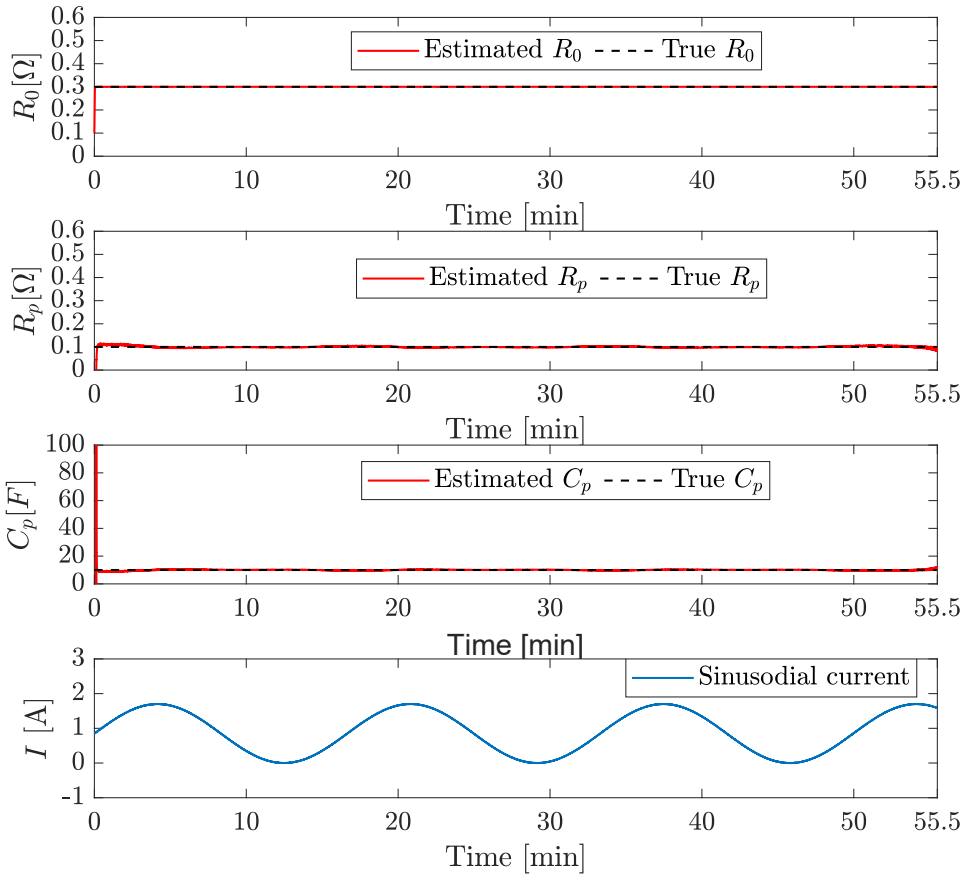

Figure 3.3: Physical parameter estimation results under sine discharge

Using a large Γ increases these fluctuations in R_p. The reverse trend is observed in C_p compare to R_p. The reason for this is that the battery's time constant persists to stay constant throughout the whole simulation. Thus, C_p decreases to compensate for the increase in R_p or vice versa. The optimum Γ can be chosen considering the trade-off between tiny fluctuations and the time duration required for the parameter convergence.

When the sinusoidal current input is applied to the algorithm, the convergence time

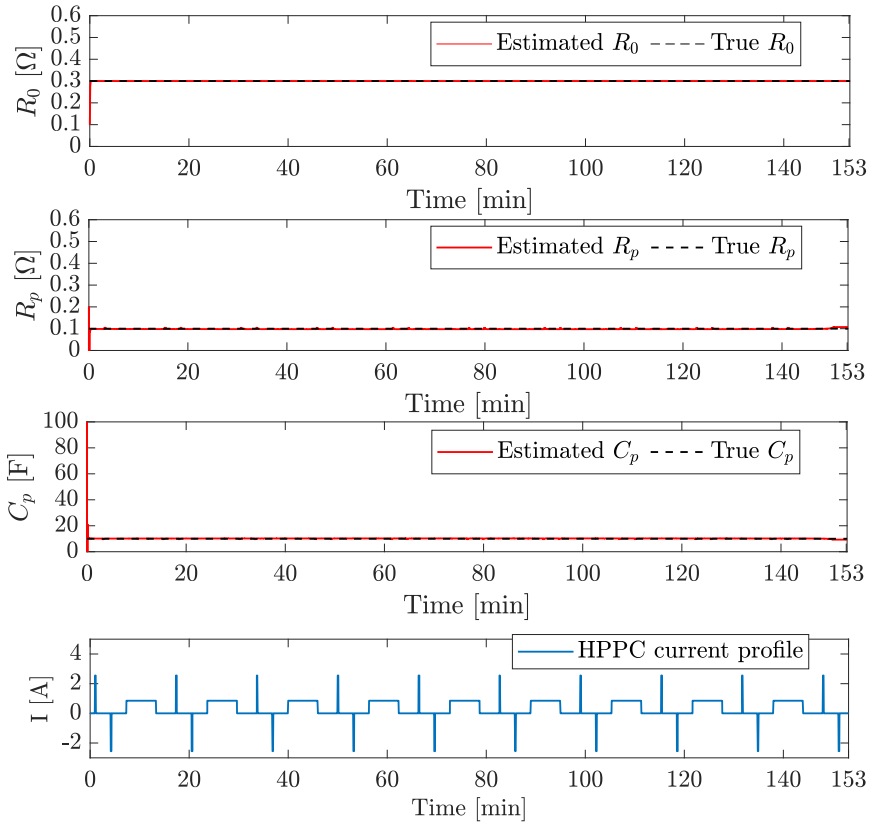

Figure 3.4: Physical parameter estimation results under HPPC current profile

does not change significantly as shown in Figure 3.3. Even though Γ is reduced, the convergence time is almost the same due to the higher frequency of the sinusoidal input profile. Moreover, fluctuations due to the noisy current input almost disappeared.

The trend in the input current profile is softly reflected in the estimated R_p. Decreasing Γ may prevent the estimated R_p from having the same trend as the input current. However, this would make the initial convergence time longer.

Figure 3.4 shows the parameter estimation results under HPPC current profile. When the input current profile is switched to more complicated profiles similarly to HPPC and DST cycles, Γ is significantly reduced. Therefore, sudden fluctuations and significant reflection of the current profile trend in estimated parameters are avoided. Furthermore, the input current frequency is greater in these simulations, therefore adopting a lower Γ would not significantly affect the convergence speed. Although Γ is 1.5 times greater in the HPPC cycle than that in the DST cycle, the convergence speed is higher under the DST cycle as shown in Figure 3.5. This is also explained by the input current frequency. Hence, it can be concluded that the input with a higher

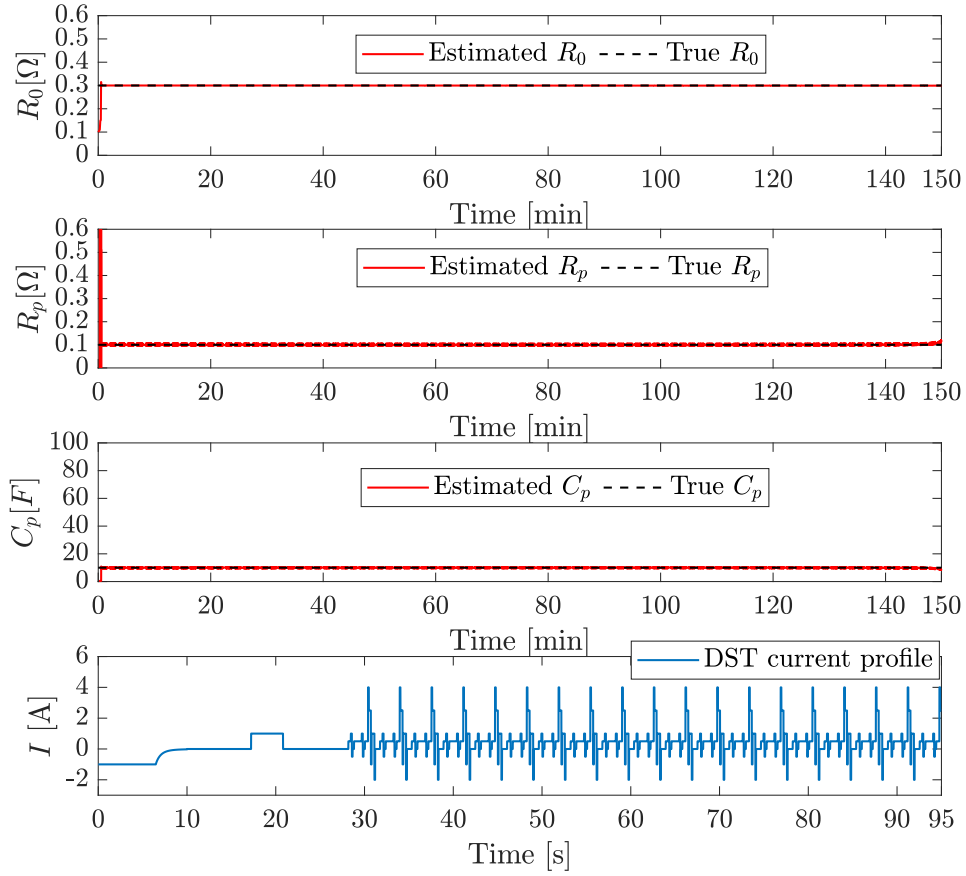

Figure 3.5: Physical parameter estimation results under dynamic stress test

frequency increases the parameter convergence speed.

3.5 Battery experiment

Figure 3.6 shows a battery test rig with three DC motors powered by a fresh LiPo battery whose capacity is 1 Ah. During battery operation, I and V_t are the measurable signals and they are acquired via NI 9505 and NI 9215 devices. CompactRio is the microprocessor used in the test rig. A graphical user interface is designed on LabVIEW software to control the speed of DC motors. Using a constant-current constant-voltage mode, the battery has been charged via the commercial battery charger. The charger can also discharge the battery under a constant current. In order to prevent electrodes from being overcharged, a 8.4V upper cut-off voltage is set. In the same manner, when the terminal voltage reaches 6.4V, the battery is considered fully discharged. The room temperature is at 25°C ±3°C and remains constant during the experiment. The

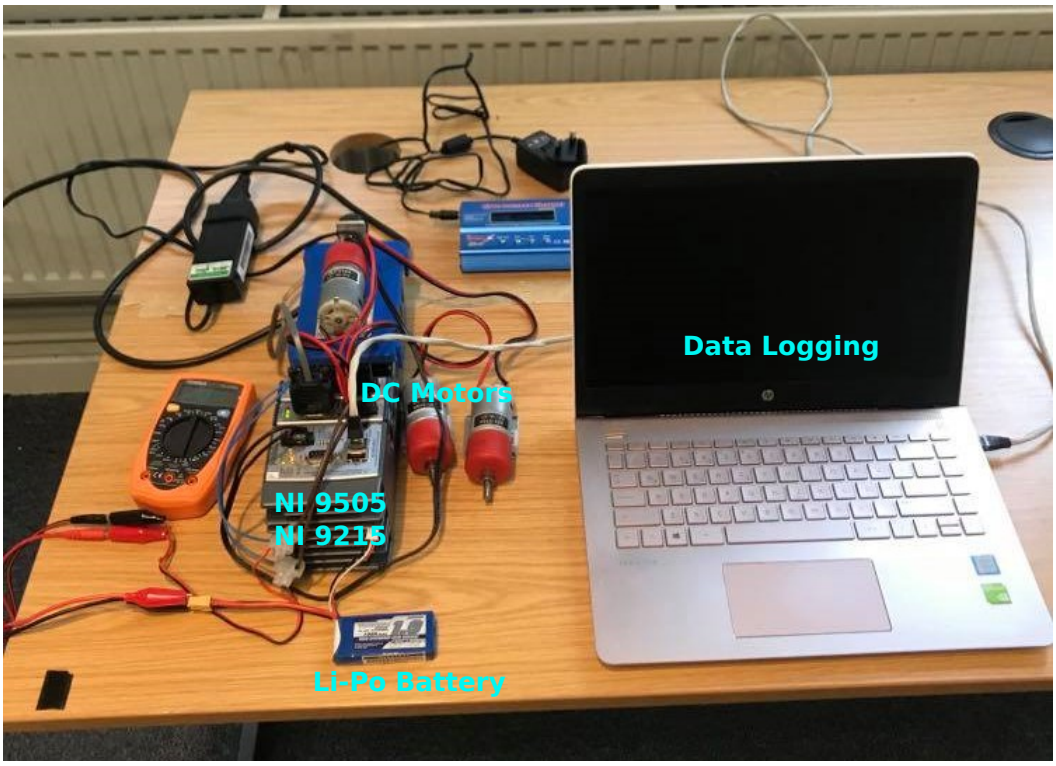

Figure 3.6: Battery test rig

motor speed is set to 50 rpm (revolutions per minute) and it remains constant during the experiment. Data is saved every 0.01 seconds.

Figure 3.7 shows the experimental results of the parameter estimation algorithm. The model parameters of the actual battery converge fast. The internal resistance R_0 almost remains constant during the experiment. However, R_p slightly decreases until the moderate SoC regions, and then it starts increasing. In low SoC regions, it increases drastically as the SoC decreases. Similar to the simulation results, C_p has the reverse trend to balance the battery's time constant.

To sum up, the model parameter identification algorithm based on the adaptive law is a reliable candidate for SoC estimation since its stability is proved in the sense of Lyapunov stability. Furthermore, the PE input guarantees the convergence of the model parameter to their actual values. The results indicate that the adaptive law-based parameter identification method can be implemented to accurately calculate battery model parameters in practice.

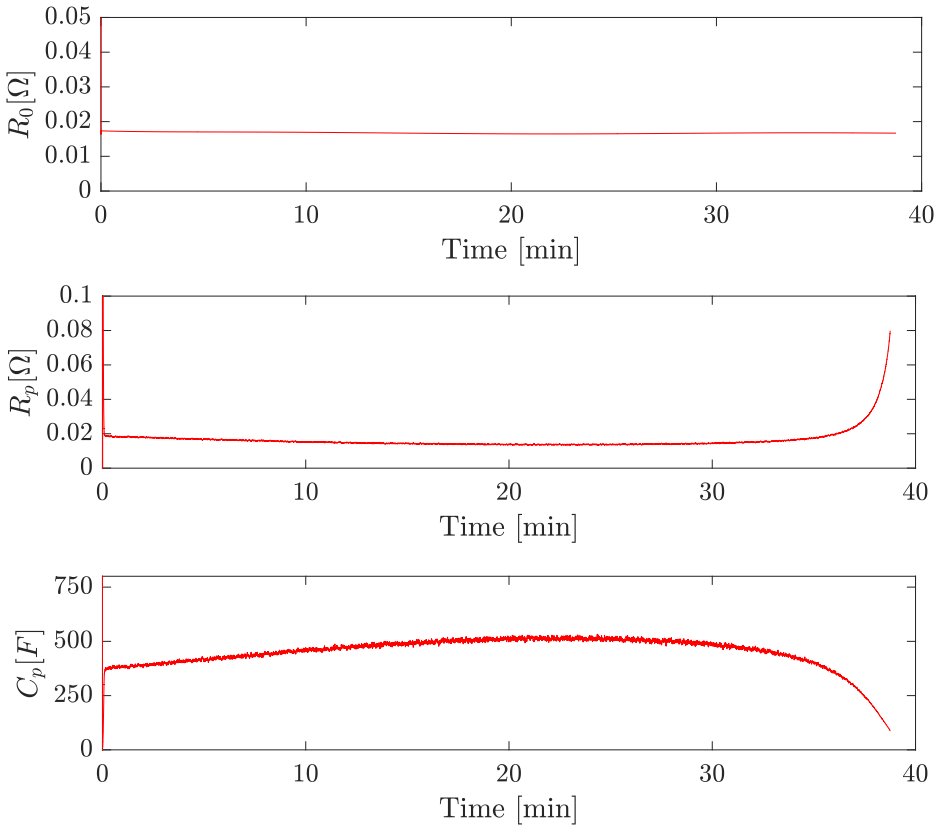

Figure 3.7: Battery model parameter estimation results by a battery experiment

3.6 Discussion

This chapter provides the details of the first order Thevenin ECM and the designing procedure of an online parameter estimation algorithm based on the adaptive law. It also explains the design of the battery test rig. The first-order Thevenin ECM is widely used in practical applications including EVs. It successfully mimics the polarisation characteristic of the battery by adopting a parallel RC branch. The battery model is validated by the battery experiment. In order to design an online parameter estimation algorithm, the battery model is firstly converted into the LPM form. This allows us to build an online parameter estimation algorithm by correcting the estimated parameters based on the difference between the measured output and the estimated output. The adaptive law-based parameter identification method is designed to estimate the battery model parameters in real-time. The designing procedure also includes the stability analysis of the parameter identification algorithm based on the Lyapunov direct method.

The stability analysis shows that the proposed method guarantees that the estimated output converges to the measured output. However, the convergence of the model parameters to their actual values can be guaranteed only if the system is persistently excited by the input signal. In most of the practical situations, the input vector is PE if the battery is charged or discharged. In detail, the measured ϕ usually carries sufficient information to the parameter estimation algorithm. Therefore, the model parameters usually converged to the actual values in the simulations. However, the convergence speed varies depending on the current input profile and Γ.

In conclusion, the proposed battery model and the parameter identification method are validated by the simulations and the battery experiment. Simulation and experimental results show that the first-order Thevenin ECM can accurately reflect the battery dynamics. The results also demonstrate the effectiveness of the online parameter estimation algorithm under noisy sensor measurements. Especially, if stability is the requirement to meet in any state estimation algorithm, the adaptive law gains more importance to calculate the model parameters. The first-order Thevenin model with the adaptive law-based parameter estimation algorithm can be used for the SoC estimation algorithms in real-time applications including EVs.

Chapter 4

The SoC and OCV Relationship

A relationship between the SoC and the OCV is essential for all ECM-based SoC estimation algorithms. This relationship must be predefined to execute the SoC estimation algorithm. It is challenging to define an accurate relationship because the relationship changes due to operational conditions, battery ageing, and battery hysteresis. Battery hysteresis is a complex phenomenon that causes OCV voltage differences between the charging and discharging cycles. Battery ageing and the ambient temperature significantly affect the SoC-OCV characteristic. Despite the relationship is affected by these aforementioned factors, it is commonly obtained by an offline SoC drop test. After SoC and OCV data points are collected, the nonlinear model is determined by applying a curve fitting to the data. The most widely used nonlinear model is the polynomial function, but there are other types of functions used to model the relationship. For example, a combination of a linear function, a power function, and a logarithmic function is proposed to describe the OCV model by Plett 2004b. Rui Xiong, Sun, et al. 2013 modified Plett's SoC-OCV model by adding a polynomial function. Tong et al. 2015 proposed another SoC-OCV model by removing the power functions from the model proposed by Plett 2004b.

The nonlinear SoC-OCV relation is commonly assumed to be known and is used to map a value of OCV to its corresponding SoC value. However, the true SoC-OCV relation changes due to battery ageing and temperature change. This difference is directly reflected as an error in SoC estimation by Zheng et al. 2018. Similar to the parameter estimation, the SoC-OCV relation could be obtained through an experimen-

tal procedure explained by Shehab El Din et al. 2018, which is vulnerable to a change in operational conditions. The effect of the SoC-OCV model and characterisation tests on the accuracy of SoC estimation is investigated by Knap et al. 2021. Different types of tests are performed to acquire the SoC-OCV characteristic depending on various operational conditions. Nonetheless, this relationship can only be applied to a specific battery and condition used during the test. The SoC-OCV curve at different temperatures is identified offline and mapped by using the polynomial electrochemical equation by Shu et al. 2020. The equation does not consider the effect of battery ageing on the SoC-OCV curve, which deteriorates the accuracy of SoC estimation eventually. Song et al. 2019 obtained the curve by sorting the estimated OCV according to SoC calculated using the CC technique. However, it is expected that the accuracy of the curve decreases with time since the CC technique stores the error at each calculation step. Dewangga et al. 2018 modelled the relation by using piece-wise linear functions and it is assumed that the SoC-OCV relation is fixed, which does not take into account the changes in the true relation. We propose an adaptive estimation algorithm for the SoC with a new nonlinear SoC-OCV curve. The algorithm estimates the parameters describing the SoC-OCV curve based on the battery boundary conditions and current measurement. Unlike other algorithms, the proposed method does not require hybrid methods and high experimental labour. In our work, the average SoC estimation error is calculated as less than 1.53% in computer simulations and 2.48% in battery experiment. To the best of the authors' knowledge, these results show superiority over the results in the literature.

The error in the curve fitting or the error due to the change in the actual relationship degrades the SoC estimation accuracy. These foreknown error sources can be mitigated by estimating the nonlinear relationship in real time. This chapter introduces a novel technique to obtain the relationship online. Thus, the estimated SoC-OCV relationship considers the changes in operational conditions, battery ageing, and battery hysteresis.

4.1 The SoC-OCV relationship modelling

A novel online method is proposed to establish the SoC-OCV relationship in real-time. The proposed method obtains the SoC-OCV relationship by establishing a parameter estimation problem. Firstly, the OCV estimation is required for the real-time

SoC-OCV curve construction. Therefore the KF based OCV estimation algorithm is introduced in the following section.

4.1.1 OCV Estimation Using Kalman Filter

As OCV slowly varies in most of the practical cases, it is assumed to be a piece-wise constant, hence

$$V_{oc,k+1} = V_{oc,k} + w_{V_{oc},k} \tag{4.1}$$

where V_{oc} is the OCV, $w_{V_{oc},k}$ is the zero-mean Gaussian random process noise. The propagation of the current, I_a, is given by

$$I_{a,k+1} = \hat{\alpha}_k I_{a,k} + (1 - \hat{\alpha}_k) I_k + w_{I_a,k} \tag{4.2}$$

where $\hat{\alpha}_k = \hat{\theta}_k^{(1)}$, $w_{I_a,k}$ is the zero-mean Gaussian random process noise. $w_{V_{oc},k}$ and $w_{I_a,k}$ are independent to each other. Equations (4.1) and (4.2) are the governing state-space equations. The measurement equation is given by

$$\tilde{V}_{t,k} = V_{oc,k} - I_{a,k}\hat{R}_p - I_k\hat{R}_0 + v_{y,k} \tag{4.3}$$

where $\tilde{V}_{t,k}$ is the measured terminal voltage, I_k is the charging or discharging terminal current at k-th sample and $v_{y,k}$ is the measurement noise. In a compact form,

$$\begin{aligned} x_{k+1} &= A_k x_k + B_k u_k + w_{x,k} \\ y_k &= C_k x_k + D_k u_k + v_{y,k} \end{aligned} \tag{4.4}$$

where

$$\begin{aligned} x_k &= \begin{bmatrix} I_{a,k} & V_{oc,k} \end{bmatrix}^T, \;\; y_k = \tilde{V}_{t,k}, \;\; u_k = I_k \\ A_k &= \begin{bmatrix} \hat{\alpha}_k & 0 \\ 0 & 1 \end{bmatrix}, \;\; B_k = \begin{bmatrix} 1 - \hat{\alpha}_k \\ 0 \end{bmatrix}, \; Cw_{x,k} = \begin{bmatrix} w_{V_{oc},k} \\ w_{I_a,k} \end{bmatrix} \\ C_k &= \begin{bmatrix} -\hat{R}_p & 1 \end{bmatrix}, \;\; D_k = -\hat{R}_0, \end{aligned} \tag{4.5}$$

the covariance of $w_{x,k}$ is Q and the variance of $v_{y,k}$ is r. Note that the measurement noise is independent from the process noise.

4.1.2 Model construction in real-time

In general, the slopes of the SoC-OCV curve change drastically from the low values to the high values. The nonlinear function must be a one-to-one increasing nonlinear function as SoC increases. Firstly, the potential candidate model of the SoC-OCV relationship must meet these two requirements. Secondly, the number of model parameters to be identified must not be more than three. The latter requirement allows us to estimate the model parameters in real-time based on the boundary conditions and measurements.

Considering these two requirements, we establish the following novel nonlinear model to capture these characteristics with three modelling parameters:

$$V_{oc} = a\log(z) + be^{z^3} + c \tag{4.6}$$

where a, b and c are the coefficients to be estimated, which are different for every battery and vary for each condition, z is the SoC in $[\delta, 1]$ and δ is a small positive number. The SoC below δ is considered to be zero. This nonlinear equation expresses the typical shape of the SoC-OCV curve and their variations. The logarithmic term is to capture relatively fast change in the OCV in low SoC regions. The exponential term is to capture the OCV change in the rest of the SoC regions. The constant term describes the nominal OCV value. By estimating the three parameters, the estimated SoC-OCV curve in real-time adapts to the variations caused by the operational condition and battery condition.

In electronics, the lower cut-off voltage is the voltage at which the battery is fully discharged. At this voltage, the battery SoC is equal to 0 as follows:

$$V_{\text{low}} = V_{oc}|_{z=0} \approx V_{oc}|_{z=\delta} \approx a\log\delta + b + c \tag{4.7}$$

where V_{low} is the lower cut-off voltage of the battery, which is given in the battery specifications. Similarly, V_{oc} is equal to the higher cut-off voltage, V_{high}, when the battery is fully charged, as follows:

$$V_{\text{high}} = V_{oc}|_{z=1} = be + c \tag{4.8}$$

Subtract (4.7) from (4.8)

$$V_{\text{high}} - V_{\text{low}} = b(e-1) - a\log\delta \tag{4.9}$$

Solve for b as follows:

$$b = b(a) = \frac{\Delta V_{hl} + a\log\delta}{e-1} \tag{4.10}$$

where $\Delta V_{hl} = V_{\text{high}} - V_{\text{low}}$. Substitute (4.10) into (4.8), and solve for c as follows:

$$c = c(a) = V_{\text{high}} - b(a)e \tag{4.11}$$

The derivative of (4.6) with respect to z is

$$\frac{dV_{oc}}{dz} = \frac{a}{z} + 3be^{z^3}z^2 \tag{4.12}$$

Solve the equation for a

$$a = \frac{f(dV_{oc}/dz, z)}{g(z,\delta)} = \frac{(dV_{oc}/dz)\,z\,(e-1) - 3\Delta V_{hl}e^{z^3}z^3}{(e-1) + 3e^{z^3}z^3\log\delta} \tag{4.13}$$

The number of the parameter to be estimated for the SoC-OCV curve is reduced to 1, i.e., estimating a given by (4.13). The denominator of (4.13), $g(z,\delta)$, may approach zero depending upon z and δ and it would cause the numerical problem.

Algorithm 1 is to prevent the numerical problem to calculate a. The current value of b is assumed to be constant for the neighbourhood of the singular point and (4.12) is used directly to calculate a. The calculated a in the algorithm denoted by $\tilde{a}_k$, is treated as the measurement in the estimation algorithm presented later.

Algorithm 1 Calculation of $\tilde{a}_k$

1: Set $\epsilon_1 > 0$, a small positive number
2: Calculate $g(\hat{z}_k, \delta) = (e-1) + 3e^{\hat{z}_k^3}\hat{z}_k^3\log\delta$
3: **if** $|g(\hat{z}_k,\delta)| < \epsilon_1$ **then**
4: Let $\hat{b}_k = \hat{b}_{k-1}$
5: Calculate $\tilde{a}_k$ from (4.12)
6: $\tilde{a}_k = \hat{z}_k(dV_{oc}/dz)_k - 3\hat{b}_k e^{\hat{z}_k^3}\hat{z}_k^3$
7: **else**
8: Calculate $\tilde{a}_k$ using (4.13)

To calculate (4.12) or (4.13), the OCV derivative with respect to the SoC is required.

Providing the estimates of the OCV, $\hat{V}_{oc}$, the following difference is calculated:

$$\Delta\hat{V}_{oc,k+1} = \hat{V}_{oc,k+1} - \hat{V}_{oc,k} \tag{4.14}$$

where $\hat{V}_{oc,k+1}$ and $\hat{V}_{oc,k}$ are provided by the KF designed in Algorithm 2. In addition, as the SoC propagation equation is given by T. Ouyang et al. 2021

$$z_{k+1} = z_k - \frac{I_k \Delta t}{Q_{\max}} \tag{4.15}$$

where $Q_{\max}$ is the battery capacity constant and Δt_s is the sampling time, the differential z at step $k+1$ is calculated as follows:

$$\Delta z_{k+1} = -\frac{I_k \Delta t}{Q_{\max}} \tag{4.16}$$

where $\Delta z_{k+1} = z_{k+1} - z_k$. Therefore, the derivative can be approximated by the first-order difference as follows:

$$\left.\frac{dV_{oc}}{dz}\right|_{k+1} \approx \frac{\Delta\hat{V}_{oc,k+1}}{\Delta z_{k+1}} = -\frac{\Delta\hat{V}_{oc,k+1} Q_{\max}}{I_k \Delta t} \tag{4.17}$$

and the approximation with the current z are substituted into (4.13). Equation (4.6) is now written as a function of z only. Therefore, the estimation of z leads to the estimation of SoC-OCV curve.

The SoC estimation problem has the linear state propagation equation, (4.15), and the nonlinear measurement equation, (4.6). The EKF for estimation z, i.e., $\hat{z}$, is given in Algorithm 2, where the observation matrix is defined by the following Jacobian

$$H_k = \left.\frac{\partial V_{oc}}{\partial z}\right|_{z=\hat{z}_k, a=\hat{a}_k} = \frac{\hat{a}_k}{\hat{z}_k} + 3b(\hat{a}_k)e^{\hat{z}_k^3}\hat{z}_k^2 \tag{4.18}$$

where $\hat{a}_k$ is to be estimated.

The direct substitution of $\tilde{a}_k$ in Algorithm 1 into (4.18), however, would amplify undesirable noises in the measurements and the estimated values. Additional KF is designed for estimating a, where it is assumed that a varies slowly in each sampling interval, i.e.,

$$a_{k+1} = a_k + w_{a,k} \tag{4.19}$$

where $w_{a,k}$ is the process noise with the zero-mean and the variance equal to q_a. To apply the KF design procedure, $\tilde{a}_k$ from Algorithm 1 is treated as the measurement and assumed to have the following measurement noise characteristic:

$$\tilde{a}_k = a + v_{a,k} \tag{4.20}$$

where $\tilde{a}_k$ is the measurement of the true a. $v_{a,k}$ is the zero mean Gaussian measurement noise, which is independent to the process noise, $w_{a,k}$. To calculate the variance of $v_{a,k}$, $z_k^{(i)}$ samples are generated as follows:

$$z_k^{(i)} = \hat{z}_k + v_{z,k}^{(i)} \tag{4.21}$$

where $i = 1, 2, \ldots, N_s$, N_s is the number of samples and $v_{z,k}^i$ is the zero-mean Gaussian with the variance equal to $r_{z,k}$. The $\tilde{a}_k^{(i)}$ particles are calculated by substituting $z_k^{(i)}$ samples into Algorithm 1. The variance of $v_{a,k+1}$ is then calculated by the samples as follows:

$$r_{a,k} = \frac{\sum_{i=1}^{N_s} \left[\tilde{a}_k^{(i)} - \bar{a}_k\right]^2}{N_s - 1} \tag{4.22}$$

where $\bar{a}_k = \sum \tilde{a}_k^{(i)}/N_s$. Finally, the algorithm to estimate SoC is summarized in Algorithm 2, where $(\cdot)_{k+1|k}$ is the priori prediction of $(\cdot)$ and $(\cdot)_{k+1|k+1}$ is the posteriori estimation of $(\cdot)$. Using separate KF algorithms to estimate OCV, coefficient a and SoC is recommended in order to reduce computational cost.

Algorithm 2 includes three separate KF algorithms. The standard KF algorithm is used to estimate the OCV and a separately and the EKF is utilised to estimate the SoC.

4.2 Simulations

A battery with 100% SoC is discharged under different current profiles including constant current profile, sinusoidal current profile, HPPC current profile and DST cycle current profile. Note that the battery's SoC is 99.95% in the DST cycle simulation not to overcharge the battery at the start. These testing profiles are adopted to assess the performance of the SoC-OCV curve construction algorithm under various dynamic

Algorithm 2 Adaptive SoC estimation algorithm

Initialise: $\hat{\theta}_0$, $\hat{\boldsymbol{x}}_0$, P_0, $\hat{z}_0$, $p_{z,0}$, $\hat{a}_0$ and $p_{a,0}$
while true **do**
  Obtain the measurement and input: $\tilde{V}_{t,k}$, I_k
  Run the parameter estimation using (3.35), (3.36) & (3.19)
  Run **Algorithm 1** to obtain $\tilde{a}_k$
  Calculate the variance of $\tilde{a}_k$ using (4.21) & (4.22)
  Propagate
    $\hat{x}_{k+1|k} = A_k \hat{x}_{k|k} + B_k u_k$
    $P_{k+1|k} = A_k P_{k|k} A^T + Q$
    z using (4.15)
    $p_{z,k+1|k} = p_{z,k|k} + q_z$
    $\hat{a}_{k+1|k} = \hat{a}_{k|k}$
    $p_{a,k+1|k} = p_{a,k|k} + q_a$
  Update
    $L_{k+1} = P_{k+1|k} C_k^T / \left[C_k P_{k+1|k} C_k^T + r \right]$
    $\hat{x}_{k+1|k+1} = \hat{x}_{k+1|k} + L_{k+1} \left(\tilde{V}_t - \hat{V}_{t,k+1|k} \right)$
    $P_{k+1|k+1} = (1 - L_{k+1} C_k) P_{k+1|k}$
    $K_{z,k+1} = p_{z,k+1|k} H_k^T / (H p_{z,k+1|k} H_k^T + r_z)$
    $K_{a,k+1} = p_{a,k+1|k} / (p_{a,k+1|k} + r_{a,k+1})$
    $\hat{a}_{k+1|k+1} = \hat{a}_{k+1|k} + K_{a,k+1} \left(\tilde{a} - \hat{a}_{k+1|k} \right)$
    $p_{a,k+1|k+1} = (1 - K_{a,k+1}) p_{a,k+1|k}$
    $\hat{z}_{k+1|k+1} = \hat{z}_{k+1|k} + K_{z,k+1} \left(\tilde{V}_{oc} - \hat{V}_{oc,k+1|k} \right)$
    $p_{z,k+1|k+1} = (1 - K_{z,k+1} H) p_{z,k+1|k}$
  Repeat

loading conditions. The battery's maximum capacity is 0.85 Ah. The battery model parameters are estimated online based on the adaptive law and fed into the algorithm. For the simulation purpose, the actual SoC-OCV curve is modelled by a rational function given by

$$V_{oc}(z) = \frac{\sum_{j=0}^{4} k_j z^j}{\sum_{j=0}^{4} q_j z^j} \tag{4.23}$$

where $k_0 = 16.65$, $k_1 = 516.2$, $k_2 = 519.9$, $k_3 = 5.696$, $k_4 = -4.523$, $q_0 = 2.591$, $q_1 = 70.68$, $q_2 = 61.26$, $q_3 = 14.07$, $q_4 = -24.92$. The initial values of V_{oc}, I_a, a, and z are 7V, 0A, 0.1, and 0, respectively. The covariance and the variance of OCV estimation are $Q = 0.01\mathrm{I}_{2\times2}$ and $r = 0.1$, where $\mathrm{I}_{2\times2}$ is the 2-by-2 identity matrix. V_{high} is 8.4756V and V_{low} is 6.4735V. δ is set to 0.001 and ϵ_1 is set to 0.1. The initial p_z, p_a, r_z and r_a are set to 0.001. N_s is set to 100.

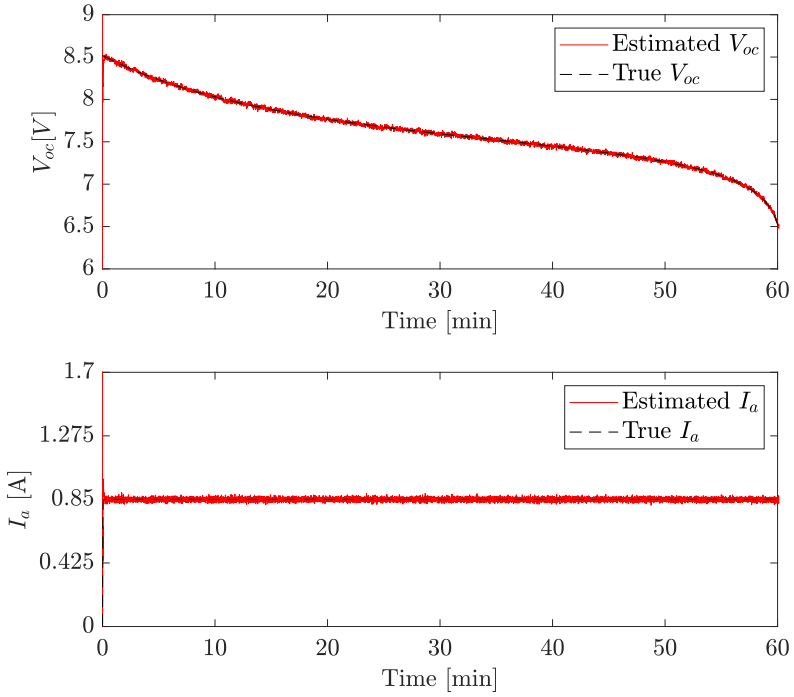

Figure 4.1: V_{oc} and I_a estimation under constant current discharge

4.3 Battery experiment

The battery test rig introduced in the previous chapter is used to validate the SoC-OCV curve construction algorithm. The LiPo battery's actual capacity is firstly calculated. The SoC-OCV data points are then collected to acquire the relationship experimentally. The experimental SoC-OCV relationship is compared to the SoC-OCV relationship estimated using the proposed algorithm.

4.3.1 Battery capacity calculation

Battery specifications include the capacity of the battery along with the lower and upper cut-off voltages. The real capacity may, however, differ slightly from the one stated by the manufacturer. Consequently, the accuracy of the SoC estimation may be affected. Therefore, the battery capacity needs to be experimentally calculated before the estimation algorithm is executed. The experimental battery capacity is calculated by drawing a constant current, i.e. 1C, from the fully charged battery. A battery is considered fully discharged when it reaches the lower cut-off voltage value. This process involves measuring how much current is drained from the battery and how long it takes. In other words, the experimental capacity can be calculated from the

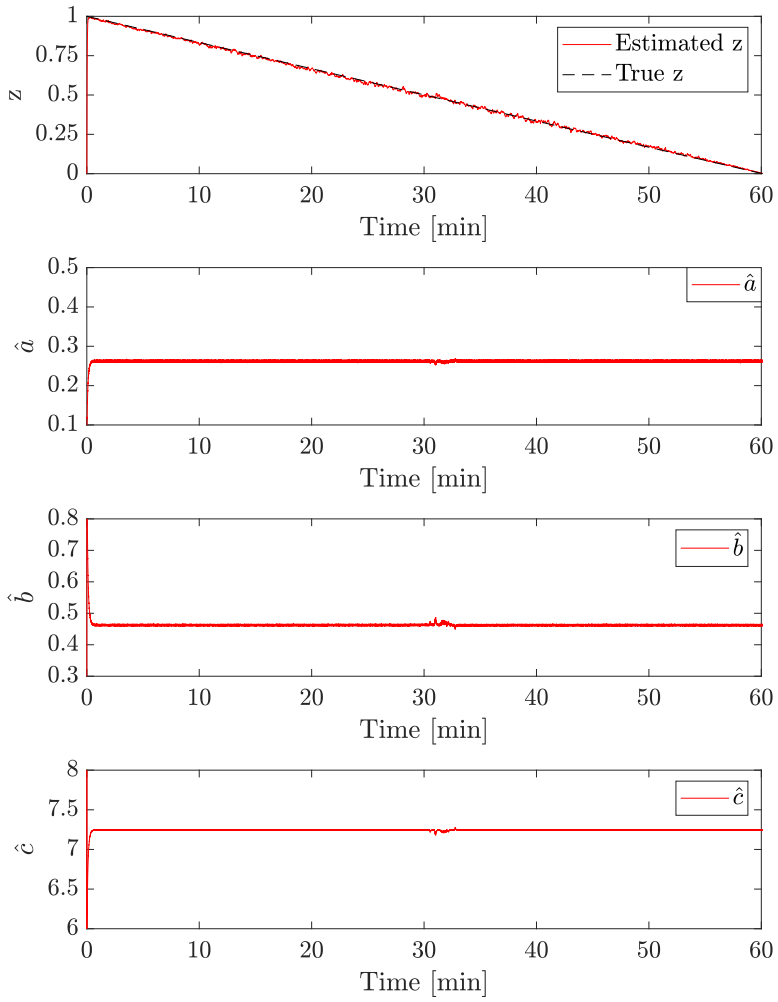

Figure 4.2: SoC and SoC-OCV curve coefficients estimation under constant current discharge

area under the time versus the current graph. This procedure is repeated 5 times and the average capacity is calculated as 0.96 Ah.

4.3.2 The SoC-OCV relationship calculation

The fully charged battery is discharged by 5% intervals until SoC reaches 80% to establish the experimental SoC-OCV relation. After that, the SoC drop interval is increased to 10% until the SoC reaches 20%. The SoC drop rate is again reduced to 5% until the battery is completely discharged. The SoC drop rate was changed to better capture non-linearity at low and high SoC regions.

After each discharging step, the battery is left for resting for an hour. This is because

the battery needs to reach the steady-state so that the measured terminal voltage can be treated as V_{oc} measurement. In the meanwhile, the corresponding SoC is calculated using Coulomb counting method. The same process is repeated by charging the battery with the same SoC drop rates to consider the V_{oc} variations between charging and discharging due to hysteresis. Finally, mean V_{oc} and SoC values are calculated and given in Table 4.1.

Table 4.1: SoC-OCV relation obtained from SoC drop test

z	0	0.05	0.1	0.15	0.2
V_{oc} [V]	6.5688	7.2294	7.365	7.4088	7.4625
z	0.3	0.4	0.5	0.6	0.7
V_{oc} [V]	7.5363	7.5813	7.6401	7.7304	7.8663
z	0.8	0.85	0.9	0.95	1
V_{oc} [V]	8.0011	8.1325	8.2151	8.3038	8.3801

4.4 Results

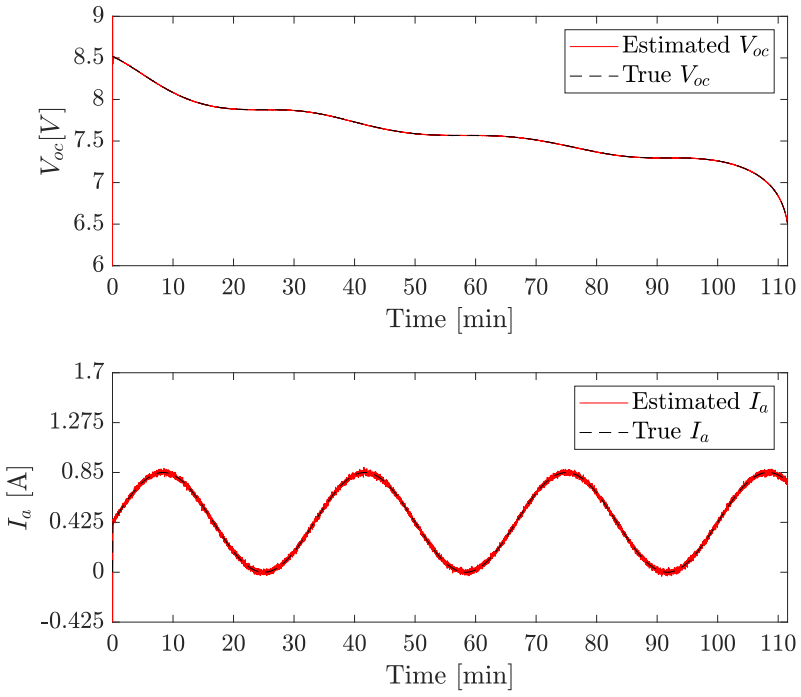

Figure 4.3: V_{oc} and I_a estimation under sinusoidal current discharge

Figure 4.1 shows the estimation result of V_{oc} and I_a under constant current discharge profile. In the parameter estimation results, it is observed that the estimate of the model parameter R_p has tiny fluctuations due to the noise in the input current es-

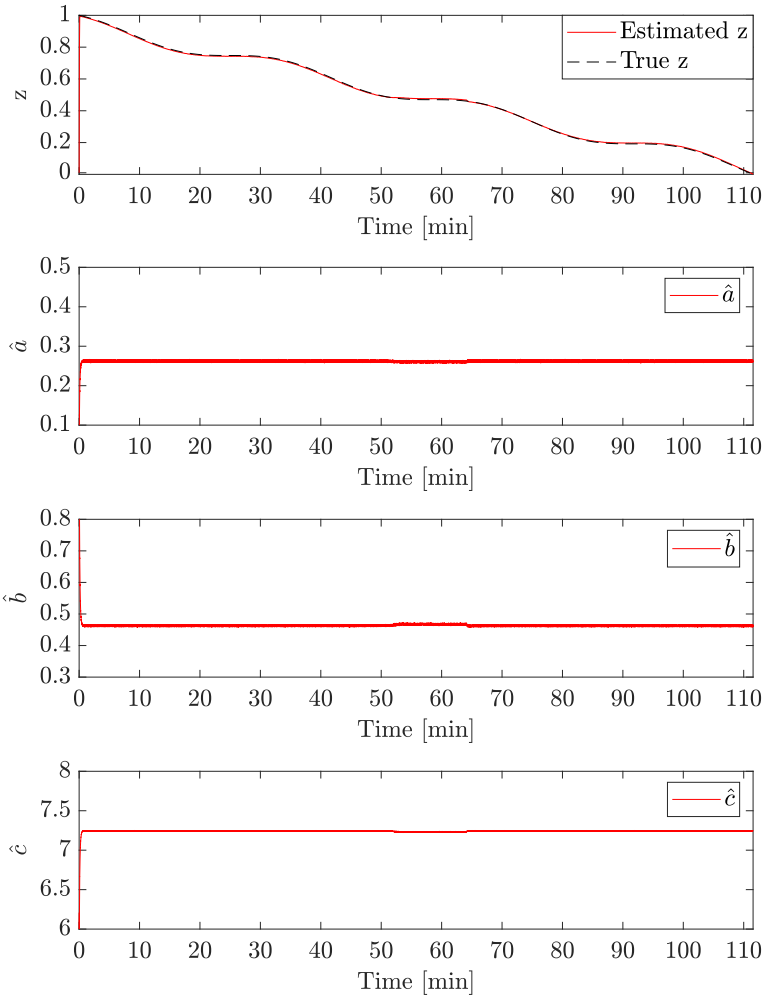

Figure 4.4: SoC and SoC-OCV curve coefficients estimation under sinusoidal current discharge

pecially when the large Γ is used. Therefore, these fluctuations have been observed in the V_{oc} and I_a estimation. However, this does not have a serious impact on the convergence of the state vector. As it is seen in Figure 4.1, estimated states converge to their actual values around 15s, and the convergence is maintained to the end of the simulation.

Figure 4.2 shows estimation results of the SoC and the coefficients a, b, and c under constant current discharge. The SoC converges to its true value within 15s as shown at the top of Figure 4.2. The coefficient a converges to the constant value which is around 0.27 whereas b and c converge to constant values that are around 0.47 and 7.25, respectively.

The slight fluctuations in the estimated coefficients are observed in the middle SoC region, i.e. around 52% of SoC. In this neighborhood, the denominator of (4.13) approaches zero. Algorithm 1 mitigates the singular issues. However, these fluctuations do not affect the convergence of the SoC. Once the singular point is passed, these fluctuations disappeared.

Figure 4.3 demonstrates the V_{oc} and I_a estimation results under the sinusoidal current input profile. These two states converge to their true values very fast within 10s. The sinusoidal current excites the system better compared to the constant current discharge profile. Thus, the model parameters converge faster compared to the constant current discharge scenario. This improves the convergence performance of the V_{oc} estimation algorithm. Compared to the V_{oc} convergence under the constant current discharge profile, the estimated V_{oc} converges to true V_{oc} faster under sinusoidal input current profile as it is in Figure 4.3.

Figure 4.4 illustrates the estimation results of the SoC and the coefficients a, b and c under sinusoidal input current discharge. The coefficients converged to the same constant values as the coefficients calculated in the constant current discharge case. Relatively faster convergence of V_{oc} increased the SoC-OCV curve algorithm performance as well. As shown in Figure 4.4, the SoC converges less than 15s and the coefficients converge relatively faster compared to the result under constant current discharge. Moreover, when the denominator of (4.13) approaches zero, the estimated coefficients show smaller fluctuations compared to the fluctuations in the coefficients in the constant current discharge case.

The proposed algorithm is performed under more complicated dynamic loading profiles. Firstly, the battery is discharged under the DST current profile. Figure 4.5 shows the V_{oc} estimation result along with the current input profile. Figure 4.6 demonstrates the estimated I_a. These two states converge to their true values within 10s. The high frequency in the DST current profile causes tiny fluctuations in the estimated V_{oc} and I_a values. However, the proposed algorithm robustly estimated the states until the end of the simulation.

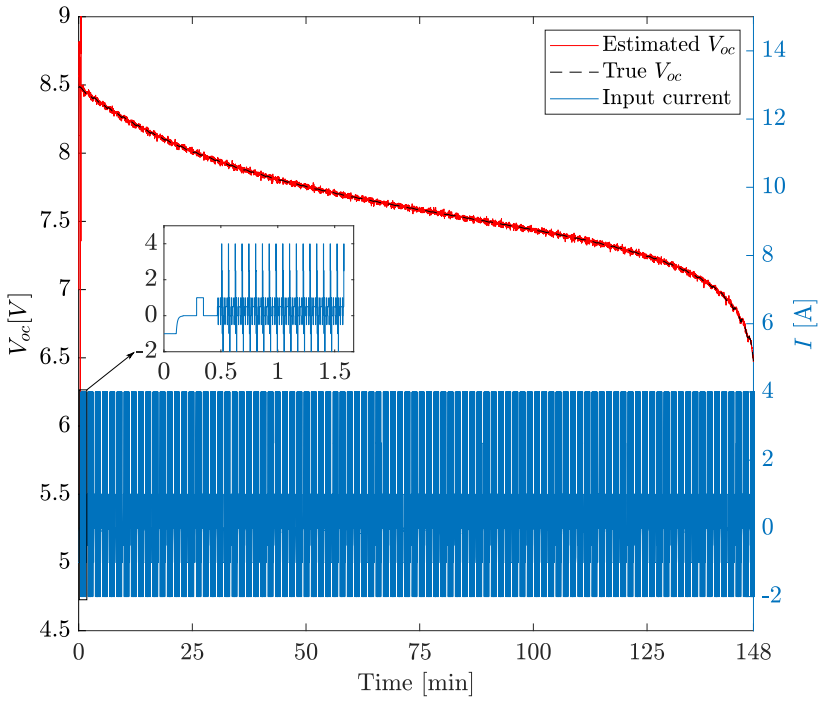

Figure 4.5: Dynamic stress test Voc estimation

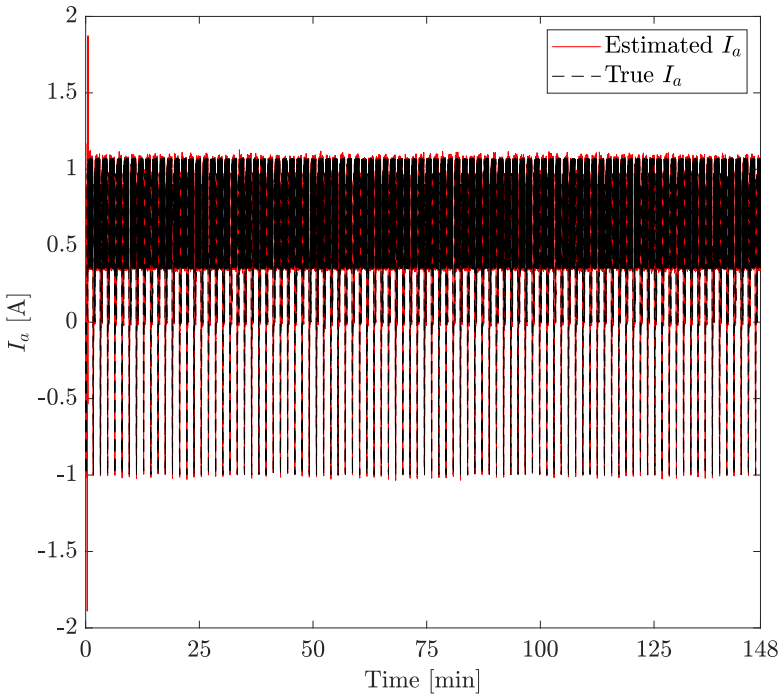

Figure 4.6: Dynamic stress test I_a estimation

Figure 4.7 demonstrates the SoC and the coefficient a, b, and c estimation result under the DST current profile. The coefficients converged to the same constant values

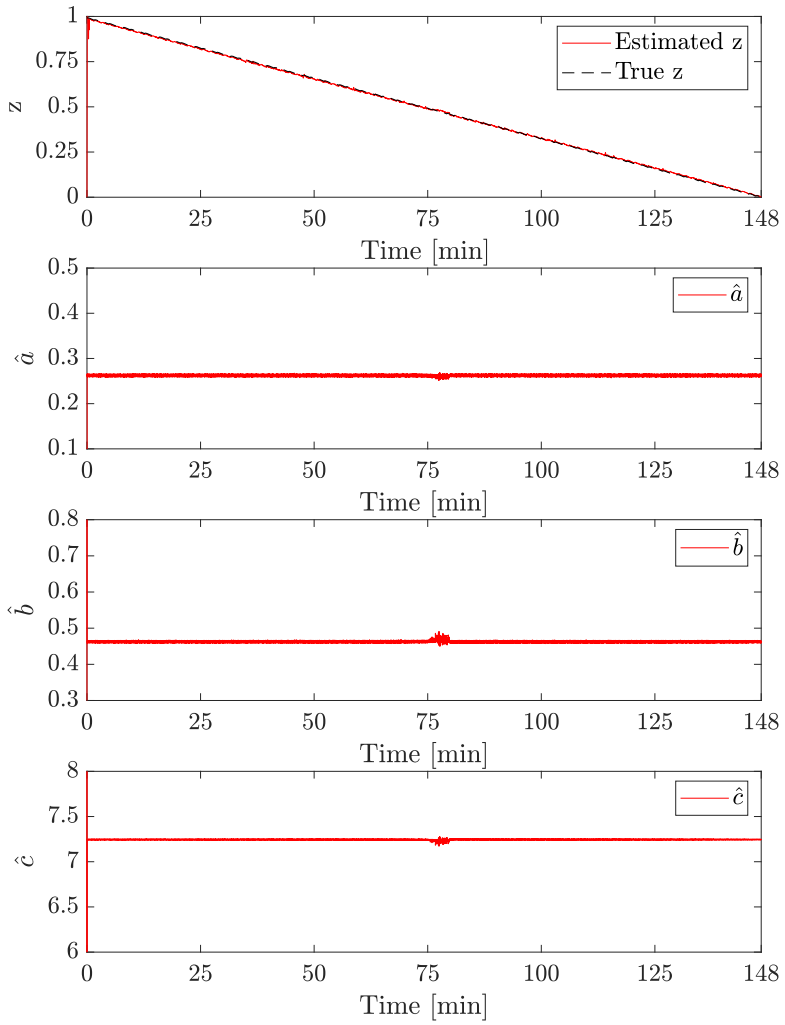

Figure 4.7: SoC and SoC-OCV curve coefficients estimation under DST cycle discharge

same as the constants in the constant current discharge and the sinusoidal discharge cases. The convergence speed of SoC is almost the same as the convergence speed of V_{oc}. The coefficients a, b, and c converge faster compared to those under constant current and sinusoidal current input discharging profiles. This is due to the faster convergence of the model parameters under DST current profile. The fluctuations in the coefficients around the singular point are more obvious in this case. However, these tiny fluctuations do not have a significant effect on the SoC estimation accuracy.

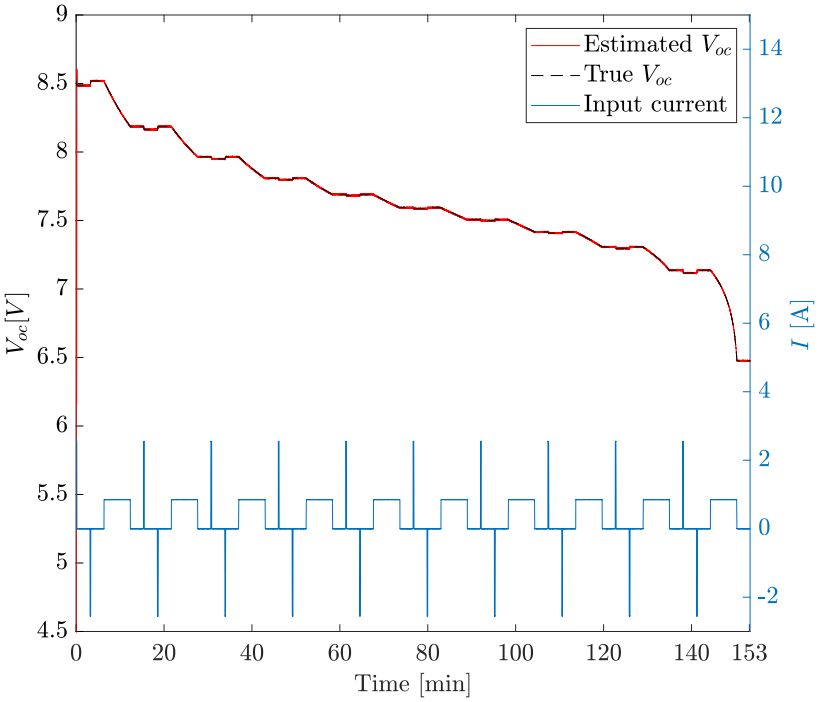

Figure 4.8: HPPC Voc estimation

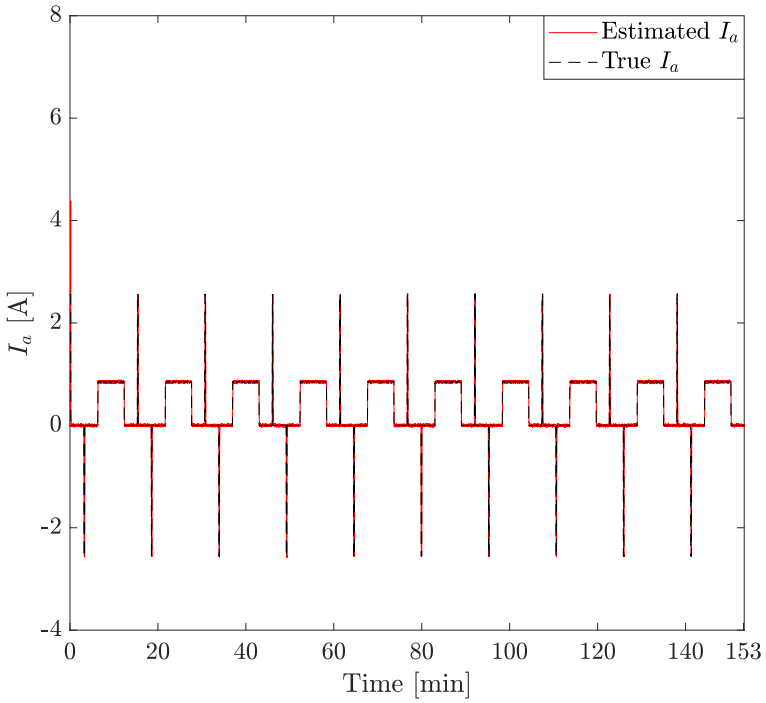

Figure 4.9: HPPC I_a estimation

Figures 4.8 and 4.9 show the convergence of V_{oc} and I_a under HPPC current profile. These two states converged to their true values and remained converged until the end

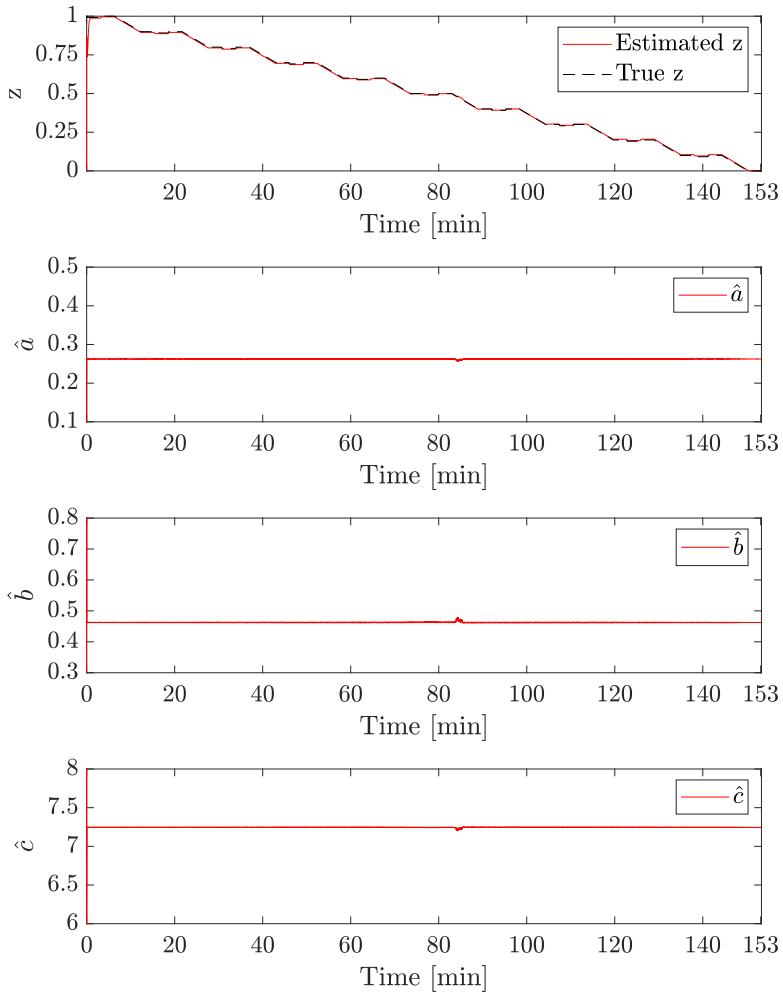

Figure 4.10: SoC and SoC-OCV curve coefficients estimation under HPPC cycle discharge

of the simulation. The pulses in the current input do not cause any jumps in the estimated states. Figure 4.10 shows the convergence of the SoC and the coefficients a, b, and c. The SoC and the coefficients converge fast under HPPC current profile similarly to the previous cases. The proposed algorithm can accurately estimate the battery states under different dynamic loading conditions.

The new nonlinear SoC-OCV model is tested to assess its performance in terms of capturing the variations in the actual SoC-OCV relationship. The SoC-OCV characteristic is dependent on the ambient temperature. When the ambient temperature is lower, the OCV becomes higher or vice versa, however, this behavior is not observed at high SoC regions, i.e. SoC $> 80\%$, (R. Zhang et al. 2018), (Choi et al. 2020). Figure

4.11 shows that the proposed model adequately represents the nonlinear SoC-OCV relation and adapts to the curve variations at different temperatures.

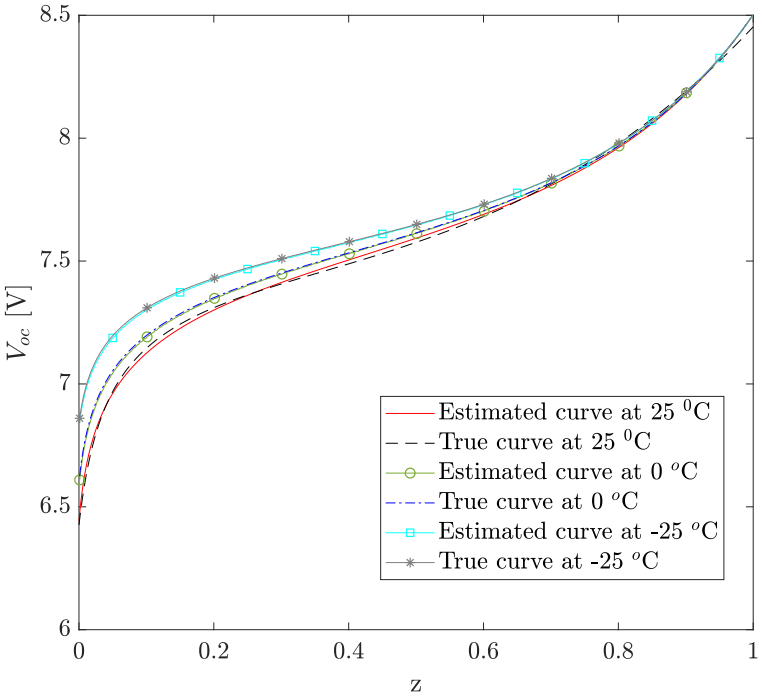

Figure 4.11: Estimated & True SoC-OCV curves at different temperatures

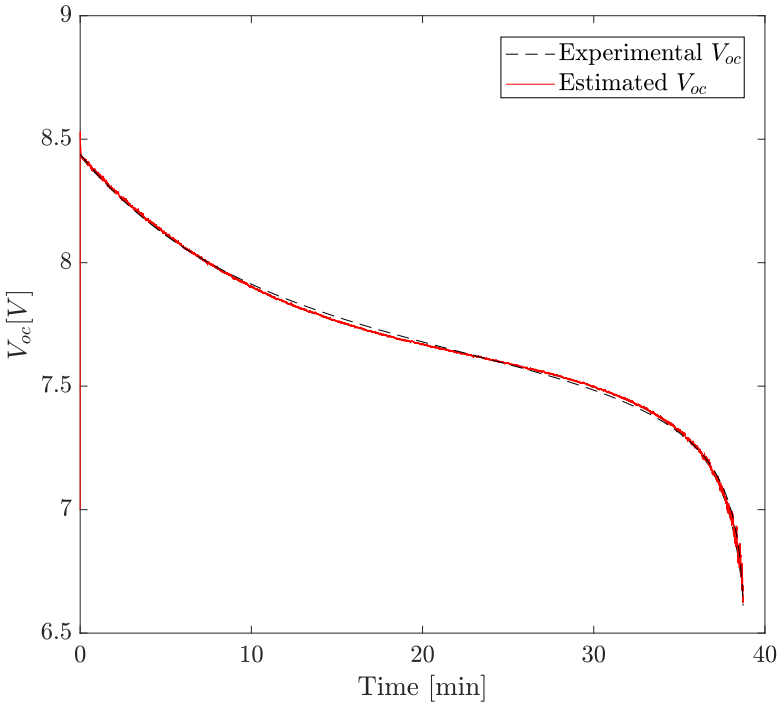

Figure 4.12: Real battery's V_{oc} estimation in comparison with the experimental V_{oc}

The battery experiment is conducted to validate the proposed algorithm. Figure 4.12

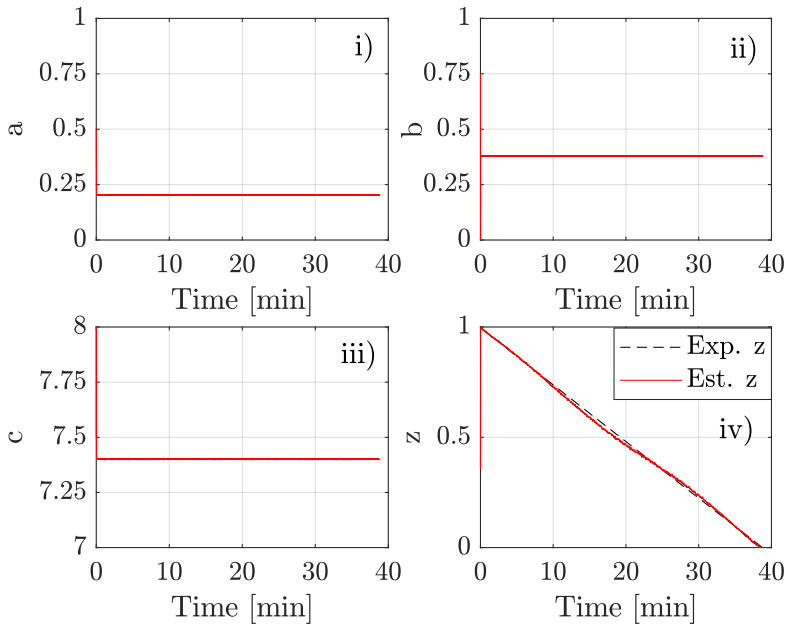

Figure 4.13: Real battery's SoC estimation in comparison with the experimental SoC & Real battery's SoC-OCV curve coefficients

shows the estimated V_{oc} in a solid red line whereas the experimental V_{oc} is in the dashed black line. The experimental V_{oc} is obtained from the data given in Table 4.1. The estimated V_{oc} converges to the experimental V_{oc} less than 1s. The accuracy in V_{oc} estimation is requisite for the accurate estimation of SoC.

The estimates of SoC-OCV curve coefficients are shown in Figure 4.13 (i-iii) and Figure 4.13 (iv) illustrates the SoC convergence. The SoC converges to its experimental value in less than 1s. It is vital to accurately estimate the SoC at low and high SoC values because it is necessary to know when to stop charging or discharging the battery. In these nonlinear regions, the estimated SoC agrees well with the experimental SoC as shown in Figure 4.13 (iv).

4.5 Discussion

The real-time SoC estimation algorithm is proposed based on a new SoC-OCV model. The OCV is estimated using the KF, the SoC is estimated using the EKF and another KF is used to develop the nonlinear curve estimation algorithm. The proposed algorithm is validated by performing the computer simulation under different dynamic loading conditions. All results show that the proposed algorithm can accurately construct the SoC-OCV relationship in real-time. In all cases, the SoC is accurately

estimated. The proposed algorithm is also validated by the battery experiment. The experimental results validate that the proposed method provides an accurate estimation of SoC. According to the experimental results, the SoC estimation error is less than 2.5%, which is given in Figure 4.14 iii).

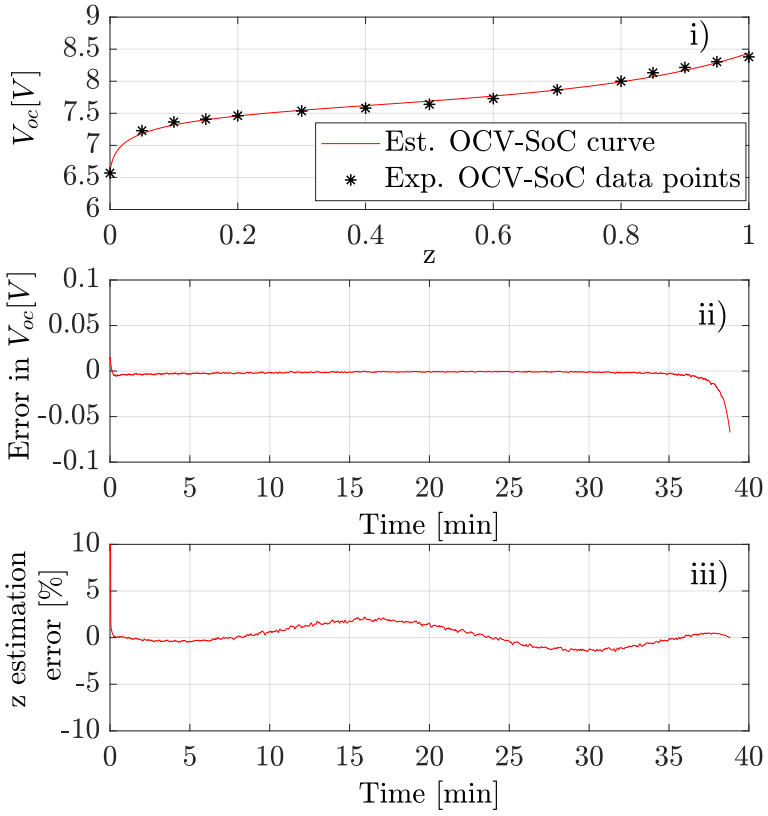

Figure 4.14: Errors in OCV and SoC

The simulation results demonstrated that the proposed algorithm also captures the variations in the SoC-OCV relationship. The proposed algorithm has two major benefits: The first benefit is that using the proposed algorithm in real-time application eliminates the requirement of preliminary laborious lab work. The second one is that it mitigates one of the error sources in the SoC estimation. To be more precise, the actual relationship is expected to change with the operational conditions and battery ageing. The proposed algorithm updates the nonlinear relationship according to the available measurements. Therefore, any changes in the actual relationship are reflected in the estimated relationship. This reduces the SoC estimation error due to the bias in the relationship. These results show that the proposed algorithm is a promising candidate to develop a real-time SoC estimation algorithm. The proposed method could be directly implemented for many applications including EVs.

Chapter 5

Current measurement noise mitigation

Although various SoC estimation algorithms have been developed to design a reliable BMS, an insufficient effort has been made to mitigate the error sources in SoC estimation methods in the literature. One of these error sources is the noisy current input measurement corrupted by two stochastic noises: zero-mean Gaussian white noise and the current bias noise. This error source needs to be mitigated to develop a more realistic and reliable battery SoC estimation algorithm.

Xingtao Liu et al. 2014 found that the bias noise can reach up to 1% in the battery experiments. It can reach up to 200 mA in practice due to the electromagnetic environment and temperature. However, the maximum value of bias noise depends on the application. Xingtao Liu et al. 2014 treated the bias noise as a constant parameter to be estimated with battery model parameters. The convergence of battery model parameters to their actual values is not guaranteed. Therefore, the bias convergence to its actual value cannot be guaranteed. Incorrect bias estimation would lead to erroneous SoC estimation. The maximum SoC error is calculated as 7.25% with 0.15A bias noise. Y. Xu et al. 2020 proposed a dual KF algorithm to filter the SoC twice to reduce the current measurement error and battery modelling error. The SoC estimation error is calculated to be within 2%. Despite the increased computational cost, this method cannot provide certain mitigation of the bias noise. Chun et al. 2016 developed a method to estimate the SoC without sensing the current measurement. The

method only uses the filtered terminal voltage measurements of each cell in the battery pack. To estimate the load current based on terminal voltage sensor measurements, it is necessary to use a high-quality but costly voltage sensor; otherwise, the current estimate is likely to be less accurate. An improved fuzzy adaptive KF is designed by Yan et al. 2013 to estimate the SoC of EVs working under poor sensor measurements. The system noise and the measurement noise are assumed to be zero-mean white noise and the proposed method only updates their statistical properties. However, the current sensor is also corrupted by the bias noise and it is neglected. To the best of the authors' knowledge, our work is the first direct attempt to consider two stochastic noises in the current measurement in the SoC estimation. Our proposed method reduced the SoC estimation error from around 11.3% to 0.56% in computer simulations. In the battery experiment, the SoC error is reduced from 1.74% to 1.12%. These results show that our proposed method reduces the SoC estimation error more compared to the methods in the literature.

The majority of the SoC estimation algorithms neglect the noise in the current input. This allows the use of the standard KF and its nonlinear filtering versions to estimate SoC. The standard KF provides an optimal estimation of the system states when the input signal includes the zero-mean Gaussian white noise with a known variance or it is noiseless. Considering noisy current input with non-Gaussian noises restricts the use of standard KF and its different versions. Therefore, the mitigation of the error source generated by the current sensor has two requirements: estimation of the current bias and modification of the standard KF considering the current measurement model.

5.1 Current sensor model

The current sensor measurement is modelled as follows:

$$\tilde{I} = I + \beta + v_i \tag{5.1}$$

where $\tilde{I}$ is the current sensor measurement, I is the true current, β is the random walk current measurement bias and v_i is the zero-mean Gaussian white noise with variance r_{v_i}.

5.1.1 Gaussian white noise with zero mean

The Gaussian white noise is a typical sensor noise with zero mean and the fundamental property given as follows:

$$E[v_{i,k}] = 0 \tag{5.2a}$$

$$E[v_{i,k_1} v_{i,k_2}^T] = \sigma_v^2 \delta \Delta t \tag{5.2b}$$

where for all k and any k_1 and k_2 are in $[0, \infty)$, σ_v^2 is the noise variance. The direct delta function $f_{dd}(\delta, k_1, k_2) = \delta \Delta t$ is defined as follows:

$$f_{dd}(\delta, k_1, k_2) = \begin{cases} 1, & \text{only if } k_1 = k_2 \\ 0, & \text{otherwise} \end{cases}$$

5.1.2 Current bias noise

The second stochastic noise corrupting the current measurement is the bias, β. The bias is the random walk, which means the difference between two adjacent sample points is the independent random increment that follows the normal distribution. Its mean and variance are given as follows:

$$\mathrm{E}[\beta_k - \beta_{k-1}] = 0 \tag{5.3a}$$

$$\mathrm{E}\{[\beta_k - \beta_{k-1}][\beta_k - \beta_{k-1}]^T\} = \sigma_\beta^2 \Delta t \tag{5.3b}$$

where σ_β^2 is a positive constant. β is propagated by the following equation:

$$\beta_k = \beta_{k-1} + \Delta\beta_k \tag{5.4}$$

where $\Delta\beta_k$ is the random increment. $\Delta\beta_k$ is expressed by

$$\Delta\beta_k = \eta_k \Delta t \tag{5.5}$$

where η_k is a random number generated from the normal distribution. The properties given in (5.3) must be separately satisfied. Rearrange (5.4) and substitute into (5.3a) as follows:

$$\mathrm{E}[\beta_k - \beta_{k-1}] = \mathrm{E}[\Delta\beta_k] = \mathrm{E}[\eta_k \Delta t] = \mathrm{E}[\eta_k]\Delta t = 0 \tag{5.6}$$

Therefore the mean value of η_k must be zero, i.e., $\mathrm{E}[\eta_k] = 0$. Secondly, the random increment property given in (5.3b) must be satisfied. Thus, rearranging (5.4) and substituting into (5.3b) yield

$$\mathrm{E}\{[\beta_k - \beta_{k-1}][\beta_k - \beta_{k-1}]^T\} = \mathrm{E}[\eta_k \Delta t \eta_k^T \Delta t] = \mathrm{E}[\eta_k \eta_k^T](\Delta t)^2 = \sigma_\beta^2 \Delta t \tag{5.7}$$

Hence the variance of η_k can be calculated by

$$\mathrm{E}[\eta_k \eta_k^T] = \sigma_\beta^2 / \Delta t \tag{5.8}$$

It is expected that estimating the SoC based on the corrected current input increases the accuracy of the estimated SoC. The measured current can be corrected by calculating its estimate based on (5.1). The estimated current input can be expressed as follows:

$$\begin{aligned} \mathrm{E}[I] =& \mathrm{E}[\tilde{I} - \beta - v_i] = \mathrm{E}[\tilde{I}] - \mathrm{E}[\beta] - \mathrm{E}[v_i] \\ \hat{I} =& \tilde{I} - \hat{\beta} \end{aligned} \tag{5.9}$$

Equation (5.9) implies that the estimation of β is required to calculate $\hat{I}$. Therefore, the current bias estimation algorithm is firstly introduced in this chapter. Afterward, the KF algorithm given in Algorithm 3 is modified taking into account the aforementioned noises.

5.2 Battery modelling for bias estimation

The current bias β is modelled as follows:

$$\beta_k = \beta_{k-1} + \Delta\beta_k \tag{5.10}$$

where $\Delta\beta_k$ is the variation in β between two sampling points. The calculation of β requires $\Delta\beta_k$. Therefore, the expression of $\Delta\beta_k$ is sought based on the one step difference of the measurement residual.

The measured $\tilde{V}_t$ at sampling time k is written as follows:

$$\tilde{V}_{t,k} = V_{oc,k} - I_k R_0 - I_{a,k} R_p + v_{V_t,k} \tag{5.11}$$

where unadorned symbols represents the true values and v_k is a zero-mean white noise. Rewrite (5.11) for sampling time $k-1$

$$\tilde{V}_{t,k-1} = V_{oc,k-1} - I_{k-1} R_0 - I_{a,k-1} R_p + v_{V_t,k-1} \tag{5.12}$$

Subtract (5.12) from (5.11)

$$\Delta\tilde{V}_{t,k} = \Delta V_{oc,k} - \Delta I_k R_0 - \Delta I_{a,k} R_p + \Delta v_{V_t,k} \tag{5.13}$$

where $\Delta[\cdot]_{k+1} = [\cdot]_{k+1} - [\cdot]_k$ and $\Delta v_{V_t,k} = v_{V_t,k} - v_{V_t,k-1}$.

The estimate of $V_{t,k}$ is calculated according to the noisy current input measurement as follows:

$$\hat{V}_{t,k} = \hat{V}_{oc,k} - \tilde{I}_k \hat{R}_0 - \hat{I}_{a,k} \hat{R}_p \tag{5.14}$$

Similarly, the estimate of V_t at sampling time $k-1$ can be written as follows:

$$\hat{V}_{t,k-1} = \hat{V}_{oc,k-1} - \tilde{I}_{k-1} \hat{R}_0 - \hat{I}_{a,k-1} \hat{R}_p \tag{5.15}$$

Subtract (5.15) from (5.14)

$$\Delta\hat{V}_{t,k} = \Delta\hat{V}_{oc,k} - \Delta\tilde{I}_k \hat{R}_0 - \Delta\hat{I}_{a,k} \hat{R}_p \tag{5.16}$$

In (5.16), to calculate the difference of OCV at two sampling points, we could use the estimated SoC at two sampling points and convert them to the corresponding OCV using the SoC-OCV relationship. However, two estimated SoC could have inconsistent values to charging (increasing SoC) or discharging (decreasing SoC) of the battery. Instead, firstly, the previous value of SoC is calculated using the following Coulomb

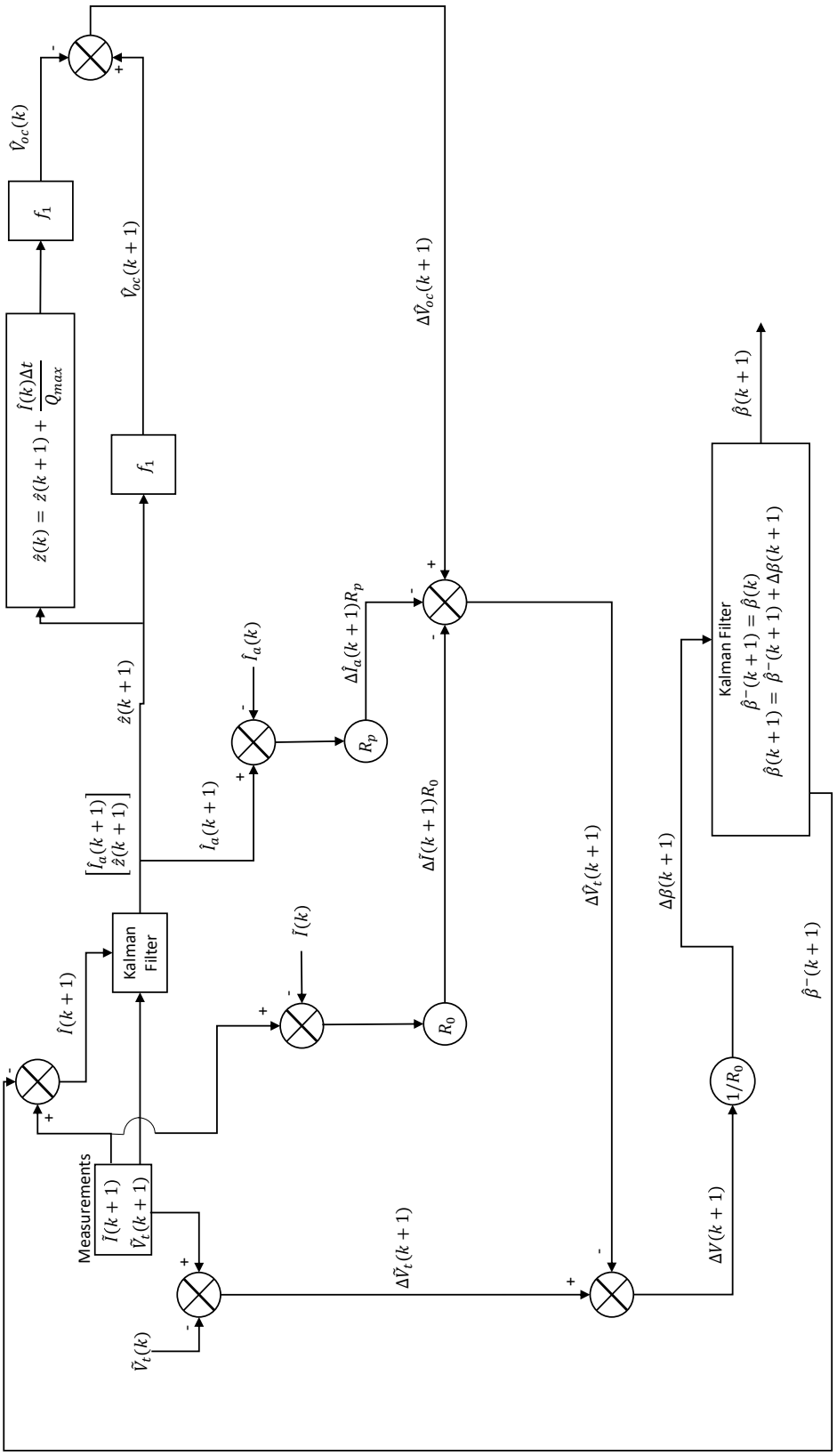

Figure 5.1: Beta estimatior

counting equation:

$$\hat{z}_{k-1} = \hat{z}_k + \frac{[\tilde{I}_k - \hat{\beta}_k]\Delta t}{Q_{max}} \tag{5.17}$$

where z_k is substituted by the estimated z_k from the KF. Then, the calculated $\hat{z}_{k-1}$ is transformed into the estimated $\hat{V}_{oc,k-1}$ through the SoC-OCV relationship. The OCV difference is calculated by subtracting $\hat{V}_{oc,k-1}$ from $\hat{V}_{oc,k}$, i.e., $\Delta\hat{V}_{oc,k} = \hat{V}_{oc,k} - \hat{V}_{oc,k-1}$.

The one sampling step difference of the measurement residual can be calculated by subtracting (5.16) from (5.13) as follows:

$$\begin{aligned}
\Delta[\Delta V_{t,k}] =& \Delta\tilde{V}_{t,k} - \Delta\hat{V}_{t,k} \\
=& \Delta V_{oc,k} - \Delta I_k R_0 - \Delta I_{a,k} R_p + \Delta v_{V_t,k} - \Delta\hat{V}_{oc,k} - \Delta\tilde{I}_k\hat{R}_0 - \Delta\hat{I}_{a,k}\hat{R}_p \\
=& (\Delta V_{oc,k} - \Delta\hat{V}_{oc,k}) + (\Delta I_k - \Delta\tilde{I}_k)\hat{R}_0 + (\Delta I_{a,k} - \Delta\hat{I}_{a,k})\hat{R}_p + \Delta v_{V_t,k} \\
=& -\Delta\beta_k\hat{R}_0 - \Delta v_{i,k}\hat{R}_0 + \Delta v_{V_t,k}
\end{aligned} \tag{5.18}$$

The difference $\Delta\beta_k$ can be calculated as follows:

$$\Delta\beta_k = -\frac{\Delta[\Delta V_{t,k}]}{\hat{R}_0} + e_{s,k} \tag{5.19}$$

where $e_{s,k} = \Delta v_{V_t,k}\hat{R}_0 - \Delta v_{i,k}$ is a zero-mean white noise. Directly substituting $\Delta\beta_k$ into (5.10) would amplify undesired noises in the estimated β values. Thus, the standard KF is designed for estimating β_k and provided in the Algorithm 5. Figure 5.1 shows the block diagram of the beta estimation algorithm.

5.3 Modification of standard Kalman filter for batteries

The standard Kalman filter given in Algorithm 3 is widely used to solve linear optimal estimation problems. Consider the following generic model for a battery system:

$$x_{k+1} = Ax_k + Bu_k + w_k \tag{5.20a}$$

$$y_k = Cx_k + Du_k + v_k \tag{5.20b}$$

where

$$
\begin{aligned}
x_k &= \begin{bmatrix} I_{a,k} & z_k \end{bmatrix}^T, \;\; y_k = \tilde{V}_{t,k}, \;\; u_k = \hat{I}_k \\
A &= \begin{bmatrix} \hat{\alpha}_k & 0 \\ 0 & 1 \end{bmatrix}, \;\; B = \begin{bmatrix} 1 - \hat{\alpha}_k \\ -\Delta t / Q_{max} \end{bmatrix}, \; w_k = \begin{bmatrix} w_{I_a,k} \\ w_{z,k} \end{bmatrix} \\
C &= \left. \frac{\partial V_t}{\partial x} \right|_{x=\hat{x}_k} \quad D = -\hat{R}_0,
\end{aligned}
\tag{5.21}
$$

x_k is the state vector, y_k is the V_t measurement and u is the input. A is the system matrix, B is the control matrix, C is the measurement-system matrix and D is the measurement-control matrix. w_k and v_k are the process and measurement Gaussian noises with zero mean and known covariance matrices Q and R, respectively. Note that w_k is independent of v_k and they are assumed to be stationary over time. The covariance of the process noise model and that of the measurement noise model are assumed to be stationary over time.

Algorithm 3 Standard Kalman Filter Algorithm (Crassidis et al. 2004)

Initialise: $\hat{x}_0^- = \mathrm{E}[x_0]$, $P_0^- = \mathrm{E}[(x_0 - \hat{x}_0)(x_0 - \hat{x}_0)^T]$.
while true **do**
  Update:
    $K_k = P_k^- C^T (C P_k^- C^T + R)^{-1}$
    $\hat{x}_k = \hat{x}_k^- + K_k[y_k - (C\hat{x}_k^- + Du_k)]$
    $P_k = (\mathrm{I} - K_k C) P_k^-$
  Propagate:
    $\hat{x}_{k+1}^- = A\hat{x}_k + Bu_k$
    $P_{k+1}^- = AP_kA^T + Q$
  Repeat

The input u in (5.20) is replaced with $\tilde{I}$ in battery systems to modify the KF to consider the aforementioned two stochastic noises in the input. The derivation of the noisy input Kalman filter (NiKF) starts with updating the priori prediction of the state vector as follows:

$$
\hat{x}_k = \hat{x}_k^- + K_k(y_k - \hat{y}_k) \tag{5.22}
$$

where K_k is the Kalman gain and the $(y_k - \hat{y}_k)$ term is the measurement residual. Similar to the propagation part, the derivation of the updated part starts with defining

the posterior state estimation error given as follows:

$$\begin{aligned} e_k &= x_k - \hat{x}_k \\ &= x_k - \hat{x}_k^- - K_k(Cx_k + DI_k + v_k - C\hat{x}_k^- - D\hat{I}_k) \\ &= x_k - \hat{x}_k^- - K_k[Cx_k + D(\tilde{I}_k - \beta_k - v_{i,k}) + v_k - C\hat{x}_k^- - D(\tilde{I}_k - \hat{\beta}_k)] \\ &= (\mathrm{I} - K_kC)e_k^- - K_kv_k + K_kDv_{i,k} + K_kD(\hat{\beta}_k - \beta_k) \end{aligned} \tag{5.23}$$

where $K_kD(\hat{\beta}_k - \beta_k)$ term is neglected since $\lim_{t\to\infty} \hat{\beta} \to \beta$ in most of the practical cases. The approximation of (5.23) is given by:

$$e_k = (\mathrm{I} - K_kC)e_k^- - K_kv_k + K_kDv_{i,k} \tag{5.24}$$

The posterior state estimation error covariance matrix is as follows:

$$\begin{aligned} P_k &= \mathrm{E}[e_ke_k^T] \\ &= \mathrm{E}[((\mathrm{I} - K_kC)e_k^- + K_kDv_{i,k} - K_kv_k)((\mathrm{I} - K_kC)e_k^- + K_kDv_{i,k} - K_kv_k)^T] \\ &= (\mathrm{I} - K_kC)P_k^-(\mathrm{I} - K_kC)^T + K_kDr_{v_{i,k}}D^TK_k^T + K_kR_kK_k^T \end{aligned} \tag{5.25}$$

where $E[\cdot]$ represents the expectation operator, R_k is the covariance of v_k, $r_{v_{i,k}}$ is the variance of $v_{i,k}$. Note that v_k, $v_{i,k}$ and e_k^- are independent of each other.

The Kalman gain matrix is derived by minimising the trace of P_k. The trace of P_k is the sum of the mean squared errors. Expand (5.25) as follows:

$$P_k = P_k^- - K_kCP_k^- - P_k^-C^TK_k^T + K_k(CP_k^-C^T + Dr_{v_{i,k}}D^T + R_k)K_k^T \tag{5.26}$$

Taking the trace of (5.26) gives

$$T[P_k] = T[P_k^-] - 2T[K_kCP_k^-] + T[K_k(CP_k^-C^T + Dr_{v_{i,k}}D^T + R_k)K_k^T] \tag{5.27}$$

Differentiate (5.27) with respect to K_k

$$\frac{dT[P_k]}{dK_k} = -2(CP_k^-)^T + 2K_k(CP_k^-C^T + Dr_{v_{i,k}}D^T + R_k) \tag{5.28}$$

Equalising (5.28) to zero and solving for K_k yield

$$K_k = (P_k^- C^T)(CP_k^- C^T + R_k + Dr_{v_{i,k}} D^T)^{-1} \tag{5.29}$$

The state is propagated as follows:

$$x_{k+1} = Ax_k + B\tilde{I}_k \tag{5.30}$$

The posterior error covariance matrix is propagated as follows:

$$\begin{aligned} e_{k+1}^- =& x_{k+1} - \hat{x}_{k+1}^- \\ =& Ax_k + BI_k + w_k - A\hat{x}_k^- - B\hat{I}_k \\ =& Ax_k + B(\tilde{I}_k - \beta_k - v_{i,k}) + w_{k-1} - A\hat{x}_k^- - B(\tilde{I}_k - \hat{\beta}_k) \\ =& A(x_k - \hat{x}_k^-) + w_k - Bv_{i,k} - B(\hat{\beta}_k - \beta_k) \end{aligned} \tag{5.31}$$

where $(\cdot)_k^-$ represents the priori prediction of $(\cdot)_k$. In (5.31), $B(\hat{\beta}_k - \beta_k)$ term is neglected because the estimated $\hat{\beta}$ converges to its actual value β in most of the practical cases, i.e., $\lim_{t\to\infty} \hat{\beta} \to \beta$. The final expression of the priori state prediction error is given as follows:

$$e_{k+1}^- = Ae_k + w_k - Bv_{i,k} \tag{5.32}$$

The prior covariance matrix is expressed as follows:

$$\begin{aligned} P_{k+1}^- =& E[e_{k+1}^- {e_{k+1}^-}^T] \\ =& E[(Ae_k + w_k - Bv_{i,k})(Ae_k + w_k - Bv_{i,k})^T] \\ =& AP_kA^T + Br_{v_{i,k}}B^T + Q \end{aligned} \tag{5.33}$$

where $r_{v_{i,k}}$ is the variance of $v_{i,k}$. Note that e_k, w_k, and $v_{i,k}$ are independent of each other.

The summary of the NiKF is given in Algorithm 4 where the covariance of w_k is Q and the variance of v_k is r. Note that the measurement noise is independent from the process noise.

Algorithm 4 NiKF Algorithm

Initialise:
  $\hat{x}_0^- = \mathrm{E}[x_0]\,, P_0^- = \mathrm{E}[(x_0 - \hat{x}_0)\,(x_0 - \hat{x}_0)^T]$
while true **do**
  Update:
  $K_k = (P_k^- C^T)(C P_k^- C^T + R_k + D r_{v_{i,k}} D^T)^{-1}$
  $\hat{x}_k = \hat{x}_k^- + K_k[y_k - (C\hat{x}_k^- + D\hat{I}_k)]$
  $P_k = (\mathrm{I} - K_k C) P_k^- (\mathrm{I} - K_k C)^T + K_k D r_{v_{i,k}} D^T K_k^T + K_k R_k K_k^T$
  Propagate:
  $\hat{x}_{k+1}^- = A\hat{x}_k + B\hat{I}_k$
  $P_{k+1}^- = A P_k A^T + B r_{v_{i,k}} B^T + Q$
  Repeat

5.4 Simulation

The fully charged battery with 0.85Ah capacity is discharged under different current profiles to assess the performance of the bias estimator algorithm. The battery sensor bias is generated according to the theoretical aspect introduced in 5.1.2. The bias β is generated and added to the true current input I along with the Gaussian

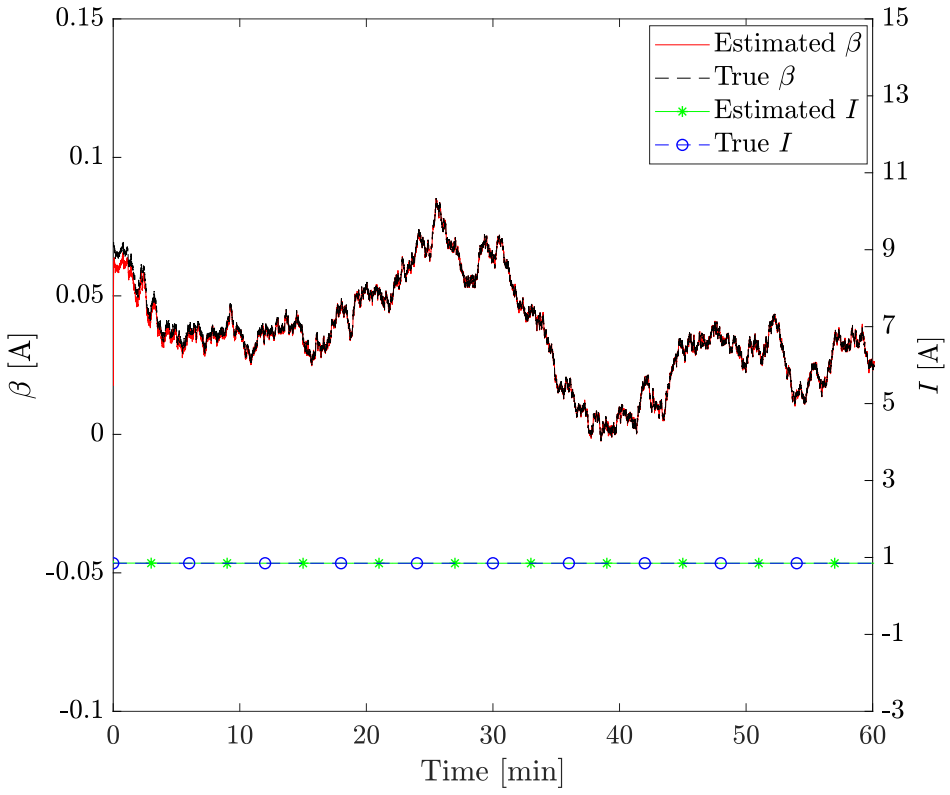

Figure 5.2: Current bias estimation under constant current discharge

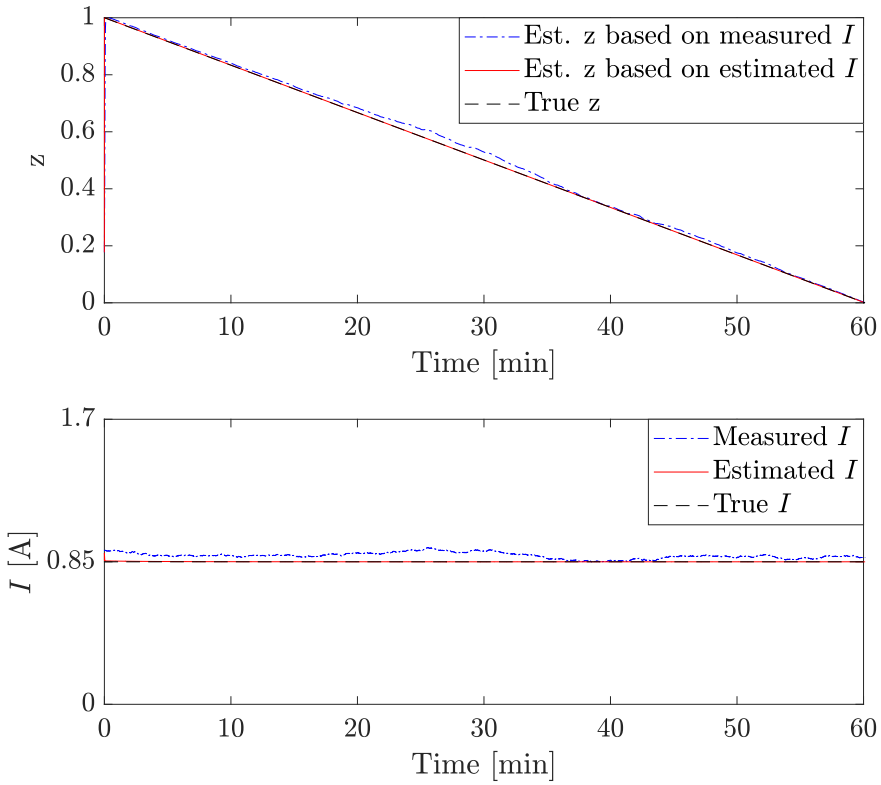

Figure 5.3: SoC estimation under constant current discharge

white noise. The available voltage sensors can measure $\tilde{V}_t$ with the error of 1–2 mV (Zheng et al. 2018). Therefore, we assume the $\pm 3\sigma_V = \pm 1.5$mV and the standard deviation in V_t, σ_V, is calculated to be $\sigma_V = 0.05$mV. We also tested the algorithm with larger σ_V values such as $\sigma_V = 1$mV, $\sigma_V = 2$mV, $\sigma_V = 5$mV, and $\sigma_V = 10$mV. In comparison with the current bias noise, Zheng et al. 2018 concluded that the white noise in the current measurement does not have a significant effect on the SoC estimation. Therefore, the standard deviation in v_i, σ_i, is chosen as same as the one in σ_V. The sampling period is 0.01s. The true battery physical parameters are as follows: $R_0 = 0.3\Omega$, $R_p = 0.1\Omega$, and $C_p = 10$F. The standard deviation in β, σ_β, is set to 0.001. To initialise the beta estimation algorithm, the initial β is randomly produced within the sample space of β which is $\Omega_\beta = [0, 100\text{mA}]$ The initial p_β is set to 0.001. The initial state I_a is set to 0 whereas the initial estimate z is randomly drawn from the uniform distribution in [0,1]. Note that the initial true z is 1 or 0.995.

Algorithm 5 SoC estimation algorithm with current input noise mitigation

Initialise: $\hat{x}_0^-$, P_0^-, $\hat{\beta}_0^-$, $p_{\beta,0}^-$
    Generate β_0 using a random number generator
while $0 < z < 1$ **do**
    Generate true β:
        $\eta_\beta \sim N(0, \sigma_\beta^2/\Delta t)$
        $\Delta\beta_k = \eta_k \Delta t$
        $\beta_{k+1} = \beta_k + \Delta\beta_k$
    Add noise to the true current:
        $\tilde{I}_k = I_k + \beta_k + N(0, \sigma_i^2)$
    Update β
        $K_{\beta,k} = p_{\beta,k}^-(p_{\beta,k}^- + r_\beta)^{-1}$
        $\hat{\beta}_k = \hat{\beta}_k^- + K_{\beta,k}\Delta\beta_k$
        $p_{\beta,k} = (1 - K_{\beta,k})p_{\beta,k}^-$
    Propagate $\hat{\beta}$ and p_β:
        $\hat{\beta}_{k+1} = \hat{\beta}_k$
        $p_{\beta,k+1} = p_{\beta,k} + q_\beta$
    Estimate SoC using NiKF
    Update:
        $K_k = (P_k^- C^T)(C P_k^- C^T + R_k + D r_{v_{i,k}} D^T)^{-1}$
        $\hat{x}_k = \hat{x}_k^- + K_k[y_k - (C\hat{x}_k^- + D\hat{I}_k)]$
        $P_k = (\mathrm{I} - K_k C)P_k^-(\mathrm{I} - K_k C)^T + K_k D r_{v_{i,k}} D^T K_k^T + K_k R_k K_k^T$
    Propagate:
        $\hat{x}_{k+1}^- = A\hat{x}_k + B\hat{I}_k$
        $P_{k+1}^- = A P_k A^T + B r_{v_{i,k}} B^T + Q$
Repeat

The initial priory error covariance matrix is given as follows:

$$P_0^- = \begin{bmatrix} 10^{-3} & 0 \\ 0 & 10^{-3} \end{bmatrix}$$

The nonlinear SoC-OCV curve model introduced in Chapter 4 is used to convert the estimated $\hat{V}_{oc}$ into the estimated $\hat{z}$. The nonlinear equation has the following coefficients: $a = 0.2539$V, $b = 0.4566$V, $c = 7.245$V and $\delta = 0.008$. The variance q_β is set to 0.001 and Q is set to $Q = [10^{-3}\,0; 0\,10^{-3}]$.

5.5 Results

The bias estimation algorithm was tested under four different current input profiles, including constant current profile, sinusoidal current profile, DST cycle current profile, and HPPC cycle current profile. The results show that our input current bias noise mitigation algorithm corrects the input current measurement so that it increases the

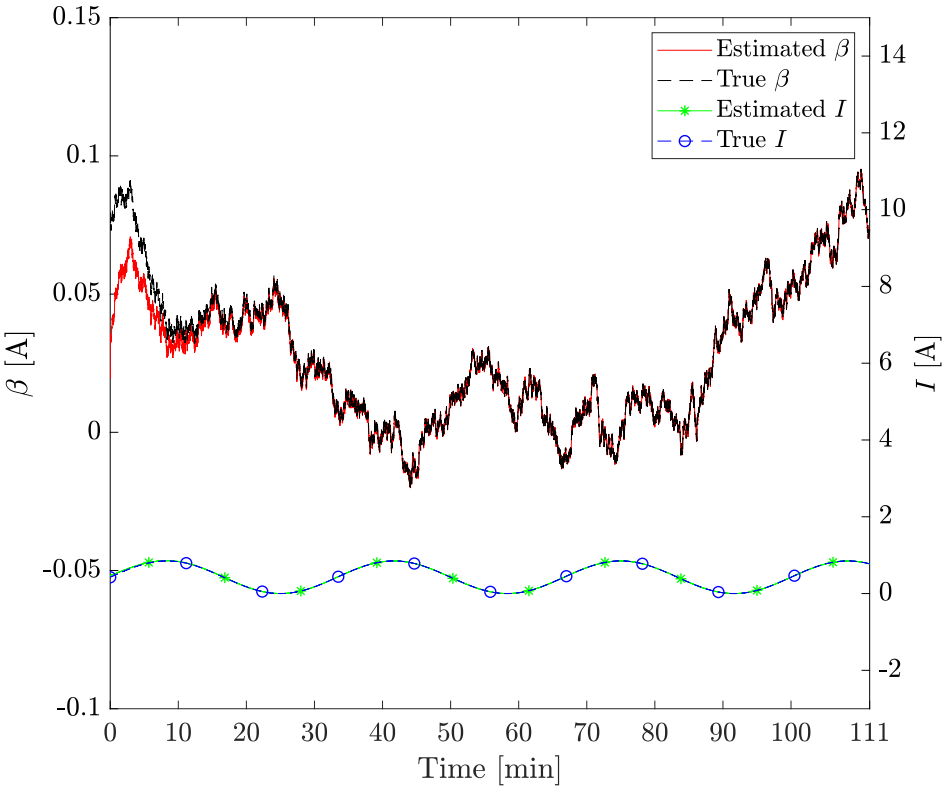

Figure 5.4: Bias estimation under sinusoidal current discharge

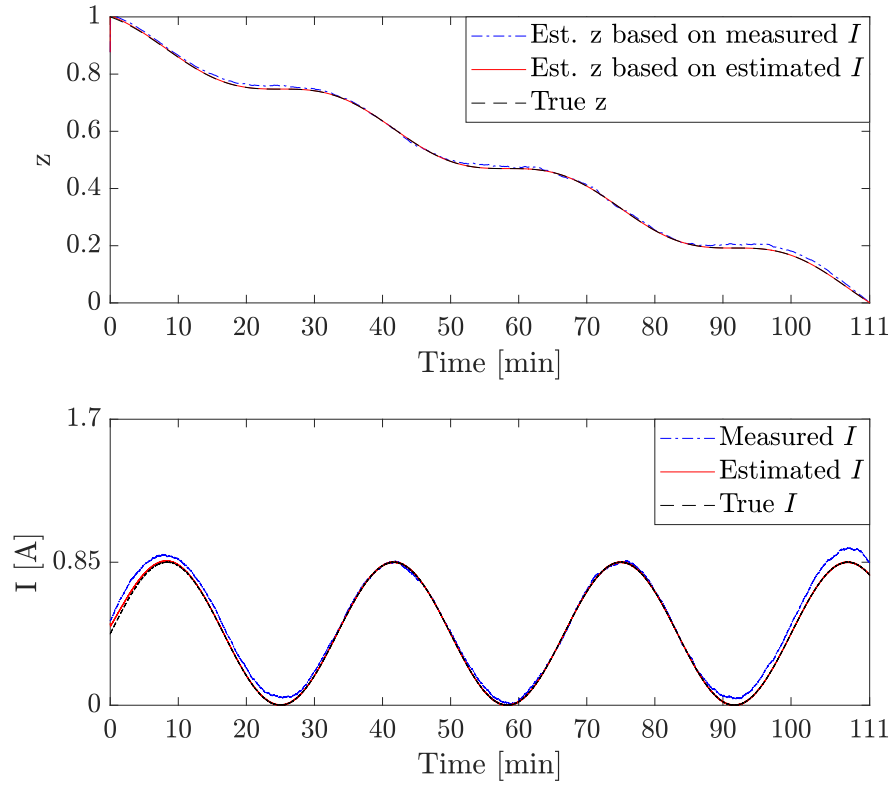

Figure 5.5: SoC estimation under sinusoidal current discharge

accuracy of the SoC estimation.

Figures 5.2, 5.4, 5.6, and 5.8 show the added true bias noise to the current measurement and its estimation under different dynamic loading conditions. In these figures, the true β is shown in a dashed black line and the estimated $\hat{\beta}$ is shown in a red solid line. These figures also show the true current input in a dashed blue line with a marker 'o' and the estimated current input in a solid green line with a marker '*'. The

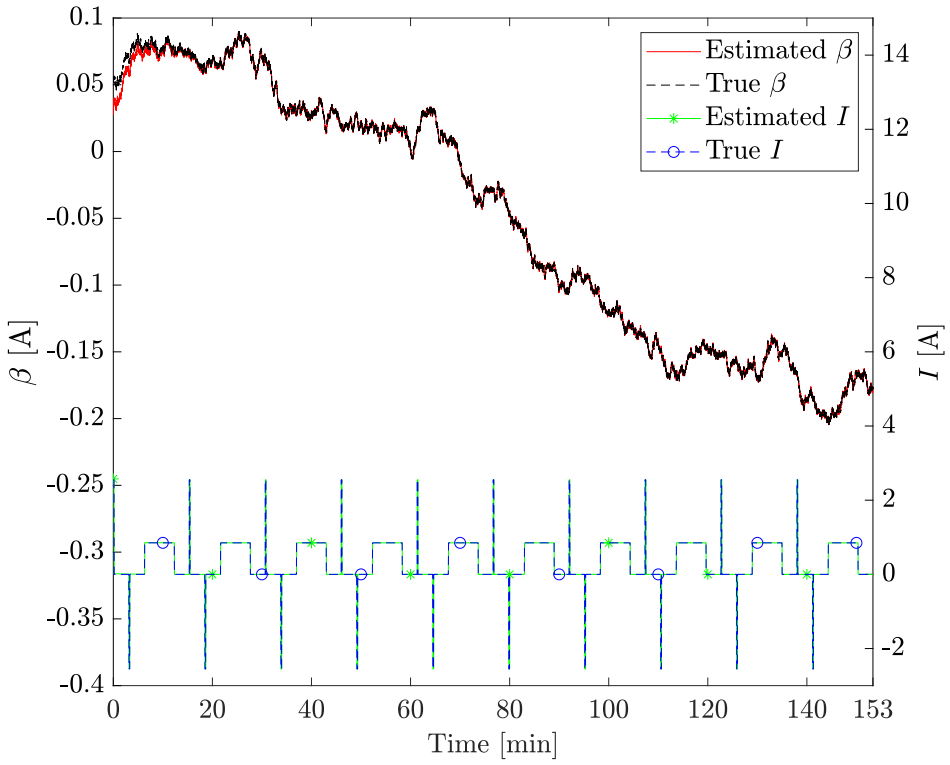

Figure 5.6: Bias estimation under HPPC current discharge

estimation result of β under constant current discharge profile is given in Figure 5.2. The current bias β has the maximum value of around 90mA which is equal to 11% of the true current input. In the simulation, the bias changes significantly. The proposed algorithm manages to calculate β and corrects the current input measurement. The estimated current and the true current signals are shown at the bottom of Figure 5.2.

The SoC estimation result under constant current discharge profile using the current input measurement is shown in blue dash-dotted in Figure 5.3. The estimated SoC using the estimated current measurement is shown in a red solid line whereas the true SoC is shown in a black-dashed line. The SoC estimation using the current input measurement directly shows large errors because of the current bias.

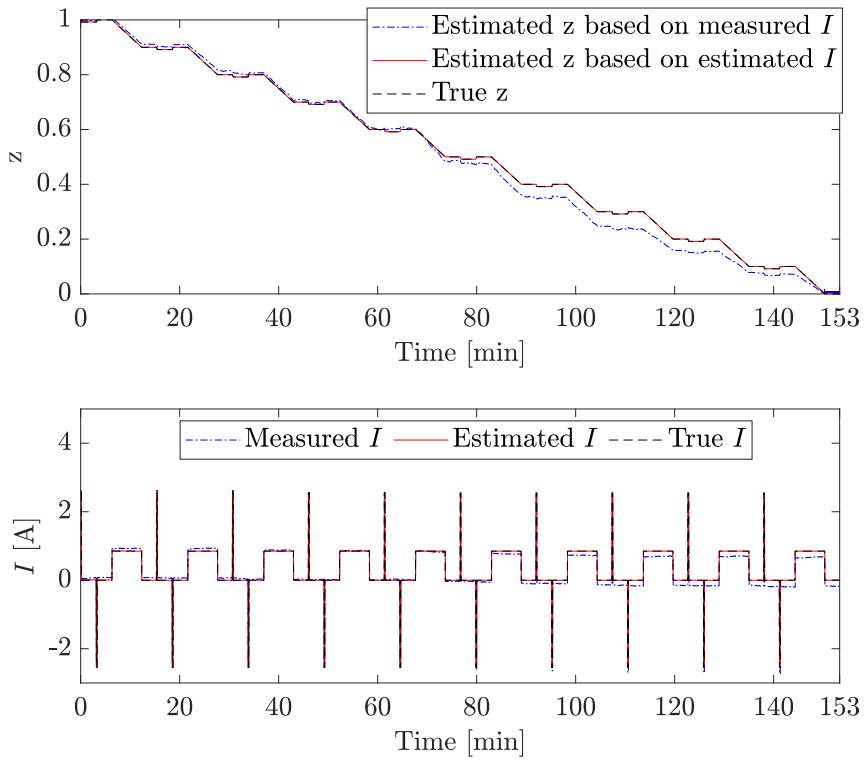

Figure 5.7: SoC estimation under HPPC current discharge

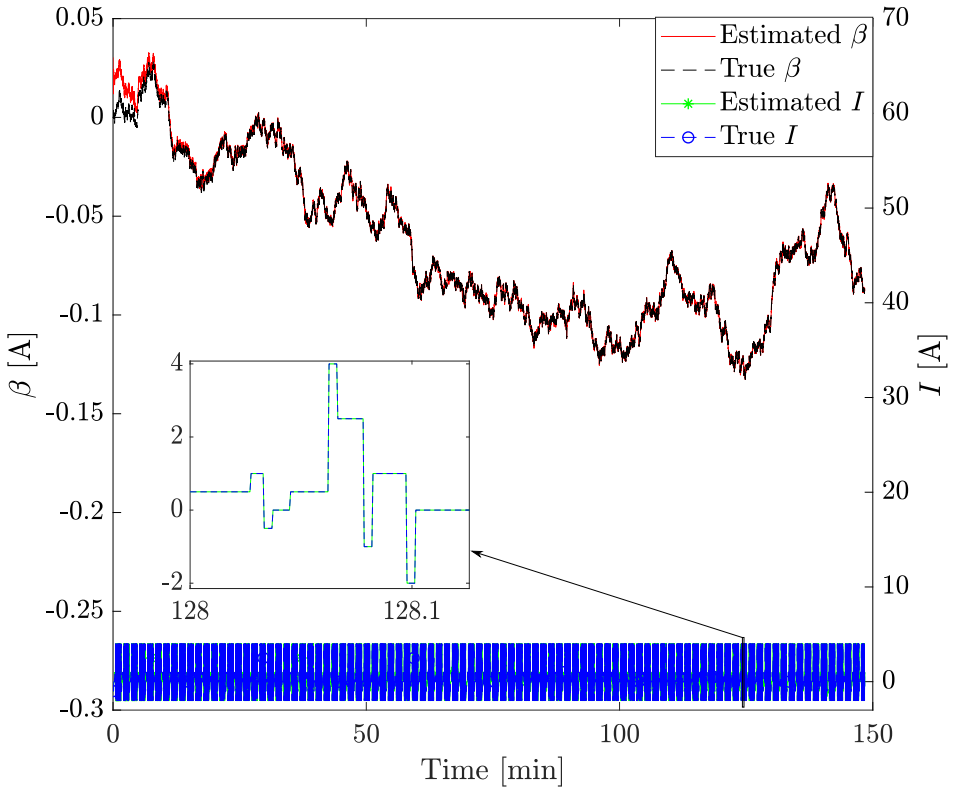

Figure 5.8: Bias estimation under DST current discharge

On the other hand, the SoC estimation using the estimated current input converges to the true SoC reasonably close. It shows that the proposed algorithm accurately calculates the estimated β and corrects the current input measurement during the entire simulation.

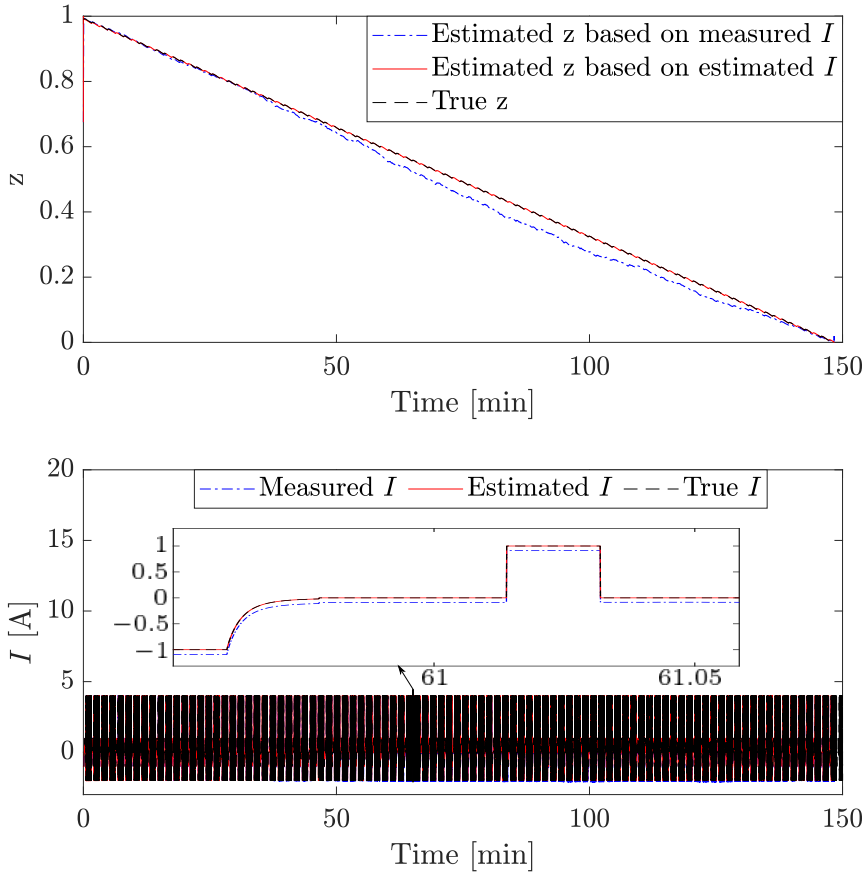

Figure 5.9: SoC estimation under DST current discharge

Figure 5.5 shows the SoC estimation result according to the current input measurement along and corrected current input along with the true SoC under the sinusoidal current input profile. Figure 5.4 shows the true β and the estimated β. The true β reached almost 100mA at the beginning and the end of the simulation. Therefore, the error in the SoC estimation calculated according to the current input measurement is high at the beginning and the end of the simulation. However, the proposed algorithm accurately corrected the current input measurement. Thus, the SoC estimation based on the estimated current input is accurately calculated using the NiKF. The convergence of β required a longer time due to the higher initial error in β compared to the time required in the constant current discharge simulation.

Figure 5.6 shows β estimation result under HPPC current profile. The bias β reaches around 200mA at the end of the simulation. Therefore, the error is increased in the SoC estimation when it is calculated according to the current input measurement as shown in Figure 5.7. However, the estimated β converged to its true value very fast. Hence, the corrupted current input measurement is corrected and the SoC estimation error due to the corrupted current measurement is significantly removed as shown in Figure 5.7.

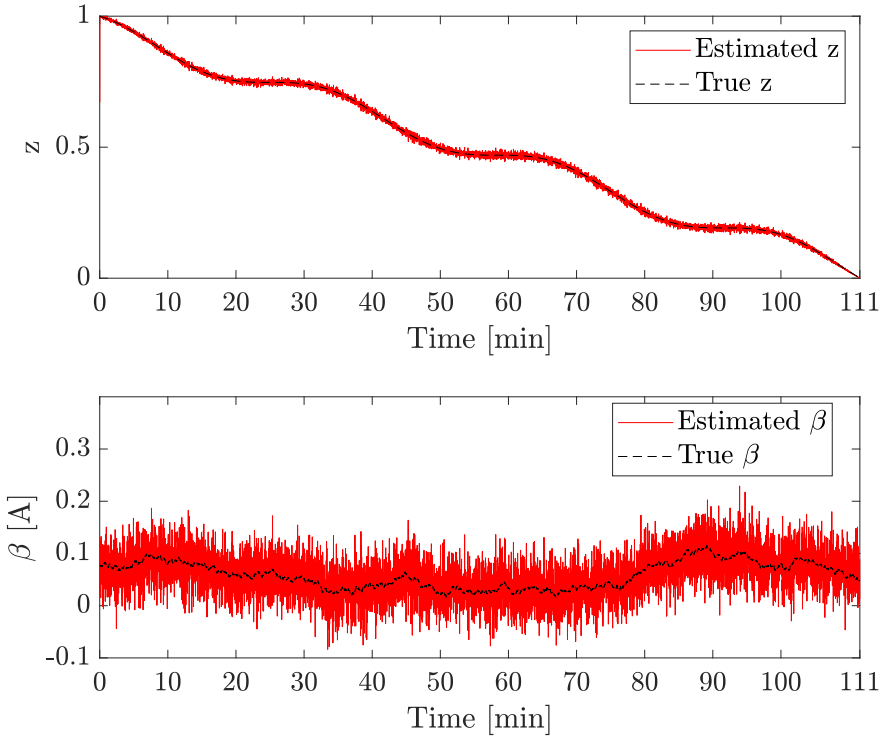

Figure 5.10: The SoC and β estimation when $\sigma_{V_t} = 0.01$ and $\sigma_i = 0.01$

The DST current profile is also adopted to assess the accuracy of β estimation as shown in Figure 5.8. In this simulation, β reaches the maximum value of 120mA. When the bias in the current input measurement is the maximum, the SoC estimation according to the measured current input has the largest error as shown in Figure 5.9. Similar to previous results, our algorithm corrects the current input measurement by estimating β accurately and subtracting it from the current input measurement. Therefore, the SoC estimation calculated according to the estimated current input is well aligned with the true SoC until the battery is fully discharged as shown in Figure 5.9.

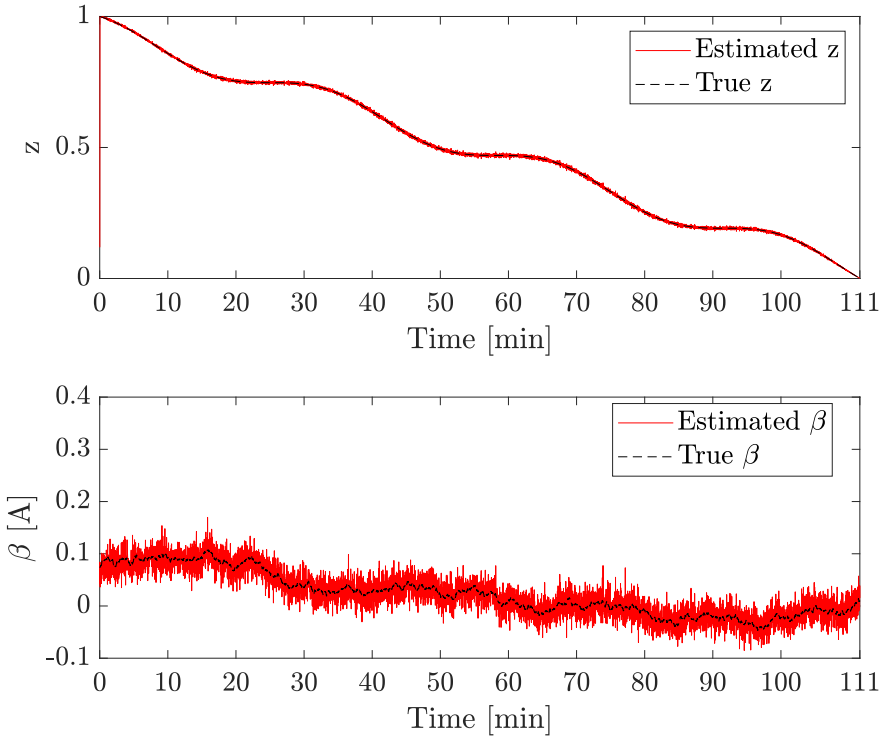

Figure 5.11: The SoC and β estimation when $\sigma_V = 0.005$ and $\sigma_i = 0.005$

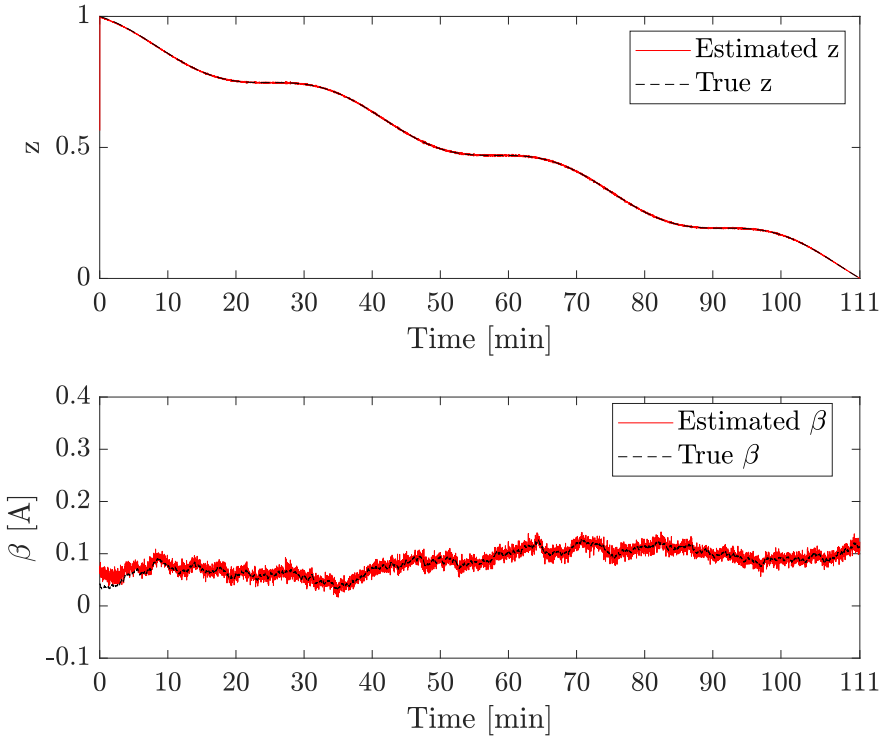

Figure 5.12: The SoC and β estimation when $\sigma_V = 0.002$ and $\sigma_i = 0.002$

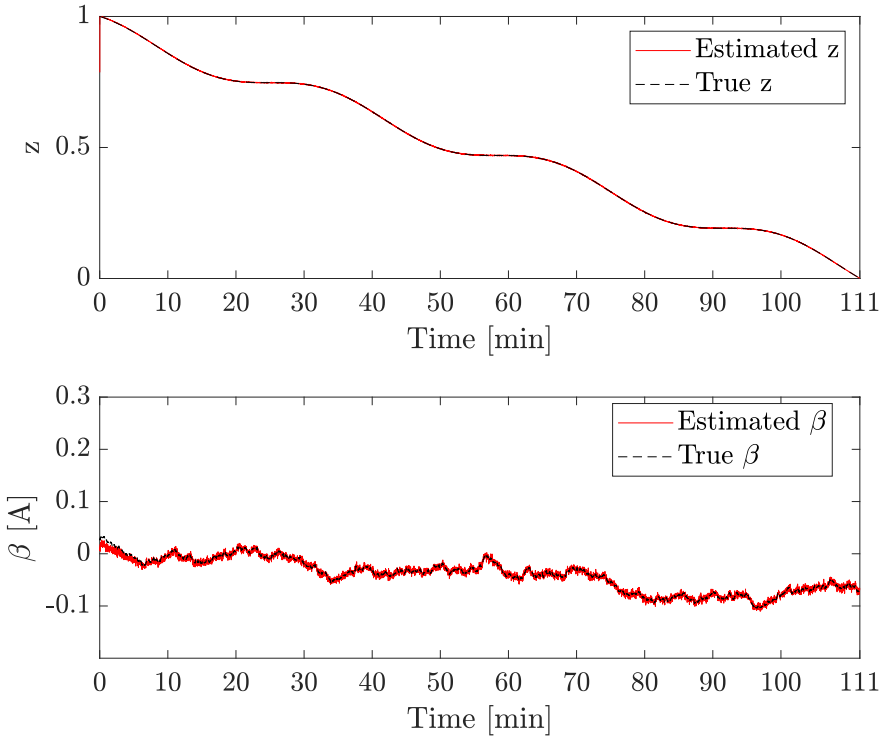

Figure 5.13: The SoC and β estimation when $\sigma_V = 0.001$ and $\sigma_i = 0.001$

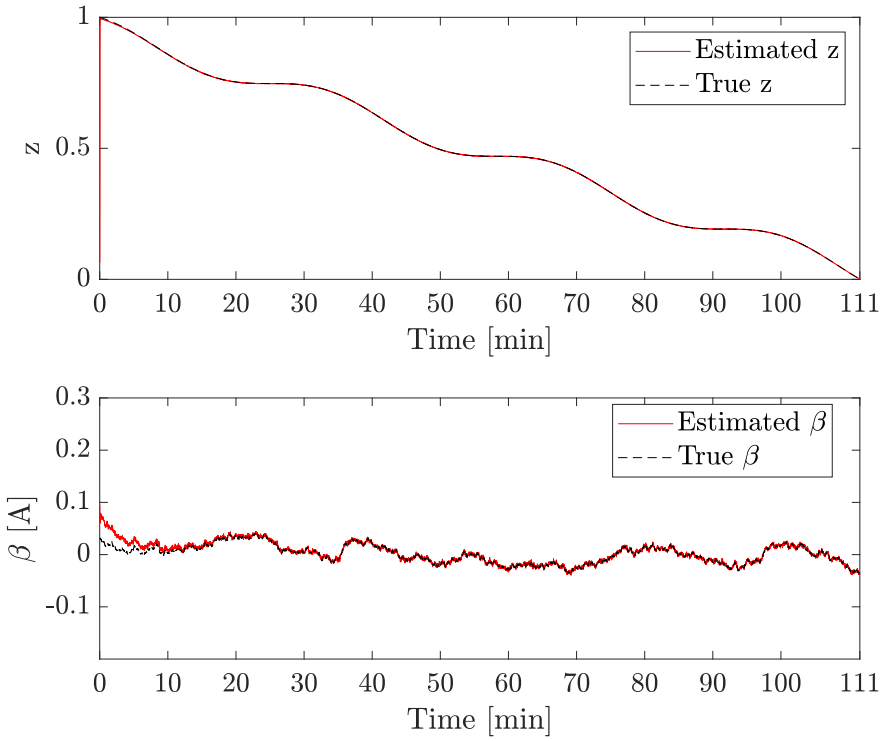

Figure 5.14: The SoC and β estimation when $\sigma_{V_t} = 0.0005$ and $\sigma_i = 0.0005$

The effect of the noise in measured V_t on the robustness of the proposed algorithm

is also investigated. To assess the performance of the proposed algorithm, 5 different standard deviation values of the white noises in V_t and I are used. Figure 5.10 shows the SoC and β estimation when the white noise standard deviation in V_t and I is 0.01, i.e., $\sigma_{V_t} = 0.01$ and $\sigma_i = 0.01$. Note that the white noise in the input current does not significantly affect the SoC estimation accuracy (Zheng et al. 2018). Therefore, σ_i is chosen similar to σ_{V_t}. As it is seen in Figure 5.10, β estimation has fluctuations due to the white noise in V_t. However, this does not change the accuracy of the SoC estimation using the estimated current input. σ_{V_t} and σ_i are then decreased to 0.005 and β and SoC estimation results are given in Figure 5.11. As expected, fluctuations in the estimated β become smaller compared to the previous β estimation result when σ_{V_t} and σ_i are decreased. The fluctuations in the SoC estimation are also reduced due to the smaller white noise in V_t measurement and smaller fluctuations in β estimates. Moreover, σ_{V_t} and σ_i values are set to 0.002, 0.001, and 0.0005. The estimation results are given in Figure 5.12, 5.13, and 5.14. It is observed that as σ_{V_t} and σ_i get smaller, the fluctuations in the β estimates and SoC estimates get smaller. However, the change in the fluctuations in the estimated β and SoC is more obvious when σ_{V_t} and σ_i are decreased from 0.01 to 0.005 and from 0.005 to 0.002. When σ_{V_t} and σ_i are decreased to 0.001 from 0.002, the estimation of β and SoC have slightly smaller fluctuations. Therefore, current measurement and voltage measurement sensors with $\sigma_{V_t} = 0.002$ and $\sigma_i = 0.002$ accuracy would provide a reasonably accurate SoC estimation using the proposed algorithm.

The proposed algorithm is also validated by the battery experiment. Figure 5.15 shows the β and SoC estimation results according to the experimental data. Around 20mA bias noise is calculated during the battery experiment. The value of calculated bias shows that he significant bias is not generated due to the short duration of the battery experiment. Once the β estimate is available, the measured current input is corrected. The SoC is calculated based on the measured current input and the estimated current input. The true SoC is calculated using the CC method and the estimated current input. The results show that the accuracy in the SoC estimation is increased with respect to the reference SoC values calculated using the corrected current measurement.

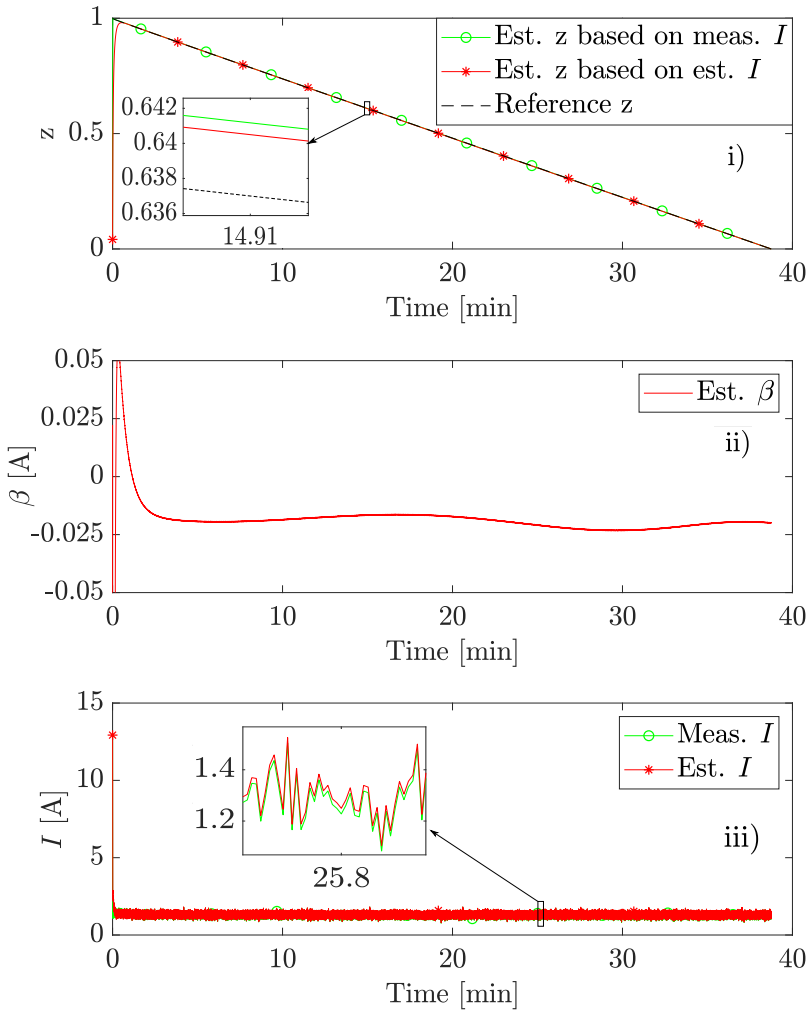

Figure 5.15: The experimental β estimation result

5.6 Discussion

The SoC estimation algorithm considering the input current measurement noise is proposed. The input current sensor is modelled as the summation of I, β and v_i. The β is estimated based on the difference between the one-step sampling step difference in the measured V_t and that in the estimated V_t. Additionally, the standard KF algorithm is modified according to the current input model. The proposed algorithm is validated by computer simulations and the battery experiment. The computer simulations are conducted under 4 different dynamic loading profiles including the constant current profile, sinusoidal current profile, HPPC current profile, and DST current profile. The proposed algorithm is also tested under 5 different standard deviation values in the white noises in V_t and I to assess the robustness of the proposed algorithm.

The current input measurement is then corrected by subtracting the estimated β from

the measured I. The estimated I is used in the NiKF to estimate the SoC. The results show that the proposed algorithm can accurately estimate β in the current input measurement. The SoC is also calculated using the measured current input. The comparison plots of the SoC estimation demonstrate that correcting the current measurement significantly reduces the SoC estimation error.

The proposed algorithm removes one of the error sources in the SoC estimation problem. This is an important development in the BMS design. It is the first successful attempt to mitigate the current sensor noise with an accurate bias noise modelling.

Chapter 6

Conclusion and future work

6.1 Conclusion

To date, available SoC-OCV calculation methods have severe limitations. The most common method is to calculate the relationship offline, which restricts its use for different operational conditions and different batteries. Alternate methods construct this relationship using hybrid techniques (where the OCV and SoC are estimated using KF-based state estimators and the CC method, respectively). The major shortcoming in this context is that the CC method requires a perfect initial guess and a noise-free current measurement, making these methods inapplicable in practice. In addition, the majority of these algorithms neglect the current measurement bias. We introduce our solutions to both issues in this research.

The presented research is the first attempt to estimate SoC in real-time based on battery boundary conditions (cut-off voltages) and current and voltage measurements. It also presents the first direct attempt at current noise mitigation by considering the corrupted current measurement including white noise and random-walk bias noise.

The real-time SoC estimation algorithm presented in Chapter 4 is based on a new SoC-OCV model, where the physical battery parameters are estimated using the adaptive law (as this guarantees parameter convergence). The OCV is estimated using the KF, the SoC is estimated using the EKF and another KF is used to develop the nonlinear curve estimation algorithm. Estimating the SoC-OCV relationship not only removes the laborious preliminary laboratory work but also makes the SoC estimation algorithm adaptive to the changes in operational conditions, battery ageing and different

batteries. The proposed algorithm is validated by performing the use of computer simulation and battery experiments. The battery experiments show that the maximum SoC estimation error is less than 2.5%. In computer simulations, the error is within 1.8% under the DST current profile whereas it is 1.53% under the HPPC current profile. Both results confirm that the proposed method provides an accurate estimation of SoC in real-time.

Current measurement bias is estimated based on the difference between $\Delta\tilde{V}_t$ and $\Delta\hat{V}_t$. The current sensor output is then corrected by subtracting the estimated bias from the measured current. Moreover, the standard KF is modified according to the input current model and SoC is estimated using the modified KF. Correcting the current input measurement significantly reduces the SoC estimation error. The proposed algorithm is assessed by computer simulations and the battery experiment. In the simulations, the maximum SoC estimation error is reduced from 7.2% to 0.78% under the DST cycle. The error in the SoC estimation using measured current is calculated as 11.3% in the HPPC cycle simulations. By using the corrected current measurement input, this error is reduced to 0.56%. In the battery experiment, the error in the SoC estimation using measured current is calculated to be 1.74%. It is reduced to 1.12% using the corrected current measurement input. It can be concluded that one of the error sources in the SoC estimation problem is significantly eliminated by the proposed method. Our current bias mitigation algorithm provides a more realistic SoC estimation under the noisy current measurement taking place in practice.

In summary, there are two novel methods added to the current SoC estimation literature. In the first method, changes in the SoC-OCV curve by operational condition and battery ageing are automatically reflected in the SoC estimation in real-time. In the second method, the current input measurement is corrected by estimating the noise added by the current measurement sensor. The proposed methods reduce the SoC estimation error due to the inaccuracy in the SoC-OCV nonlinear curve obtained offline and the inaccurate current input measurement. These methods are validated by computer simulations and the battery experiment. These results show that the proposed algorithms can be implemented in real-time applications.

6.2 Future work

This research has developed an engineering practice and a theoretical framework that are essential in advancing the current SoC estimation techniques. Two methods have been developed that tackle the real-time calculation of the SoC-OCV relationship and corrupted current measurement. Both of these advancements are essential in making the long-awaited leap of estimation algorithms from ideal setups to real-time applications. Equally, this work alludes to further questions that must be addressed in order to see the industrial implementation of these algorithms. These points are outlined as follows:

1. The model parameter convergence to true model parameters under different dynamic loading conditions will be investigated to see if the model parameters always converge to the true ones.

2. The effect of the variations in the battery cut-off voltages on constructing the SoC-OCV relationship will be investigated. Intentionally inaccurate battery boundary conditions will be used to see the effect on the SoC-OCV curve construction algorithm.

3. The proposed SoC-OCV nonlinear model will be assessed for different battery types to see if the proposed model captures different battery characteristics. Different batteries in terms of battery chemistry will be chosen and their SoC-OCV relationship will be calculated by a battery drop test. Then, the calculated data will be curve-fitted by the proposed nonlinear model.

4. The observability of the SoC estimation problem and the behaviour of the SoC estimation error when the slope of the SoC-OCV curve gets closer to zero will be investigated.

5. The behaviour of the SoC estimation error due to the difference between the model and the truth will be investigated by realistic and extreme condition experiments.

6. The impact of the small positive constant (δ) on the SoC estimation accuracy and the optimal online calculation of δ will be investigated. The idea of collecting data in 4 calculation steps will be investigated to calculate the optimal δ.

7. The effect of the time interval (Δt) on the accuracy of the calculation of dV_{oc}/dz along with the behaviour of the SoC estimation error will be investigated.

8. The influence of the parameter estimation accuracy on the bias noise estimation will be investigated. Additionally, the effect of the different types of voltage measurement noises on the bias noise estimation accuracy will be investigated.

9. In order to observe larger bias noises in the current measurement, longer battery experiments in terms of the time duration are needed. Further experimental analysis of the bias noise estimation algorithm will be conducted.

References

Aburakhis, Mohamed, Ordóñez, Raúl, and Djaneye-Boundjou, Ouboti (2022). "A Discrete Fractional Order Adaptive Law for Parameter Estimation and Adaptive Control". In: *IEEE Open Journal of Control Systems* 1, pp. 113–125. DOI: 10.1109/OJCSYS.2022.3185002.

Adaikkappan, Maheshwari and Sathiyamoorthy, Nageswari (2022). "Modeling, state of charge estimation, and charging of lithium-ion battery in electric vehicle: A review". In: *International Journal of Energy Research* 46.3, pp. 2141–2165.

Ali, Muhammad U., Khan, Hafiz F., Masood, Haris, Kallu, Karam D., Ibrahim, Malik M., Zafar, Amad, Oh, Semin, and Kim, Sangil (2022). "An adaptive state of charge estimator for lithium-ion batteries". In: *Energy Science & Engineering* 10.7, pp. 2333–2347. DOI: https://doi.org/10.1002/ese3.1141. eprint: https://onlinelibrary.wiley.com/doi/pdf/10.1002/ese3.1141. URL: https://onlinelibrary.wiley.com/doi/abs/10.1002/ese3.1141.

Atlung, S., West, K., and Jacobsen, T. (1979). "Dynamic aspects of solid solution cathodes for electrochemical power sources". In: *J. Electrochem. Soc*, pp. 1311–1321.

Aung, H., Soon Low, K., and Ting Goh, S. (2015). "State-of-Charge Estimation of Lithium-Ion Battery Using Square Root Spherical Unscented Kalman Filter (Sqrt-UKFST) in Nanosatellite". In: *IEEE Transactions on Power Electronics* 30.9, pp. 4774–4783. DOI: 10.1109/TPEL.2014.2361755.

Baba, Naoki, Yoshida, Hiroaki, Nagaoka, Makoto, Okuda, Chikaaki, and Kawauchi, Shigehiro (2014). "Numerical simulation of thermal behavior of lithium-ion secondary batteries using the enhanced single particle model". In: *Journal of Power*

Sources 252, pp. 214–228. ISSN: 0378-7753. DOI: https://doi.org/10.1016/j.jpowsour.2013.11.111. URL: http://www.sciencedirect.com/science/article/pii/S037877531301954X.

Barcellona, Simone, Colnago, Silvia, Dotelli, Giovanni, Latorrata, Saverio, and Piegari, Luigi (2022). "Aging effect on the variation of Li-ion battery resistance as function of temperature and state of charge". In: *Journal of Energy Storage* 50, p. 104658. ISSN: 2352-152X. DOI: https://doi.org/10.1016/j.est.2022.104658. URL: https://www.sciencedirect.com/science/article/pii/S2352152X22006727.

Barsali, S. and Ceraolo, M. (2002). "Dynamical models of lead-acid batteries: implementation issues". In: *IEEE Transactions on Energy Conversion* 17.1, pp. 16–23. DOI: 10.1109/60.986432.

Beelen, Henrik, Bergveld, Henk Jan, and Donkers, M. C. F. (2021). "Joint Estimation of Battery Parameters and State of Charge Using an Extended Kalman Filter: A Single-Parameter Tuning Approach". In: *IEEE Transactions on Control Systems Technology* 29.3, pp. 1087–1101. DOI: 10.1109/TCST.2020.2992523.

Bian, Xiaolei, Wei, Zhongbao, He, Jiangtao, Yan, Fengjun, and Liu, Longcheng (2020). "A two-step parameter optimization method for low-order model-based state-of-charge estimation". In: *IEEE Transactions on Transportation Electrification* 7.2, pp. 399–409.

Bo, Cheng, Zhifeng, Bai, and Binggang, Cao (2008). "State of charge estimation based on evolutionary neural network". In: *Energy Conversion and Management* 49.10, pp. 2788–2794. ISSN: 0196-8904. DOI: https://doi.org/10.1016/j.enconman.2008.03.013. URL: https://www.sciencedirect.com/science/article/pii/S0196890408001131.

Çelikten, Baran, Eren, Ozan, and Karataş, Yusuf Selim (2022). "An execution time optimized state of charge estimation method for lithium-ion battery". In: *Journal of Energy Storage* 51, p. 104307. ISSN: 2352-152X. DOI: https://doi.org/10.1016/j.est.2022.104307. URL: https://www.sciencedirect.com/science/article/pii/S2352152X22003334.

Chaoui, H. and Gualous, H. (2017). "Adaptive State of Charge Estimation of Lithium-Ion Batteries With Parameter and Thermal Uncertainties". In: *IEEE Transactions on Control Systems Technology* 25.2, pp. 752–759. DOI: 10.1109/TCST.2016.2572362.

Chaoui, Hicham, Golbon, Navid, Hmouz, Imad, Souissi, Ridha, and Tahar, Sofiène (2015). "Lyapunov-Based Adaptive State of Charge and State of Health Estimation for Lithium-Ion Batteries". In: *IEEE Transactions on Industrial Electronics* 62.3, pp. 1610–1618. DOI: 10.1109/TIE.2014.2341576.

Chen, Cheng, Xiong, Rui, Yang, Ruixin, and Li, Hailong (2022). "A Novel Operational Data-Driven Battery Open-Circuit Voltage Characterization mining method for Large-Scale Applications". In: *Green Energy and Intelligent Transportation*, pp. 827–841. ISSN: 2773-1537. DOI: https://doi.org/10.1016/j.geits.2022.100001. URL: https://www.sciencedirect.com/science/article/pii/S2773153722000019.

Chen, Bo-Chiuan and Chuang, Guo-Shun (2017). "State of Charge Estimation for Lithium-Ion Batteries Using Extended Kalman Filter with Local Linearization". In: *The 13th International Conference on Automotive Engineering*. SAE International. DOI: https://doi.org/10.4271/2017-01-1734. URL: https://doi.org/10.4271/2017-01-1734.

Chen, Xiaokai, Lei, Hao, Xiong, Rui, Shen, Weixiang, and Yang, Ruixin (2019). "A novel approach to reconstruct open circuit voltage for state of charge estimation of lithium ion batteries in electric vehicles". In: *Applied Energy* 255, p. 113758.

Chen, Zhenggang, Zhou, Jianxiong, Zhou, Fei, and Xu, Shuai (2021). "State-of-charge estimation of lithium-ion batteries based on improved H infinity filter algorithm and its novel equalization method". In: *Journal of Cleaner Production* 290, pp. 125–138.

Choi, Eunseok and Chang, Sekchin (2020). "A Temperature-Dependent State of Charge Estimation Method Including Hysteresis for Lithium-Ion Batteries in Hybrid Electric Vehicles". In: *IEEE Access* 8, pp. 129857–129868. DOI: 10.1109/ACCESS.2020.3009281.

Chun, Chang Yoon, Cho, Bohyung, and Kim, Jonghoon (2016). "Implementation of discharging/charging current sensorless state-of-charge estimator reflecting cell-to-cell variations in lithium-ion series battery packs". In: *International Journal of Automotive Technology* 17, pp. 909–916.

Ciochina, Silviu, Paleologu, Constantin, Benesty, Jacob, and Enescu, Andrei (Aug. 2009). "On the influence of the forgetting factor of the RLS adaptive filter in system identification". In: pp. 1–4. DOI: 10.1109/ISSCS.2009.5206117.

Corno, Matteo, Bhatt, Nimitt, Savaresi, Sergio, and Verhaegen, Michel (Jan. 2015). "Electrochemical Model-Based State of Charge Estimation for Li-Ion Cells". In: *Control Systems Technology, IEEE Transactions on* 23, pp. 117–127. DOI: 10.1109/TCST.2014.2314333.

Crassidis, John L and Junkins, John L (2004). *Optimal estimation of dynamic systems*. Chapman and Hall/CRC.

Cui, Zhenhua, Wang, Licheng, Li, Qiang, and Wang, Kai (2022). "A comprehensive review on the state of charge estimation for lithium-ion battery based on neural network". In: *International Journal of Energy Research* 46.5, pp. 5423–5440. DOI: https://doi.org/10.1002/er.7545. eprint: https://onlinelibrary.wiley.com/doi/pdf/10.1002/er.7545. URL: https://onlinelibrary.wiley.com/doi/abs/10.1002/er.7545.

Deng, Dan, Liu, Sheng-Yong, Wang, Shunli, Xia, Li-Li, and Chen, Lei (May 2021). "An improved second-order electrical equivalent modeling method for the online high power Li-ion battery state of charge estimation". In: pp. 1725–1729. DOI: 10.1109/ECCE-Asia49820.2021.9479017.

Deng, Zhongwei, Yang, Lin, Cai, Yishan, Deng, Hao, and Sun, Liu (2016). "Online available capacity prediction and state of charge estimation based on advanced data-driven algorithms for lithium iron phosphate battery". In: *Energy* 112, pp. 469–480. ISSN: 0360-5442. DOI: https://doi.org/10.1016/j.energy.2016.06.130. URL: https://www.sciencedirect.com/science/article/pii/S0360544216309045.

Dewangga, B. R., Herdjunanto, S., and Cahyadi, A. (2018). "Battery Current Estimation Based on Simple Model with Parameter Update Strategy Using Piecewise Linear SOC-OCV". In: *2018 4th International Conference on Science and Technology (ICST)*, pp. 1–6. DOI: 10.1109/ICSTC.2018.8528694.

Ding, Xiaofeng, Zhang, Donghuai, Cheng, Jiawei, Wang, Binbin, and Luk, Patrick Chi Kwong (2019). "An improved Thevenin model of lithium-ion battery with high accuracy for electric vehicles". In: *Applied Energy* 254, p. 113615. ISSN: 0306-2619. DOI: https://doi.org/10.1016/j.apenergy.2019.113615. URL: https://www.sciencedirect.com/science/article/pii/S0306261919312899.

Dong, Guangzhong, Chen, Zonghai, and Wei, Jingwen (2019). "Sequential Monte Carlo Filter for State-of-Charge Estimation of Lithium-Ion Batteries Based on Auto Regressive Exogenous Model". In: *IEEE Transactions on Industrial Electronics* 66.11, pp. 8533–8544. DOI: 10.1109/TIE.2018.2890499.

Doyle, Marc, Fuller, Thomas F, and Newman, John (1993). "Modeling of galvanostatic charge and discharge of the lithium/polymer/insertion cell". In: *Journal of the Electrochemical society* 140.6, pp. 1526–1537.

Eddahech, A., Briat, O., and Vinassa, J.M. (2012). "Adaptive voltage estimation for EV Li-ion cell based on artificial neural networks state-of-charge meter". In: *2012 IEEE International Symposium on Industrial Electronics*, pp. 1318–1324. DOI: 10.1109/ISIE.2012.6237281.

Fang, Chao, Jin, Zhiyang, Wu, Jingjin, and Liu, Chenguang (2021). "Estimation of Lithium-Ion Battery SOC Model Based on AGA-FOUKF Algorithm". In: *Frontiers in Energy Research* 9. ISSN: 2296-598X. DOI: 10.3389/fenrg.2021.769818. URL: https://www.frontiersin.org/article/10.3389/fenrg.2021.769818.

Farmann, Alexander, Waag, Wladislaw, Marongiu, Andrea, and Sauer, Dirk Uwe (2015). "Critical review of on-board capacity estimation techniques for lithium-ion batteries in electric and hybrid electric vehicles". In: *Journal of Power Sources* 281, pp. 114–130. ISSN: 0378-7753. DOI: https://doi.org/10.1016/j.jpowsour.2015.01.129. URL: http://www.sciencedirect.com/science/article/pii/S0378775315001457.

Gao, Ruizhi, Liu, Shulin, and Cui, Naxin (2017). "Online parametric adaptive state of charge estimation for lithium batteries". In: *2017 Chinese Automation Congress (CAC)*, pp. 1442–1447. DOI: 10.1109/CAC.2017.8242994.

Gholizadeh, Mehdi and Salmasi, Farzad R. (2014). "Estimation of State of Charge, Unknown Nonlinearities, and State of Health of a Lithium-Ion Battery Based on a Comprehensive Unobservable Model". In: *IEEE Transactions on Industrial Electronics* 61.3, pp. 1335–1344. DOI: 10.1109/TIE.2013.2259779.

Grewal, S. and Grant, D.A. (2001). "A novel technique for modelling the state of charge of lithium ion batteries using artificial neural networks". In: *2001 Twenty-Third International Telecommunications Energy Conference INTELEC 2001*, pp. 174–179. DOI: 10.1049/cp:20010596.

Guo, Meng, Sikha, Godfrey, and White, Ralph E. (2011). "Single-Particle Model for a Lithium-Ion Cell: Thermal Behavior". In: *Journal of The Electrochemical Society* 158.2, A122. DOI: 10.1149/1.3521314. URL: https://doi.org/10.1149/1.3521314.

Han, Xuebing, Ouyang, Minggao, Lu, Languang, and Li, Jianqiu (2014). "Cycle Life of Commercial Lithium-Ion Batteries with Lithium Titanium Oxide Anodes in Electric Vehicles". In: *Energies* 7.8, pp. 4895–4909. ISSN: 1996-1073. DOI: 10.3390/en7084895. URL: https://www.mdpi.com/1996-1073/7/8/4895.

Hannan, M.A., Lipu, M.S.H., Hussain, A., and Mohamed, A. (2017). "A review of lithium-ion battery state of charge estimation and management system in electric vehicle applications: Challenges and recommendations". In: *Renewable and Sustainable Energy Reviews* 78, pp. 834–854. ISSN: 1364-0321. DOI: https://doi.org/10.1016/j.rser.2017.05.001. URL: https://www.sciencedirect.com/science/article/pii/S1364032117306275.

Hannan, Mahammad Abdul, Lipu, MS, Hussain, Aini, Ker, Pin Jern, Mahlia, TM Indra, Mansor, Muhamad, Ayob, Afida, Saad, Mohamad H, and Dong, ZY (2020). "Toward enhanced state of charge estimation of lithium-ion batteries using optimized machine learning techniques". In: *Scientific reports* 10.1, pp. 1–15. DOI: https://doi.org/10.1038/s41598-020-61464-7.

Hashemzadeh, Pouya, Désilets, Martin, Lacroix, Marcel, and Jokar, Ali (2022). "Investigation of the P2D and of the modified single-particle models for predicting the nonlinear behavior of Li-ion batteries". In: *Journal of Energy Storage* 52, pp. 104–119. ISSN: 2352-152X. DOI: https://doi.org/10.1016/j.est.2022.104909. URL: https://www.sciencedirect.com/science/article/pii/S2352152X22009161.

Haus, Benedikt and Mercorelli, Paolo (2020). "Polynomial Augmented Extended Kalman Filter to Estimate the State of Charge of Lithium-Ion Batteries". In: *IEEE Transactions on Vehicular Technology* 69.2, pp. 1452–1463. DOI: 10.1109/TVT.2019.2959720.

He, Hongwen, Xiong, Rui, Zhang, Xiaowei, Sun, Fengchun, and Fan, JinXin (2011). "State-of-Charge Estimation of the Lithium-Ion Battery Using an Adaptive Extended Kalman Filter Based on an Improved Thevenin Model". In: *IEEE Transactions on Vehicular Technology* 60.4, pp. 1461–1469. DOI: 10.1109/TVT.2011.2132812.

He, Lin, Wang, Yangyang, Wei, Yujiang, Wang, Mingwei, Hu, Xiaosong, and Shi, Qin (2022). "An adaptive central difference Kalman filter approach for state of charge estimation by fractional order model of lithium-ion battery". In: *Energy* 244, pp. 122–136. ISSN: 0360-5442. DOI: https://doi.org/10.1016/j.energy.2021.122627. URL: https://www.sciencedirect.com/science/article/pii/S0360544221028760.

He, Zhicheng, Yang, Ziming, Cui, Xiangyu, and Li, Eric (2020). "A Method of State-of-Charge Estimation for EV Power Lithium-Ion Battery Using a Novel Adaptive Extended Kalman Filter". In: *IEEE Transactions on Vehicular Technology* 69.12, pp. 14618–14630. DOI: 10.1109/TVT.2020.3032201.

Hong, Seonri, Kang, Moses, Park, Hwapyeong, Kim, Jonghoon, and Baek, Jongbok (2022). "Real-Time State-of-Charge Estimation Using an Embedded Board for Li-Ion Batteries". In: *Electronics* 11.13, pp. 142–158. ISSN: 2079-9292. DOI: 10.3390/electronics11132010. URL: https://www.mdpi.com/2079-9292/11/13/2010.

Hongwen, He et al. (2011). "Evaluation of lithium-ion battery equivalent circuit models for state of charge estimation by an experimental approach". In: *energies* 4.4, pp. 582–598.

Hongwen, He, Rui, Xiong, Hongqiang, Guo, and Shuchun, Li (2012). "Comparison study on the battery models used for the energy management of batteries in electric vehicles". In: *Energy Conversion and Management* 64, pp. 113–121.

Hu, Xiaosong et al. (2021). "Research directions for next-generation battery management solutions in automotive applications". In: *Renewable and Sustainable Energy Reviews* 152, p. 111695. ISSN: 1364-0321. DOI: https://doi.org/10.1016/j.rser.2021.111695. URL: https://www.sciencedirect.com/science/article/pii/S1364032121009692.

Hu, Xiaosong, Yuan, Hao, Zou, Changfu, Li, Zhe, and Zhang, Lei (2018). "Co-Estimation of State of Charge and State of Health for Lithium-Ion Batteries Based on Fractional-Order Calculus". In: *IEEE Transactions on Vehicular Technology* 67.11, pp. 10319–10329. DOI: 10.1109/TVT.2018.2865664.

Huang, Chao, Wang, Zhenhua, Zhao, Zihan, Wang, Long, Lai, Chun Sing, and Wang, Dong (2018). "Robustness Evaluation of Extended and Unscented Kalman Filter for Battery State of Charge Estimation". In: *IEEE Access* 6, pp. 27617–27628. DOI: 10.1109/ACCESS.2018.2833858.

Huang, Cong-Sheng and Chow, Mo-Yuen (2021). "Robust State-of-Charge Estimation for Lithium-Ion Batteries Over Full SOC Range". In: *IEEE Journal of Emerging and Selected Topics in Industrial Electronics* 2.3, pp. 305–313. DOI: 10.1109/JESTIE.2021.3078253.

Ioannou, Petros and Fidan, Bariş (2006). *Adaptive Control Tutorial*. Philadelphia, PA: Society for Industrial and Applied Mathematics. DOI: 10.1137/1.9780898718652. eprint: https://epubs.siam.org/doi/pdf/10.1137/1.9780898718652. URL: https://epubs.siam.org/doi/abs/10.1137/1.9780898718652.

Jarrraya, Imen, Degaa, Laid, Rizoug, Nassim, Chabchoub, Mohamed Hedi, and Trabelsi, Hafedh (2022). "Comparison study between hybrid Nelder-Mead particle swarm

optimization and open circuit voltage—Recursive least square for the battery parameters estimation". In: *Journal of Energy Storage* 50, p. 104424. ISSN: 2352-152X. DOI: https://doi.org/10.1016/j.est.2022.104424. URL: https://www.sciencedirect.com/science/article/pii/S2352152X22004479.

Jiang, Xue, Zhang, Bowen, Yufeng, Wang, Xiang, Yi, and Li, Weilin (Nov. 2020). "Modeling and state of charge estimation of Lithium-ion Battery using the autoregressive exogenous model". In: pp. 1–7. DOI: 10.1109/CIYCEE49808.2020.9332582.

Jibhkate, Ujwal N. and Mujumdar, Uday B. (2022). "Development of low complexity open circuit voltage model for state of charge estimation with novel curve modification technique". In: *Electrochimica Acta* 429, pp. 1409–1424. ISSN: 0013-4686. DOI: https://doi.org/10.1016/j.electacta.2022.140944. URL: https://www.sciencedirect.com/science/article/pii/S001346862201101X.

Johnson, V.H. (2002). "Battery performance models in ADVISOR". In: *Journal of Power Sources* 110.2, pp. 321–329. ISSN: 0378-7753. DOI: https://doi.org/10.1016/S0378-7753(02)00194-5. URL: https://www.sciencedirect.com/science/article/pii/S0378775302001945.

Jokić, Ivan, Zečević, Žarko, and Krstajić, Božo (2018). "State-of-charge estimation of lithium-ion batteries using extended Kalman filter and unscented Kalman filter". In: *2018 23rd International Scientific-Professional Conference on Information Technology (IT)*, pp. 1–4. DOI: 10.1109/SPIT.2018.8350462.

Kim, J., Shin, J., Chun, C., and Cho, B. H. (2012). "Stable Configuration of a Li-Ion Series Battery Pack Based on a Screening Process for Improved Voltage/SOC Balancing". In: *IEEE Transactions on Power Electronics* 27.1, pp. 411–424. DOI: 10.1109/TPEL.2011.2158553.

Kim, Woo-Yong, Lee, Pyeong-Yeon, Kim, Jonghoon, and Kim, Kyung-Soo (2019). "State of Charge and Equivalent Internal Resistance Estimation for a Multi-cell Application based on Cell-Difference-Model". In: *2019 IEEE Energy Conversion Congress and Exposition (ECCE)*, pp. 2664–2668. DOI: 10.1109/ECCE.2019.8912623.

Knap, Vaclav and Stroe, Daniel-Ioan (2021). "Effects of open-circuit voltage tests and models on state-of-charge estimation for batteries in highly variable temperature environments: Study case nano-satellites". In: *Journal of Power Sources* 498, p. 229913. ISSN: 0378-7753. DOI: https://doi.org/10.1016/j.jpowsour.2021.229913. URL: https://www.sciencedirect.com/science/article/pii/S0378775321004444.

Ko, Younghwi, Cho, Kangcheol, Kim, Minseong, and Choi, Woojin (2022). "A Novel Capacity Estimation Method for the Lithium Batteries Using the Enhanced Coulomb Counting Method With Kalman Filtering". In: *IEEE Access* 10, pp. 38793–38801. DOI: 10.1109/ACCESS.2022.3165639.

Lee, Seongjun, Kim, Jonghoon, Lee, Jaemoon, and Cho, B.H. (2008). "State-of-charge and capacity estimation of lithium-ion battery using a new open-circuit voltage versus state-of-charge". In: *Journal of Power Sources* 185.2, pp. 1367–1373. ISSN: 0378-7753. DOI: https://doi.org/10.1016/j.jpowsour.2008.08.103. URL: https://www.sciencedirect.com/science/article/pii/S0378775308017965.

Li, Yigang, Chen, Jiqing, and Lan, Fengchong (2020). "Enhanced online model identification and state of charge estimation for lithium-ion battery under noise corrupted measurements by bias compensation recursive least squares". In: *Journal of Power Sources* 456, p. 227984. ISSN: 0378-7753. DOI: https://doi.org/10.1016/j.jpowsour.2020.227984. URL: https://www.sciencedirect.com/science/article/pii/S0378775320302871.

Lin, Xinfan (2018). "Theoretical Analysis of Battery SOC Estimation Errors Under Sensor Bias and Variance". In: *IEEE Transactions on Industrial Electronics* 65.9, pp. 7138–7148. DOI: 10.1109/TIE.2018.2795521.

Ling, Liuyi and Wei, Ying (2021). "State-of-Charge and State-of-Health Estimation for Lithium-Ion Batteries Based on Dual Fractional-Order Extended Kalman Filter and Online Parameter Identification". In: *IEEE Access* 9, pp. 47588–47602. DOI: 10.1109/ACCESS.2021.3068813.

Liu, Datong, Li, Lyu, Song, Yuchen, Wu, Lifeng, and Peng, Yu (2019). "Hybrid state of charge estimation for lithium-ion battery under dynamic operating conditions". In: *International Journal of Electrical Power & Energy Systems* 110, pp. 48–61.

ISSN: 0142-0615. DOI: https://doi.org/10.1016/j.ijepes.2019.02.046. URL: https://www.sciencedirect.com/science/article/pii/S0142061518318118.

Liu, Shuai, Wang, Zidong, Chen, Yun, and Wei, Guoliang (2020). "Protocol-Based Unscented Kalman Filtering in the Presence of Stochastic Uncertainties". In: *IEEE Transactions on Automatic Control* 65.3, pp. 1303–1309. DOI: 10.1109/TAC.2019.2929817.

Liu, X., Jin, Y., Zeng, S., Chen, X., Feng, Y., Liu, S., and Liu, H. (2020). "Online identification of power battery parameters for electric vehicles using a decoupling multiple forgetting factors recursive least squares method". In: *CSEE Journal of Power and Energy Systems* 6.3, pp. 735–742. DOI: 10.17775/CSEEJPES.2018.00960.

Liu, Xiangyong, Li, Wanli, and Zhou, Aiguo (2018). "PNGV Equivalent Circuit Model and SOC Estimation Algorithm for Lithium Battery Pack Adopted in AGV Vehicle". In: *IEEE Access* 6, pp. 23639–23647. DOI: 10.1109/ACCESS.2018.2812421.

Liu, Xingtao, Chen, Zonghai, Zhang, Chenbin, and Wu, Ji (2014). "A novel temperature-compensated model for power Li-ion batteries with dual-particle-filter state of charge estimation". In: *Applied Energy* 123, pp. 263–272.

Liu, Zhentong and He, Hongwen (2015). "Model-based Sensor Fault Diagnosis of a Lithium-ion Battery in Electric Vehicles". In: *Energies* 8.7, pp. 6509–6527. ISSN: 1996-1073. DOI: 10.3390/en8076509. URL: https://www.mdpi.com/1996-1073/8/7/6509.

Long, Yin (2022). "A novel method for obtaining open-circuit-voltage and estimating state-of-charge considering battery-pack inconsistencies". In: DOI: http://dx.doi.org/10.2139/ssrn.4151299.

Loukil, Jihen, Masmoudi, Ferdaous, and Derbel, Nabil (2017). "State of charge estimation of lead acid battery using a Kalman filter". In: *2017 14th International Multi-Conference on Systems, Signals & Devices (SSD)*, pp. 308–312. DOI: 10.1109/SSD.2017.8167026.

Ma, Wentao, Qiu, Jinzhe, Liang, Junli, and Chen, Badong (2019). "Linear Kalman Filtering Algorithm With Noisy Control Input Variable". In: *IEEE Transactions on*

Circuits and Systems II: Express Briefs 66.7, pp. 1282–1286. DOI: 10.1109/TCSII.2018.2878951.

Macioszek, Elżbieta (2020). "Electric Vehicles - Problems and Issues". In: *Smart and Green Solutions for Transport Systems*. Ed. by Grzegorz Sierpiński. Cham: Springer International Publishing, pp. 169–183. ISBN: 978-3-030-35543-2.

Meng, Jinhao, Stroe, Daniel-Ioan, Ricco, Mattia, Luo, Guangzhao, and Teodorescu, Remus (2019). "A Simplified Model-Based State-of-Charge Estimation Approach for Lithium-Ion Battery With Dynamic Linear Model". In: *IEEE Transactions on Industrial Electronics* 66.10, pp. 7717–7727. DOI: 10.1109/TIE.2018.2880668.

Mohammadi, Fazel (2022). "Lithium-ion battery State-of-Charge estimation based on an improved Coulomb-Counting algorithm and uncertainty evaluation". In: *Journal of Energy Storage* 48, p. 104061. ISSN: 2352-152X. DOI: https://doi.org/10.1016/j.est.2022.104061. URL: https://www.sciencedirect.com/science/article/pii/S2352152X22000986.

Naseri, Farshid, Schaltz, Erik, Stroe, Daniel-Ioan, Gismero, Alejandro, and Farjah, Ebrahim (2022). "An Enhanced Equivalent Circuit Model With Real-Time Parameter Identification for Battery State-of-Charge Estimation". In: *IEEE Transactions on Industrial Electronics* 69.4, pp. 3743–3751. DOI: 10.1109/TIE.2021.3071679.

Newman, John S. and Thomas-Alyea, Karen E (2004). *Electrochemical systems / John Newman and Karen E. Thomas-Alyea.* eng. 3rd ed. Hoboken, N.J.: J. Wiley. ISBN: 0471477567.

Ng, Kong Soon, Moo, Chin-Sien, Chen, Yi-Ping, and Hsieh, Yao-Ching (2009). "Enhanced coulomb counting method for estimating state-of-charge and state-of-health of lithium-ion batteries". In: *Applied Energy* 86.9, pp. 1506–1511. ISSN: 0306-2619. DOI: https://doi.org/10.1016/j.apenergy.2008.11.021. URL: https://www.sciencedirect.com/science/article/pii/S0306261908003061.

Ouyang, Q., Chen, J., and Zheng, J. (2020). "State-of-Charge Observer Design for Batteries With Online Model Parameter Identification: A Robust Approach". In:

IEEE Transactions on Power Electronics 35.6, pp. 5820–5831. DOI: 10.1109/TPEL.2019.2948253.

Ouyang, Tiancheng, Xu, Peihang, Chen, Jingxian, Lu, Jie, and Chen, Nan (2021). "An Online Prediction of Capacity and Remaining Useful Life of Lithium-Ion Batteries Based on Simultaneous Input and State Estimation Algorithm". In: *IEEE Transactions on Power Electronics* 36.7, pp. 8102–8113. DOI: 10.1109/TPEL.2020.3044725.

Pang, Hui, Guo, Long, Wu, Longxing, and Jin, Xinfang (2020). "An enhanced temperature-dependent model and state-of-charge estimation for a Li-Ion battery using extended Kalman filter". In: *International Journal of Energy Research* 44.9, pp. 7254–7267. DOI: https://doi.org/10.1002/er.5435. eprint: https://onlinelibrary.wiley.com/doi/pdf/10.1002/er.5435. URL: https://onlinelibrary.wiley.com/doi/abs/10.1002/er.5435.

Park, Saehong, Zhang, Dong, and Moura, Scott (2017). "Hybrid electrochemical modeling with recurrent neural networks for li-ion batteries". In: *2017 American Control Conference (ACC)*, pp. 3777–3782. DOI: 10.23919/ACC.2017.7963533.

Partovibakhsh, Maral and Liu, Guangjun (2015). "An Adaptive Unscented Kalman Filtering Approach for Online Estimation of Model Parameters and State-of-Charge of Lithium-Ion Batteries for Autonomous Mobile Robots". In: *IEEE Transactions on Control Systems Technology* 23.1, pp. 357–363. DOI: 10.1109/TCST.2014.2317781.

Pastor-Fernández, C., Bruen, T., Widanage, W.D., Gama-Valdez, M.A., and Marco, J. (2016). "A Study of Cell-to-Cell Interactions and Degradation in Parallel Strings: Implications for the Battery Management System". In: *Journal of Power Sources* 329, pp. 574–585. ISSN: 0378-7753. DOI: https://doi.org/10.1016/j.jpowsour.2016.07.121. URL: https://www.sciencedirect.com/science/article/pii/S0378775316309995.

Piao, Changhao, Yang, Xiaoyong, Teng, Cong, and Yang, HuiQian (2010). "An improved model based on artificial neural networks and Thevenin model for nickel metal hydride power battery". In: *2010 International Conference on Optics, Photonics and Energy Engineering (OPEE)*. Vol. 1, pp. 115–118. DOI: 10.1109/OPEE.2010.5508184.

Piller, Sabine, Perrin, Marion, and Jossen, Andreas (2001). "Methods for state-of-charge determination and their applications". In: *Journal of Power Sources* 96.1. Proceedings of the 22nd International Power Sources Symposium, pp. 113–120. ISSN: 0378-7753. DOI: https://doi.org/10.1016/S0378-7753(01)00560-2. URL: https://www.sciencedirect.com/science/article/pii/S0378775301005602.

Ping, Shen, Minggao, Ouyang, Languang, Lu, Jianqiu, Li, and Xuning, Feng (2018). "The Co-estimation of State of Charge, State of Health, and State of Function for Lithium-Ion Batteries in Electric Vehicles". In: *IEEE Transactions on Vehicular Technology* 67.1, pp. 92–103. DOI: 10.1109/TVT.2017.2751613.

Plett, Gregory L. (2004a). "Extended Kalman filtering for battery management systems of LiPB-based HEV battery packs: Part 1. Background". In: *Journal of Power Sources* 134.2, pp. 252–261. ISSN: 0378-7753. DOI: https://doi.org/10.1016/j.jpowsour.2004.02.031. URL: https://www.sciencedirect.com/science/article/pii/S0378775304003593.

– (2004b). "Extended Kalman filtering for battery management systems of LiPB-based HEV battery packs: Part 2. Modeling and identification". In: *Journal of Power Sources* 134.2, pp. 262–276. ISSN: 0378-7753. DOI: https://doi.org/10.1016/j.jpowsour.2004.02.032. URL: https://www.sciencedirect.com/science/article/pii/S037877530400360X.

Prashant, Shrivastava, Soon, Tey Kok, Mohd, Idris, and Saad, Mekhilef (May 2021). "Lithium-ion Battery Model Parameter Identification Using Modified Adaptive Forgetting Factor-Based Recursive Least Square Algorithm". In: pp. 2169–2174. DOI: 10.1109/ECCE-Asia49820.2021.9479079.

Rahimifard, Sara, Ahmed, Ryan, and Habibi, Saeid (2021). "Interacting Multiple Model Strategy for Electric Vehicle Batteries State of Charge/Health/ Power Estimation". In: *IEEE Access* 9, pp. 109875–109888. DOI: 10.1109/ACCESS.2021.3102607.

Ren, Pu, Wang, Shunli, Huang, Junhan, Chen, Xianpei, He, Mingfang, and Cao, Wen (2022). "Novel co-estimation strategy based on forgetting factor dual particle filter algorithm for the state of charge and state of health of the lithium-ion battery". In:

International Journal of Energy Research 46.2, pp. 1094–1107. DOI: https://doi.org/10.1002/er.7230. eprint: https://onlinelibrary.wiley.com/doi/pdf/10.1002/er.7230. URL: https://onlinelibrary.wiley.com/doi/abs/10.1002/er.7230.

Seaman, Aden, Dao, Thanh-Son, and McPhee, John (2014). "A survey of mathematics-based equivalent-circuit and electrochemical battery models for hybrid and electric vehicle simulation". In: *Journal of Power Sources* 256, pp. 410–423. ISSN: 0378-7753. DOI: https://doi.org/10.1016/j.jpowsour.2014.01.057. URL: https://www.sciencedirect.com/science/article/pii/S0378775314000810.

Shehab El Din, M., Hussein, A. A., and Abdel-Hafez, M. F. (2018). "Improved Battery SOC Estimation Accuracy Using a Modified UKF With an Adaptive Cell Model Under Real EV Operating Conditions". In: *IEEE Transactions on Transportation Electrification* 4.2, pp. 408–417. DOI: 10.1109/TTE.2018.2802043.

Shen, Jia-Ni, Shen, Jia-Jin, He, Yi-Jun, and Ma, Zi-Feng (2019). "Accurate State of Charge Estimation With Model Mismatch for Li-Ion Batteries: A Joint Moving Horizon Estimation Approach". In: *IEEE Transactions on Power Electronics* 34.5, pp. 4329–4342. DOI: 10.1109/TPEL.2018.2861730.

Shen, Jiangwei, Xiong, Jian, Shu, Xing, Li, Guang, Zhang, Yuanjian, Chen, Zheng, and Liu, Yonggang (2021). "State of charge estimation framework for lithium-ion batteries based on square root cubature Kalman filter under wide operation temperature range". In: *International Journal of Energy Research* 45.4, pp. 5586–5601. DOI: https://doi.org/10.1002/er.6186. eprint: https://onlinelibrary.wiley.com/doi/pdf/10.1002/er.6186. URL: https://onlinelibrary.wiley.com/doi/abs/10.1002/er.6186.

Shen, Ping, Ouyang, Minggao, Han, Xuebing, Feng, Xuning, Lu, Languang, and Li, Jianqiu (2018). "Error Analysis of the Model-Based State-of-Charge Observer for Lithium-Ion Batteries". In: *IEEE Transactions on Vehicular Technology* 67.9, pp. 8055–8064. DOI: 10.1109/TVT.2018.2842820.

Shi, Yiwei, Feng, Donghan, Yu, Sumin, Fang, Chen, Li, Hengjie, and Zhou, Yun (2022). "The projection of electric vehicle population growth considering scrappage and tech-

nology competition: A case study in Shanghai". In: *Journal of Cleaner Production* 365, p. 132673. ISSN: 0959-6526. DOI: https://doi.org/10.1016/j.jclepro.2022.132673. URL: https://www.sciencedirect.com/science/article/pii/S0959652622022727.

Shrivastava, Prashant, Soon, Tey Kok, Idris, Mohd Yamani Idna Bin, and Mekhilef, Saad (2019). "Overview of model-based online state-of-charge estimation using Kalman filter family for lithium-ion batteries". In: *Renewable and Sustainable Energy Reviews* 113, p. 109233. ISSN: 1364-0321. DOI: https://doi.org/10.1016/j.rser.2019.06.040. URL: https://www.sciencedirect.com/science/article/pii/S1364032119304332.

Shu, Xing, Li, Guang, Shen, Jiangwei, Yan, Wensheng, Chen, Zheng, and Liu, Yonggang (2020). "An adaptive fusion estimation algorithm for state of charge of lithium-ion batteries considering wide operating temperature and degradation". In: *Journal of Power Sources* 462, p. 228132. ISSN: 0378-7753. DOI: https://doi.org/10.1016/j.jpowsour.2020.228132. URL: https://www.sciencedirect.com/science/article/pii/S0378775320304353.

Siva Suriya Narayanan, S. and Thangavel, S. (2022). "Machine learning-based model development for battery state of charge–open circuit voltage relationship using regression techniques". In: *Journal of Energy Storage* 49, p. 104098. ISSN: 2352-152X. DOI: https://doi.org/10.1016/j.est.2022.104098. URL: https://www.sciencedirect.com/science/article/pii/S2352152X22001335.

Song, Y., Park, M., Seo, M., and Kim, S. W. (2019). "Improved SOC estimation of lithium-ion batteries with novel SOC-OCV curve estimation method using equivalent circuit model". In: *2019 4th International Conference on Smart and Sustainable Technologies (SpliTech)*, pp. 1–6. DOI: 10.23919/SpliTech.2019.8783149.

Tamilselvi, S., Gunasundari, S., Karuppiah, N., Razak RK, Abdul, Madhusudan, S., Nagarajan, Vikas Madhav, Sathish, T., Shamim, Mohammed Zubair M., Saleel, C. Ahamed, and Afzal, Asif (2021). "A Review on Battery Modelling Techniques". In: *Sustainability* 13.18, pp. 140–156. ISSN: 2071-1050. DOI: 10.3390/su131810042. URL: https://www.mdpi.com/2071-1050/13/18/10042.

Tang, Xidong, Mao, Xiaofeng, Lin, Jian, and Koch, Brian (2011). "Li-ion battery parameter estimation for state of charge". In: *Proceedings of the 2011 American Control Conference*, pp. 941–946. DOI: 10.1109/ACC.2011.5990963.

Tao, G. and Kokotovic, P.V. (1995). "Adaptive control of plants with unknown hystereses". In: *IEEE Transactions on Automatic Control* 40.2, pp. 200–212. DOI: 10.1109/9.341778.

Tingting, Dong, Jun, Li, Fuquan, Zhao, Yi, You, and Qiqian, Jin (2011). "Analysis on the influence of measurement error on state of charge estimation of LiFePO4 power Battery". In: *2011 International Conference on Materials for Renewable Energy Environment*. Vol. 1, pp. 644–649. DOI: 10.1109/ICMREE.2011.5930893.

Tong, Shijie, Klein, Matthew P., and Park, Jae Wan (2015). "On-line optimization of battery open circuit voltage for improved state-of-charge and state-of-health estimation". In: *Journal of Power Sources* 293, pp. 416–428. ISSN: 0378-7753. DOI: https://doi.org/10.1016/j.jpowsour.2015.03.157. URL: https://www.sciencedirect.com/science/article/pii/S0378775315005911.

Topan, Paris Ali, Ramadan, M. Nisvo, Fathoni, Ghufron, Cahyadi, Adha Imam, and Wahyunggoro, Oyas (2016). "State of Charge (SOC) and State of Health (SOH) estimation on lithium polymer battery via Kalman filter". In: *2016 2nd International Conference on Science and Technology-Computer (ICST)*, pp. 93–96. DOI: 10.1109/ICSTC.2016.7877354.

Tran, Ngoc-Tham, Khan, Abdul Basit, and Choi, Woojin (2017). "State of Charge and State of Health Estimation of AGM VRLA Batteries by Employing a Dual Extended Kalman Filter and an ARX Model for Online Parameter Estimation". In: *Energies* 10.1, pp. 254–271. ISSN: 1996-1073. DOI: 10.3390/en10010137. URL: https://www.mdpi.com/1996-1073/10/1/137.

Tulsyan, Aditya, Tsai, Yiting, Gopaluni, R. Bhushan, and Braatz, Richard D. (2016). "State-of-charge estimation in lithium-ion batteries: A particle filter approach". In: *Journal of Power Sources* 331, pp. 208–223. ISSN: 0378-7753. DOI: https://doi.org/10.1016/j.jpowsour.2016.08.113. URL: https://www.sciencedirect.com/science/article/pii/S0378775316311338.

Wadi, A., Abdel-Hafez, M. F., and Hussein, A. A. (2019). "Mitigating the Effect of Noise Uncertainty on the Online State-of-Charge Estimation of Li-Ion Battery Cells". In: *IEEE Transactions on Vehicular Technology* 68.9, pp. 8593–8600. DOI: 10.1109/TVT.2019.2928047.

Wan, Eric A. and Merwe, Rudolph van der (2001). "The Unscented Kalman Filter". In: *Kalman Filtering and Neural Networks*. John Wiley & Sons, Ltd. Chap. 7, pp. 221–280. ISBN: 9780471221548. DOI: https://doi.org/10.1002/0471221546.ch7. eprint: https://onlinelibrary.wiley.com/doi/pdf/10.1002/0471221546.ch7. URL: https://onlinelibrary.wiley.com/doi/abs/10.1002/0471221546.ch7.

Wang, Yongqi, Yin, Wei, Yan, Qingzhong, and Cheng, Yong (2021). "Impact of sensor accuracy of battery management system on SOC estimation of electric vehicle based on EKF algorithm". In: *2021 5th CAA International Conference on Vehicular Control and Intelligence (CVCI)*, pp. 1–6. DOI: 10.1109/CVCI54083.2021.9661212.

Wang, Zuolu, Feng, Guojin, Liu, Xiongwei, Gu, Fengshou, and Ball, Andrew (2022). "A novel method of parameter identification and state of charge estimation for lithium-ion battery energy storage system". In: *Journal of Energy Storage* 49, p. 104124. ISSN: 2352-152X. DOI: https://doi.org/10.1016/j.est.2022.104124. URL: https://www.sciencedirect.com/science/article/pii/S2352152X22001608.

Wei, Jingwen and Chen, Chunlin (2020). "State of Charge and Health Estimation For Lithium-Ion Batteries Using Recursive Least Squares". In: *2020 5th International Conference on Advanced Robotics and Mechatronics (ICARM)*, pp. 686–689. DOI: 10.1109/ICARM49381.2020.9195346.

Wei, Zhongbao, Dong, Guangzhong, Zhang, Xinan, Pou, Josep, Quan, Zhongyi, and He, Hongwen (2021). "Noise-Immune Model Identification and State-of-Charge Estimation for Lithium-Ion Battery Using Bilinear Parameterization". In: *IEEE Transactions on Industrial Electronics* 68.1, pp. 312–323. DOI: 10.1109/TIE.2019.2962429.

Wu, Tiezhou, Chen, Xueguang, Xia, Fangzhen, and Xiang, Jianfeng (2011). "Research on SOC Hybrid Estimation Algorithm of Power Battery Based on EKF". In: *2011*

Asia-Pacific Power and Energy Engineering Conference, pp. 1–3. DOI: 10.1109/APPEEC.2011.5748464.

Wu, X., Li, X., and Du, J. (2018). "State of Charge Estimation of Lithium-Ion Batteries Over Wide Temperature Range Using Unscented Kalman Filter". In: *IEEE Access* 6, pp. 41993–42003. DOI: 10.1109/ACCESS.2018.2860050.

Xia, Bizhong, Lao, Zizhou, Zhang, Ruifeng, Tian, Yong, Chen, Guanghao, Sun, Zhen, Wang, Wei, Sun, Wei, Lai, Yongzhi, Wang, Mingwang, and Wang, Huawen (Dec. 2017). "Online Parameter Identification and State of Charge Estimation of Lithium-Ion Batteries Based on Forgetting Factor Recursive Least Squares and Nonlinear Kalman Filter". In: *Energies* 11, p. 3. DOI: 10.3390/en11010003.

– (2018). "Online Parameter Identification and State of Charge Estimation of Lithium-Ion Batteries Based on Forgetting Factor Recursive Least Squares and Nonlinear Kalman Filter". In: *Energies* 11.1. ISSN: 1996-1073. DOI: 10.3390/en11010003. URL: https://www.mdpi.com/1996-1073/11/1/3.

Xiao, Yongsong, Wang, Dongqing, and Ding, Feng (2010). "The residual-based ESG algorithm and its performance analysis". In: *Journal of the Franklin Institute* 347.2, pp. 426–437. ISSN: 0016-0032. DOI: https://doi.org/10.1016/j.jfranklin.2009.05.008. URL: https://www.sciencedirect.com/science/article/pii/S0016003209000945.

Xiaosong, Hu, Shengbo, Li, and Huei, Peng (Jan. 2012). "A comparative study of equivalent circuit models for Li-ion batteries". In: *Journal of Power Sources* 198, pp. 359–367. DOI: 10.1016/j.jpowsour.2011.10.013.

Xiong, R., He, H., Sun, F., and Zhao, K. (2013). "Evaluation on State of Charge Estimation of Batteries With Adaptive Extended Kalman Filter by Experiment Approach". In: *IEEE Transactions on Vehicular Technology* 62.1, pp. 108–117. DOI: 10.1109/TVT.2012.2222684.

Xiong, Rui, Huang, Jintao, Duan, Yanzhou, and Shen, Weixiang (2022a). "Enhanced Lithium-ion battery model considering critical surface charge behavior". In: *Applied Energy* 314, pp. 1189–1204. ISSN: 0306-2619. DOI: https://doi.org/10.1016/

j.apenergy.2022.118915. URL: https://www.sciencedirect.com/science/article/pii/S0306261922003373.

Xiong, Rui, Huang, Jintao, Duan, Yanzhou, and Shen, Weixiang (2022b). "Enhanced Lithium-ion battery model considering critical surface charge behavior". In: *Applied Energy* 314, pp. 118–129. ISSN: 0306-2619. DOI: https://doi.org/10.1016/j.apenergy.2022.118915. URL: https://www.sciencedirect.com/science/article/pii/S0306261922003373.

Xiong, Rui, Sun, Fengchun, He, Hongwen, and Nguyen, Trong Duy (2013). "A data-driven adaptive state of charge and power capability joint estimator of lithium-ion polymer battery used in electric vehicles". In: *Energy* 63, pp. 295–308. ISSN: 0360-5442. DOI: https://doi.org/10.1016/j.energy.2013.10.027. URL: https://www.sciencedirect.com/science/article/pii/S0360544213008761.

Xu, Jun, Wang, Jing, Li, Shiying, and Cao, Binggang (2016). "A Method to Simultaneously Detect the Current Sensor Fault and Estimate the State of Energy for Batteries in Electric Vehicles". In: *Sensors* 16.8. ISSN: 1424-8220. DOI: 10.3390/s16081328. URL: https://www.mdpi.com/1424-8220/16/8/1328.

Xu, Wei, Xu, Jinli, Lang, Jinfeng, and Yan, Xiaofeng (2019). "A Multi-Timescale Estimator for Lithium-Ion Battery State of Charge and State of Energy Estimation Using Dual H Infinity Filter". In: *IEEE Access* 7, pp. 181229–181241. DOI: 10.1109/ACCESS.2019.2959396.

Xu, Yidan, Hu, Minghui, Zhou, Anjian, Li, Yunxiao, Li, Shuxian, Fu, Chunyun, and Gong, Changchao (2020). "State of charge estimation for lithium-ion batteries based on adaptive dual Kalman filter". In: *Applied Mathematical Modelling* 77, pp. 1255–1272. ISSN: 0307-904X. DOI: https://doi.org/10.1016/j.apm.2019.09.011. URL: https://www.sciencedirect.com/science/article/pii/S0307904X19305414.

Yan, Xiangwu, Yang, Yang, Guo, Qi, Zhang, Hechuan, and Qu, Wei (2013). "Electric vehicle battery SOC estimation based on fuzzy Kalman filter". In: *2013 2nd International Symposium on Instrumentation and Measurement, Sensor Network and Automation (IMSNA)*, pp. 863–866. DOI: 10.1109/IMSNA.2013.6743414.

Yann Liaw, Bor, Nagasubramanian, Ganesan, Jungst, Rudolph G., and Doughty, Daniel H. (2004). "Modeling of lithium ion cells—A simple equivalent-circuit model approach". In: *Solid State Ionics* 175.1. Fourteenth International Conference on Solid State Ionics, pp. 835–839. ISSN: 0167-2738. DOI: https://doi.org/10.1016/j.ssi.2004.09.049. URL: https://www.sciencedirect.com/science/article/pii/S0167273804006678.

Ye, Yonghuang, Shi, Yixiang, Cai, Ningsheng, Lee, Jianjun, and He, Xiangming (2012). "Electro-thermal modeling and experimental validation for lithium ion battery". In: *Journal of Power Sources* 199, pp. 227–238. ISSN: 0378-7753. DOI: https://doi.org/10.1016/j.jpowsour.2011.10.027. URL: https://www.sciencedirect.com/science/article/pii/S0378775311019768.

Ye, Yuanmao, Li, Zhenpeng, Lin, Jingxiong, and Wang, Xiaolin (2022). "State-of-charge estimation with adaptive extended Kalman filter and extended stochastic gradient algorithm for lithium-ion batteries". In: *Journal of Energy Storage* 47, p. 103611. ISSN: 2352-152X. DOI: https://doi.org/10.1016/j.est.2021.103611. URL: https://www.sciencedirect.com/science/article/pii/S2352152X21012895.

Yu, Quanqing, Xiong, Rui, and Lin, Cheng (2017). "Online Estimation of State-of-charge Based on the H infinity and Unscented Kalman Filters for Lithium Ion Batteries". In: *Energy Procedia* 105. 8th International Conference on Applied Energy, ICAE2016, 8-11 October 2016, Beijing, China, pp. 2791–2796. ISSN: 1876-6102. DOI: https://doi.org/10.1016/j.egypro.2017.03.600. URL: https://www.sciencedirect.com/science/article/pii/S1876610217306525.

Yuan, Baohe, Zhang, Binger, Yuan, Xiang, Wang, Jingyi, Chen, Lulu, Bai, Lei, and Luo, Shijun (2022). "Study on the Relationship Between Open-Circuit Voltage, Time Constant And Polarization Resistance of Lithium-Ion Batteries". In: *Journal of The Electrochemical Society* 169.6, p. 060513. DOI: 10.1149/1945-7111/ac7359. URL: https://doi.org/10.1149/1945-7111/ac7359.

Zhang, Cheng, Li, Kang, Pei, Lei, and Zhu, Chunbo (2015). "An integrated approach for real-time model-based state-of-charge estimation of lithium-ion batteries". In: *Journal of Power Sources* 283, pp. 24–36. ISSN: 0378-7753. DOI: https://doi.org/

10.1016/j.jpowsour.2015.02.099. URL: https://www.sciencedirect.com/science/article/pii/S0378775315003444.

Zhang, Hua, Mu, Hai Wei, Zhang, Yong, and Han, Jian (2014). "Calculation and characteristics analysis of lithium ion batteries' internal resistance using HPPC test". In: *Advanced Materials Research*. Vol. 926. Trans Tech Publ, pp. 915–918.

Zhang, Jingliang, Liao, Linxia, and Lee, Jay (Apr. 2010). "Prognostics and Health Monitoring of Li-ion Battery for Hybrid Electric Vehicle". In: DOI: 10.4271/2010-01-0256.

Zhang, Ruifeng, Xia, Bizhong, Li, Baohua, Cao, Libo, Lai, Yongzhi, Zheng, Weiwei, Wang, Huawen, Wang, Wei, and Wang, Mingwang (2018). "A Study on the Open Circuit Voltage and State of Charge Characterization of High Capacity Lithium-Ion Battery Under Different Temperature". In: *Energies* 11.9. ISSN: 1996-1073. DOI: 10.3390/en11092408. URL: https://www.mdpi.com/1996-1073/11/9/2408.

Zhang, Shijian, Zhang, Yunlong, Meng, Qingyu, and Zhou, Boya (2022). "Big data analysis of the influence of ambient temperature on electric vehicles". In: *2022 IEEE International Conference on Electrical Engineering, Big Data and Algorithms (EEBDA)*, pp. 239–244. DOI: 10.1109/EEBDA53927.2022.9744863.

Zhang, Shuzhi and Zhang, Xiongwen (2022). "A novel non-experiment-based reconstruction method for the relationship between open-circuit-voltage and state-of-charge/state-of-energy of lithium-ion battery". In: *Electrochimica Acta* 403, p. 139637. ISSN: 0013-4686. DOI: https://doi.org/10.1016/j.electacta.2021.139637. URL: https://www.sciencedirect.com/science/article/pii/S0013468621019216.

Zhang, Wenjie, Wang, Liye, Wang, Lifang, Liao, Chenglin, and Zhang, Yuwang (2022). "Joint State-of-Charge and State-of-Available-Power Estimation Based on the Online Parameter Identification of Lithium-Ion Battery Model". In: *IEEE Transactions on Industrial Electronics* 69.4, pp. 3677–3688. DOI: 10.1109/TIE.2021.3073359.

Zhang, Xiaoqiang, Zhang, Weiping, and Lei, Geyang (Dec. 2016). "A Review of Li-ion Battery Equivalent Circuit Models". In: *Transactions on Electrical and Electronic Materials* 17, pp. 311–316. DOI: 10.4313/TEEM.2016.17.6.311.

Zhao, Guangming and Wang, Yifan (2020). "An online model identification for state of charge estimation of lithium-ion batteries using extended kalman filter". In: *2020 IEEE 3rd International Conference on Renewable Energy and Power Engineering (REPE)*, pp. 34–38. DOI: 10.1109/REPE50851.2020.9253875.

Zheng, Yuejiu, Ouyang, Minggao, Han, Xuebing, Lu, Languang, and Li, Jianqiu (2018). "Investigating the error sources of the online state of charge estimation methods for lithium-ion batteries in electric vehicles". In: *Journal of Power Sources* 377, pp. 161–188. ISSN: 0378-7753. DOI: https://doi.org/10.1016/j.jpowsour.2017.11.094. URL: https://www.sciencedirect.com/science/article/pii/S037877531731594X.

Zhi, Li, Peng, Zhang, Zhifu, Wang, Qiang, Song, and Yinan, Rong (2017). "State of Charge Estimation for Li-ion Battery Based on Extended Kalman Filter". In: *Energy Procedia* 105. 8th International Conference on Applied Energy, ICAE2016, 8-11 October 2016, Beijing, China, pp. 3515–3520. ISSN: 1876-6102. DOI: https://doi.org/10.1016/j.egypro.2017.03.806. URL: https://www.sciencedirect.com/science/article/pii/S1876610217308810.

Zhu, Rui, Duan, Bin, Zhang, Junming, Zhang, Qi, and Zhang, Chenghui (2020). "Co-estimation of model parameters and state-of-charge for lithium-ion batteries with recursive restricted total least squares and unscented Kalman filter". In: *Applied Energy* 277, pp. 1154–1174. ISSN: 0306-2619. DOI: https://doi.org/10.1016/j.apenergy.2020.115494. URL: https://www.sciencedirect.com/science/article/pii/S0306261920310060.

Zou, Zhongyue, Xu, Jun, Mi, Chris, Cao, Binggang, and Chen, Zheng (2014). "Evaluation of Model Based State of Charge Estimation Methods for Lithium-Ion Batteries". In: *Energies* 7.8, pp. 5065–5082. ISSN: 1996-1073. DOI: 10.3390/en7085065. URL: https://www.mdpi.com/1996-1073/7/8/5065.

Appendix A

Appendix Chapter

A.1 Battery model algorithm

```
%% Simulation parameter
clear all;
dt = 10^-2;
t = 0:dt:60*112;
N = length(t);
A = 0.425;
f = 0.0005;
I = A*sin(f*2*pi*t) + A*ones(1,N);
plot(I);
%% battery design
Q_max = 0.85*60*60;
R0 = 0.3;
Rp = 0.1;
Cp = 10;
tau = Rp*Cp;
z(1) = 1;
Vp(1)= 0;
a =      0.2539;
b =      0.4566;
```

```
c =       7.245;
delta = 0.008;
Voc(1) = a*log((z(1)+delta))+b*exp((z(1)+delta).^3)+c;
%I = I + normrnd(0,5*10^-3,550001,1);
Vt(1) = Voc(1) - Vp(1) - I(1)*R0;
i = 1;
while z(i) > 10^-3
    z(i+1) = z(i) - I(i)*dt/Q_max;
    Vp(i+1) = exp(-dt/tau)*Vp(i) + (1 - exp(-dt/tau))*Rp*I(i);
    Voc(i+1) = a*log((z(i+1)+delta))+b*exp((z(i+1)+delta).^3)+c;
    Vt(i+1) = Voc(i+1) - Vp(i+1) - I(i+1)*R0;
    i = i+1;
end
save('battery.mat','Vt','I','z','Voc','Vp','dt','a','b',...
'c','delta','Q_max');
```

A.2 Parameter estimation algorithm

```
clear all;
load 'battery.mat'
%% adaptive parameter estimation
N = length(Vt);
%I = I + normrnd(0,10^-3,length(I),1);
%theta = [alpha1, alpha2, alpha3]'
theta = [0.990, -0.1, (0.9980*0.1-(1-0.990)*0.05)]';
dVt(1) = Vt(1);
dVt(2) = Vt(2) - Vt(1);
dI(1) = I(1);
dI(2) = I(2) - I(1);
Gamma = 5000*eye(3);
R0_hat(1) = -theta(2,1);
R0_hat(2) = -theta(2,1);
```

```
Rp_hat(1) = (-theta(1)*theta(2)-theta(3))/(1-theta(1));
Rp_hat(2) = (-theta(1)*theta(2)-theta(3))/(1-theta(1));
Cp_hat(1) = -dt/(Rp_hat(2)*log(theta(1)));
Cp_hat(2) = -dt/(Rp_hat(2)*log(theta(1)));
for k=2:N-1
        dVt(k+1) = Vt(k+1) - Vt(k);
        dI(k+1) = I(k+1) - I(k);
        phi = [dVt(k) dI(k+1) dI(k)]';
        epsilon(k+1) = dVt(k+1) - theta'*phi;
        theta = theta + Gamma*epsilon(k+1)*phi;
        R0_hat(k+1) = -theta(2);
        Rp_hat(k+1) = (-theta(1)*theta(2) - theta(3))/(1-theta(1));
        Cp_hat_2(k+1) = -dt/(Rp_hat(k+1)*log(theta(1)));
        Rp_hat_2(k+1) = 1/Cp_hat_2(k+1);
end
save ('para_out.mat','R0_hat','Rp_hat','Cp_hat');
figure(1);
subplot(4,1,1);hold on;axis([0 N 0 0.6]);
plot(R0_hat,'r');plot(0.3*ones(N,1),'k--');
xlabel('Time [min]');ylabel('R_0 [\Omega]');
legend('Estimated R_0','True R_0');
subplot(4,1,2);hold on;axis([0 N 0 0.6]);
plot(Rp_hat_2,'r');plot(0.1*ones(N,1),'k--');
xlabel('Time [min]');ylabel('R_p [\Omega]');
legend('Estimated R_p','True R_p');
subplot(4,1,3);hold on;axis([0 N 0 100]);
plot(Cp_hat_2,'r');plot(10*ones(N,1),'k--');
xlabel('Time [min]');ylabel('C_p [F]');
legend('Estimated C_p','True C_p');
subplot(4,1,4);hold on;
plot(I);axis([0 N -1 3]);
legend('Sinusodial current')
```

```
47 xlabel('Time [min]');ylabel('I [A]');
```

A.3 SoC-OCV curve construction algorithm

```
1  clear all;
2  load 'para_out.mat';
3  load 'battery.mat';
4  I = I - 0.1;
5  SoC=z;
6  clear z;
7  %load 'Voc.mat'
8  Voc_true = Voc;
9  tau_hat = Rp_hat.*Cp_hat;
10 N = length(R0_hat);
11 Ns = 1000;
12 C_max = 0.85*60*60;
13 Q_max = 0.85*60*60;
14 V_l = 6.4412;
15 V_h = 8.5028;
16 dV = V_h - V_l;
17 delta = 8*10^-3;
18 l = log(1+delta) - log(delta);
19 e = exp((1 + delta)^3) - exp(delta^3);
20 a_hat(3) = 0.5;
21 b_hat(3) = 0.75;
22 c_hat(3) = 7.5;
23 P(3)  = 0;
24 Q = 10^-6;
25 R = 10^-1;
26 r_noise = 10^-3;
27 q_noise = 10^-3;
```

```
Ia = zeros(Ns,1);
Voc = 6.4 + 2*rand(Ns,1);
z(3) = 0.5;
H(3) = 0.2539.*log(z(1)+8*10^-3) +...
0.4566.*exp((z(1)+8*10^-3).^3) + 7.245;
r_z = 10^-1;
q_z = 10^-6;
i = 1;
x_hat(:,3)=[0;7];
P_hat = [10^-3 0;0 10^-3];
Qx = [10^-6;10^-6];
rx = 10^-6;
% z(177920) = 0.5;
% a_hat(177920) = 0.5;
for k=3:N-1
        beta = exp(-dt/(Rp_hat(k).*Cp_hat(k)));
        A = [beta 0;0 1];
        B = [1-beta;0];
        %% Propagation
        x_hat(:,k+1) = A*x_hat(:,k)+B*I(k);
        P_hat = A*P_hat*A' + Qx;
        z(k+1) = z(k) - I(k)*dt/Q_max;
        a_hat(k+1) = a_hat(k);
        %% Kalman filter for a
        P = R + Q;
        S = P + R;
        C = [-Rp_hat(k) 1];
        L = P_hat*C'/(C*P_hat*C'+rx);
        Vt_hat = x_hat(2,k+1) - x_hat(1,k+1)*Rp_hat(k)...
        - I(k)*R0_hat(k);
        x_hat(:,k+1) = x_hat(:,k+1) + L*(Vt(k+1) - Vt_hat);
        P_hat = (1 - L*C)*P_hat;
```

```
60          Voc_hat(k+1) = abs(x_hat(2,k+1));
61          K(k+1) = (Voc_hat(k+1) - Voc_hat(k))/(- I(k)*dt/Q_max);
62          deno(k) = mean((1 - 3*l*exp(z(k+1).^3).*z(k+1).^3/e));
63          if deno(k)<0.3 & deno(k)>-0.1
64              a = K(k+1)*z(k+1)-3*b_hat(k)*exp((z(k+1))^3)*...
65              ((z(k+1))^3);
66          else
67              a = (K(k+1).*z(k+1) - 3*dV/e*exp(z(k+1).^3).*...
68              z(k+1).^3)./(1 - 3*l*exp(z(k+1).^3).*z(k+1).^3/e);
69          end
70          b = (dV - a*l)/e;
71          c = V_l - a*log(delta) - b*exp(delta^3);
72          a_mean(k+1) = a;
73          Ka = P*S;
74          ya(k) = a_mean(k) - a_hat(k);
75          a_hat(k+1) = a_hat(k) + Ka*ya(k);
76          P = (1 - Ka)*P;
77          %%
78          b_hat(k+1) = (dV - a_hat(k+1)*l)/e;
79          c_hat(k+1) = V_l - a_hat(k+1)*log(delta) -...
80          b_hat(k+1)*exp(delta^3);
81          H(k+1) = a_hat(k+1).*log(z(k+1)+8*10^-3) + b_hat(k+1).*...
82          exp((z(k+1)+8*10^-3).^3) + c_hat(k+1);
83          p_z = r_z + q_z;
84          s_z  = p_z + r_z;
85          kz = p_z*s_z;
86          y_z = Voc_hat(k) - H(k+1);
87          z(k+1) = z(k) +kz*y_z;
88          p_z = (1-kz*K(k+1))*p_z;
89  end
90  plot(x_hat(2,:));hold on;plot(Voc_true);
91  figure(2);
```

```
92 plot(SoC);hold on;plot(z)
```

A.4 Bias estimation algorithm

```
1  clear all
2  load 'battery.mat'
3  N = length(Vt);
4  R0 = 0.3;
5  Rp = 0.1;
6  Cp = 10;
7  tau = Rp*Cp;
8  alpha = exp(-dt/tau);
9  A = [alpha 0 ; 0 1];
10 B = [1-alpha ; -dt/Q_max];
11 %% %%%%%%%%%%%%%%%%%%%%%%%%%%%%%%%%%%%
12 Vt = Vt + normrnd(0,10^-6,1,N);
13 %Terminal voltage added white noise
14 %% initialisation
15 x_hat(:,1) = [0 ; rand];
16 Voc_hat(1) = a*log((x_hat(2,1)+delta))...
17 +b*exp((x_hat(2,1)+delta).^3)+c;
18 P = [10^-3 0 ;0 10^-3];
19 Q = [10^-3 0 ; 0 10^-6];
20 r = 10^-3;
21 %% %%%%%%%%%%%%%%%%%%%%%%%%%%%%%%%%%%%
22 % Drift Generator
23 a_beta = 0;
24 b_beta = 0.1;
25 sigma_beta = 10^-3;
26 P_b = 10^-3;
27 q_b = 10^-1;
```

```
r_b =10^-6;
% initial beta (t)
beta(1) = (b_beta-a_beta)*rand + a_beta;
% creates a random initial value for beta within [a,b]
I_meas(1) = I(1) + beta(1)+ normrnd(0,10^-6);
beta_hat(1) = (b_beta-a_beta)*rand + a_beta;%(b-a)*rand + a;
% creates a random initial value for beta within [a,b]
%%
for k=1:N-1
    beta(k+1) = f_beta(sigma_beta,dt,beta(k));
    %Beta function to produce random walk bias
    %in the current measurement
    I_meas(k+1) = I(k+1) + beta(k+1)+ normrnd(0,10^-6);
    % True current + Drift noise + White noise
    x_hat(:,k+1) = A*x_hat(:,k) + B*(I_meas(k)-beta_hat(k));
    P = A*P*A' + Q;
    %%Drift noise
    beta_hat(k+1) = beta_hat(k);
    P_b = P_b + q_b;
    C2 = (a + 3*b*exp(x_hat(2,k+1).^3).*x_hat(2,k+1).^3)...
    ./x_hat(2,k+1);
    C = [-Rp  C2];
    K = P*C'/(C*P*C' + r);
    Voc_hat(k+1) = a*log((x_hat(2,k+1)+delta))...
    +b*exp((x_hat(2,k+1)+delta).^3)+c;
    Vt_hat(k+1) = Voc_hat(k+1) - (I_meas(k+1)...
    -beta_hat(k+1))*R0 - x_hat(1,k+1)*Rp;
    x_hat(:,k+1) = x_hat(:,k+1) + K*(Vt(k+1) - Vt_hat(k+1));
    P = (eye(2) - K*C)*P;
    z_star(k) = x_hat(2,k);
    z_star(k+1) = z_star(k) - (I_meas(k)-beta_hat(k))*dt/Q_max;
    Voc_star(k+1) = a*log(z_star(k+1)+delta)...
```

```
    +b*exp((z_star(k+1)+delta).^3)+c;
    Voc_star(k) = a*log(z_star(k)+delta)...
    +b*exp((z_star(k)+delta).^3)+c;
    deltaVoc_star(k+1) = Voc_star(k+1) - Voc_star(k);
    deltaVt(k+1) = Vt(k+1) - Vt(k);
    deltaVp_hat(k+1) = (x_hat(1,k+1) - x_hat(1,k))*Rp;
    deltaVt_hat(k+1) = deltaVoc_star(k+1) - (I_meas(k+1)...
    -I_meas(k))*R0 - deltaVp_hat(k+1);
    delta_beta(k+1) =  (deltaVt(k+1) - deltaVt_hat(k+1))/R0;
    L_b(k+1) = P_b/(P_b + r_b);
    beta_hat(k+1) = beta_hat(k+1) ...
    + L_b(k+1)*(delta_beta(k+1));
end
z_hat = x_hat(2,:);
for k=1:N-1
    x_hat(:,k+1) = A*x_hat(:,k) + B*(I_meas(k));
    P = A*P*A' + Q;
    %%Drift noise
    C2 = (a + 3*b*exp(x_hat(2,k+1).^3)...
    .*x_hat(2,k+1).^3)./x_hat(2,k+1);
    C = [-Rp  C2];
    K = P*C'/(C*P*C' + r);
    Voc_hat(k+1) = a*log((x_hat(2,k+1)+delta))...
    +b*exp((x_hat(2,k+1)+delta).^3)+c;
    Vt_hat(k+1) = Voc_hat(k+1) - (I_meas(k+1))*R0...
    - x_hat(1,k+1)*Rp;
    x_hat(:,k+1) = x_hat(:,k+1) + K*(Vt(k+1) - Vt_hat(k+1));
    P = (eye(2) - K*C)*P;
end
save('bias_simulation.mat','beta','beta_hat'...
,'z_hat','x_hat','z','I','I_meas');
figure(1);
```

```
92  hold on;plot(beta_hat,'r');plot(beta,'k--');
93  axis([0 N -0.1 0.15]);
94  xlabel('Time [ms]');ylabel('\beta [A]')
95  yyaxis right;plot(I_meas - beta_hat,'y');axis([0 N -3 15]);
96  ylabel('I [A]');hold on;plot(I(1:length(beta)),'b')
97  legend('Estimated \beta','True \beta','Estimated I','True I');
98  figure(2);
99  subplot(2,1,1);xlabel('Time [min]');ylabel('z')
100 hold on;plot(abs(x_hat(2,:)),'g');
101 plot(z_hat,'r');plot(z,'k--');axis([0 N 0 1]);
102 legend('Estimated z based on measured I'...
103 ,'Estimated z based on estimated I','True z')
104 subplot(2,1,2);xlabel('Time [min]');ylabel('I [A]')
105 hold on;plot(I_meas,'g');plot((I_meas-beta_hat)...
106 ,'r');plot(I,'k--');axis([0 N 0 1.7]);
107 legend('Measured I','Estimated I','True I')
```